ASPECTS OF NON-ADIABATIC MOLECULAR COLLISION THEORY

A Thesis submitted for the Degree of Doctor of Philosophy

in the University of Oxford

by

M. R. Gover

Wolfson College

Oxford

Hilary Term, 1978

Theoretical Chemistry Department

Oxford

Aspects of non-adiabatic molecular collision theory

by M. R. Gover, Wolfson College, Oxford

Submitted for the Degree of Doctor of Philosophy in the University of Oxford

Hilary Term, 1978

This thesis is concerned with non-adiabatic effects in alkali / halogen collision systems. After a general survey of non-adiabatic molecular collision theory, and its application to such systems, calculations have been performed relating to three topics :

(i) Vibrational energy distributions resulting from electron transfer collisions between alkali metal atoms and halogen molecules are often treated by the multi-curve crossing approach to the classical path approximation, in the form of two approximations, one valid at high collision energy, the other at low energy; the performance of these is evaluated over a wide energy range by comparison with the results from an "exact" multi-curve crossing approach.

(ii) Classical trajectory calculations for reactive alkali / halogen collisions are performed using a simple ionic potential energy surface, developed earlier to model the weakening of the halogen bond by the metal ion immediately after the electron transfer. Detailed comparison is made between the results and those from experiment; good agreement is obtained for K/I_2 and comparison of the results for K/I_2 and Cs/I_2 indicates that this effect is not merely dependent on the charge of the ion.

(iii) The population of ground and excited sodium atoms resulting from Na/I charge neutralisation collisions is investigated using the multi-curve crossing approach. Although it has been suggested that population inversions may be produced by such a process, it is shown that this is only possible at extremely high collision energies.

Abstract

Three aspects of non-adiabatic effects in alkali / halogen collision systems are studied.

(i) Electron transfer collisions involving halogen molecules, $M + X_2 \rightarrow M^+ + X_2^-$, are currently receiving extensive experimental investigation by molecular beams. Theoretical interpretation, particularly of vibrational energy distributions resulting from such collisions, rests mainly on the classical path approximation, and two approaches to this, the surface hopping trajectory method, and the multi-curve crossing method, can be recognised. The latter is applied as one of two approximations, the Bauer, Fisher & Gilmore (BFG) method, and the Franck-Condon (FC) method, applicable in the limits of low and high collision energy respectively.

These approximations have been applied somewhat indiscriminately, and an investigation into their validity is presented. An exact formulation of the multi-curve crossing equations has been developed, and used to test the effectiveness of the two approximations by comparison of the results obtained for the vibrational energy distribution over a wide collision energy range. Solution of the Morse oscillator by a finite element method with cubic splines was investigated as a means of evaluating the overlap integrals required in these calculations. Solution of the coupled differential equations in the exact formulation was investigated by an implementation of the Magnus method of exponentiating the Hamiltonian matrix and also by straightforward treatment of the simultaneous equations as an initial value problem; the latter approach was found to be more

satisfactory computationally.

From the results obtained for transition probabilities to low vibrational levels of the covalent and ionic channels, it was found that the FC and BFG methods agree surprisingly well with each other at both high and low collision energies. The exact results oscillate as a function of energy for a particular impact parameter, the oscillations becoming less rapid as the energy is increased, and eventually dying out; the results from the two approximations appear to follow the exact results as they would be with the oscillations averaged out; such averaging might well occur in practice, since it was found that the exact transition probabilities also oscillate rapidly as a function of impact parameter.

Vibrational energy distributions within the ionic manifold and within the excited levels of the covalent channel were also considered; the FC method predicts no oscillations in these, regardless of interference between ingoing and outgoing trajectories, and it was confirmed that the oscillations in the exact results for these two distributions died out in the region in which the FC method is expected to become valid.

(ii) Throughout the history of molecular beams, experimental and theoretical investigation of alkali / halogen reactive collisions $M + X_2 \rightarrow MX + X$ has played a prominant role. In an earlier work, the physical picture of an electron jump followed by progressive weakening of the bond in the X_2^- by the electric field of the approaching M^+ was used to construct a simple ionic potential energy surface for classical trajectory calculations, with two variable parameters used to determine the extent of the bond weakening effect. It was found that the calculated scattering results were sensitive to the values of the parameters, and in this work, addition of initial

reactant vibrational energy has been used to improve the dynamical part of the calculation and permit closer comparison with experiment.

The initial vibrational energy caused a smearing out of the calculated angular and translational energy distributions of the MX; however, owing to the particular form of the Monte Carlo method used, viz. systematically chosen pseudo-random starting conditions, bunching effects in the theoretical scattering continued to make comparison with experiment difficult. Thus various properties of the scattering which involve averaging over many trajectories were selected, and, using these as a basis for comparison, best values for the variable parameters were found for $K + I_2$, giving quite good agreement with experiment. These were then used for $Cs + I_2$, but poorer agreement was obtained, indicating that the halogen bond weakening effect cannot be described as independent of the nature of the alkali ion.

(iii) Much less extensively studied have been atom-atom charge neutralisation collisions $M^+ + X^- \rightarrow M + X$. Owing to the near coincidence of the asymptotes for the curves for $M(^2P) + X$ and $M^+ + X^-$ in the system Na / I, it has been suggested that such collisions might be capable of producing a population inversion of Na(3p) with respect to Na(3s) and hence be used as a laser pumping mechanism. The multi-curve crossing approach has been used to investigate this; in order to do this, it was first necessary to calculate the variation of the off-diagonal Hamiltonian matrix elements with internuclear separation, using Whittaker function solutions for the sodium wavefunctions; the results were found to fit quite well the simple form $H_{ic}(r) = - Ar e^{-Br}$, and it was confirmed that the value of the interaction at the crossing point between the curves for $Na^+ + I^-$ and $Na(3s) + I$ was in agreement with previously published values.

The multi-curve crossing calculations indicated that production of a significant population of Na(3p) by the collisional mechanism proposed is only possible at extremely high collision energies ($\sim$ 500 keV), and at the energies used experimentally ($\sim$.5 eV) there is a negligable transition probability to the excited sodium; this is readily rationalised by the observation that the asymptotic near coincidence of the ionic and excited covalent curves is only approached at vast internuclear separations, owing to the extreme long range nature of the Coulomb potential; the interaction decreases much more rapidly than the separation between the curves. Thus it appears that the observed enhanced population of Na(3p) in shock tube experiments cannot be accounted for by a collisional charge neutralisation process. It is pointed out that such a process is much more likely to occur in some systems involving lithium, in which there is an actual crossing between the ionic and excited covalent curves.

Aknowledgements

Many thanks are due to my supervisor, Dr. Child, for providing inspiration and encouragement.

I wish also to thank the people at FOM, Amsterdam, for their hospitality and useful advice during a visit to inspect their interesting experiments.

Abbreviations

LZS	Landau - Zener - Stückelberg
SHT	Surface hopping trajectory
BFG	Bauer - Fisher - Gilmore
FC	Franck - Condon
PES	Potential energy surface
BO	Born - Oppenheimer
RRG	Rayleigh - Ritz - Galerkin

Contents

I		Introduction	1
II		Non-adiabatic molecular collision theory	13
	A	Adiabatic states and the Born-Oppenheimer approximation	13
	B	Diabatic states	18
	C	Classical Path approximation	20
	D	Two-state curve-crossing approximation	23
	(i)	Relation between the potential energy curves in the diabatic and adiabatic representations	24
	(ii)	Relation between the diabatic and adiabatic wavefunctions	26
	(iii)	The coupling in the diabatic and adiabatic representations	26
	(iv)	Coupled equations in the classical path approximation	27
	(v)	Non-adiabatic transition probability	29
	E	Multi-curve crossing approach to atom/diatom systems	34
	F	High energy limit - the Franck-Condon method	44
	G	Low energy limit - the sequential Landau-Zener BFG method	52
	H	Surface hopping trajectory approach to atom/diatom systems	56
III		Comparison of methods for calculating vibrational energy distributions in electron transfer collisions $M + X_2 \rightarrow M^+ + X_2^-$	58

A	Introduction	58
B	Description of the model system	59
(i)	Parameters and assumptions	59
(ii)	Morse oscillator wavefunctions and energies	64
(iii)	Harmonic oscillator overlap integrals	65
(iv)	Solution of Morse oscillator by finite element method	66
((v)	Morse oscillator overlap integrals	72
C	The Magnus approximation	80
D	Magnus solution to coupled equations	90
E	Krogh solution to coupled equations	101
F	Discussion of results	113
G	Summary and conclusions	117
IV	Trajectory studies of reactive scattering of alkali metal atoms with halogen molecules	121
A	Introduction	121
B	Inclusion of initial vibrational energy	125
C	Calculations for $K + I_2$	127
D	Calculations for $Cs + I_2$	139
E	Summary and conclusions	145
V	Charge neutralisation in $Na^+ + I^-$ collisions as a possible laser pumping mechanism	148
A	Introduction	148
B	The coupled equations	150
C	Calculation of the ## matrix elements	151
(i)	Diagonal elements	151
(ii)	Introduction to calculation of off - diagonal elements	153
(iii)	Calculation of wavefunctions	158

(iv) Calculation of off - diagonal elements 164

D The classical trajectory 174

E Discussion of results 176

F Summary and conclusions 179

References 181

CHAPTER I

INTRODUCTION

Over the last fifteen years, molecular beams have been extensively used to study elementary collisions in the gas phase (Ross, 1966; Schlier, 1970; Fluendy & Lawley, 1974; Lawley, 1975). Particularly well studied have been various collisions involving transfer of an electron between an alkali metal atom and a halogen, or sometimes other non-metal, atom or diatomic molecule; such collisions have also lent themselves readily to theoretical interpretation, making much use of the techniques of non-adiabatic molecular collision theory (see e.g. Baede, 1975; Janev, 1976). Aspects of the theory of such collisions form the subject of this work.

The simplest system is that of an alkali atom plus a halogen atom. The charge exchange collision

$$M + X \rightarrow M^+ + X^- \qquad (1\text{-}1)$$

(M = alkali metal; X = halogen) has been studied experimentally, although to a fairly small extent. Total (Moutinho, Aten & Los, 1971, 1974) and differential (Delvigne & Los, 1973) cross sections for the charge transfer have been measured. The total cross sections rise rapidly from threshold to a maximum, and then drop slowly with increasing collision energy; the differential cross sections show sharp peaks at low and high $E\theta$, with a broad peak between them. This is reviewed by Wexler (1973) and Baede (1975). The alkali halide molecules MX have been taken as an archetype of the curve-

crossing problem (Ewing et al, 1971). Of the various states involved, only two, viz. the covalent state $M(^2S_{\frac{1}{2}}) + X(^2P_{\frac{1}{2}})$ and the ionic state $M^+(^1S_0) + X^-(^1S_0)$, both of symmetry $^1\Sigma^+$ (Baede, 1975), need usually be considered; thus this is an ideal system for the application of the two-state approximation.

The two-state curve-crossing problem has been well studied (see e.g. Nikitin, 1968; Crothers, 1971; Delos & Thorson, 1972b). The theory was originally formulated by Landau (1932), Zener (1932), and Stückelberg (1932), based on the assumptions of linear diabatic potentials $H_{11}(r)$ and $H_{22}(r)$, constant interaction $H_{12}(r)$, and constant velocity v, in the crossing region. The result, usually called the Landau-Zener formula, is that the probability of staying on one diabatic curve during a single passage through the crossing region is given by:

$$P = e^{-2\gamma} \tag{1-2}$$

where

$$\gamma = \left. \frac{\pi \left| H_{12} \right|^2}{\hbar v (F_1 - F_2)} \right|_{r = r_c}$$

where r_c is the crossing radius, given by $H_{11}(r_c) = H_{22}(r_c)$;

$$F_i = \frac{\partial H_{ii}}{\partial r} ;$$

and r is the internuclear separation.

Particularly important is the dynamic width Δx_d, which is a velocity dependant region within which the assumptions must apply for the model to be valid. This is given by:

$$\Delta x_d = \sqrt{\frac{8\hbar v}{|F_1 - F_2|}} \tag{1-3}$$

The LZS (Landau-Zener-Stuckelberg) model has been criticised (Bates, 1960; Coulson & Zalewski, 1962) because of the inflexibility which its assumptions introduce, but it has enjoyed widespread application to $M + X$ and related collisions, and successfully predicts the observed maximum in the total cross section as a function of energy for these collisions.

The potentials generally used to describe the $M + X$ system (Delvigne & Los, 1973; Janev, 1976) are, relative to zero energy at infinitely separated $M^+ + X^-$, a simplefied Rittner (1951) potential for the diabatic ionic state (in atomic units):

$$H_{11}(r) = U_{ion}(r) = -\frac{1}{r} - \frac{(\alpha_{M^+} + \alpha_{X^-})}{2r^4} - \frac{2\alpha_{M^+}\alpha_{X^-}}{r^7} - \frac{C_{ion}}{r^6} + A_{ion}e^{-r/k_{ion}} \qquad (1\text{-}4)$$

where α_{M^+} = polarisability of M^+ ion;

α_{X^-} = polarisability of X^- ion,

and a covalent diabatic potential with a C_6 attraction and exponential repulsion:

$$H_{22}(r) = U_{cov}(r) = -\frac{C_{cov}}{r^6} + A_{cov}e^{-r/k_{cov}} - \Delta E \qquad (1\text{-}5)$$

where $\Delta E = I_M - E_{aX}$

and I_M = first ionisation potential of M;

E_{aX} = electron affinity of X.

These curves cross, usually at a fairly large internuclear separation, where $U_{cov}(r)$ is virtually flat, as shown in fig. 1;

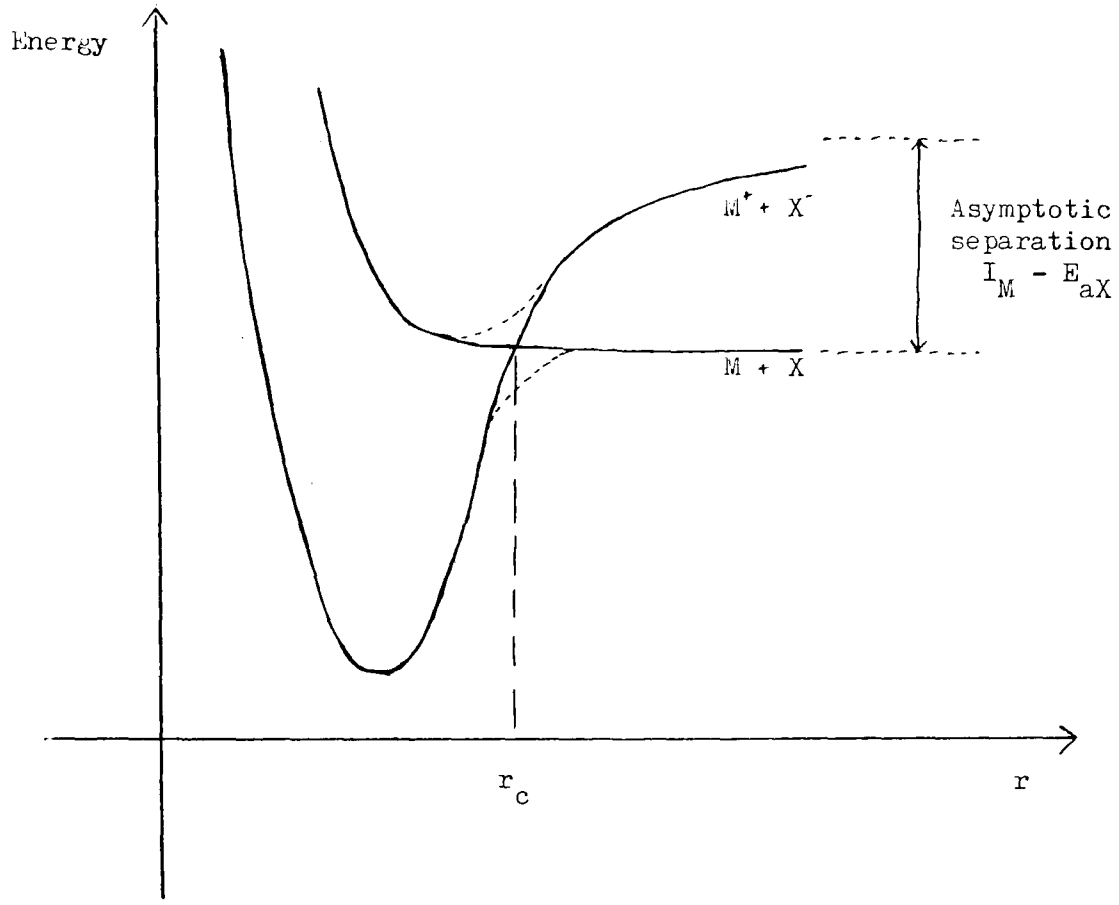

Fig. 1. The crossing at $r = r_c$ between the ground diabatic potential curves for an alkali halide MX.

the dashed curves are the adiabatic potentials, resulting from interaction between these two.

Delvigne & Los (1973) distinguished "covalent" scattering, under the influence of $U_{cov}(r)$, responsible for the peak in the differential charge transfer cross section at low $E\theta$, and "ionic" scattering, under the influence of $U_{ion}(r)$, responsible for the peaks at higher $E\theta$.

Much less clearly characterised is the interaction potential $H_{12}(r)$. Owing to its occurrence in the LZS formula, $H_{12}(r_c)$ has attracted most effort. Direct integration of $\langle \xi_1 | H | \xi_2 \rangle$, where

the ζ's are the appropriate wavefunctions, has been facilated by the fact that, at the fairly large crossing distances involved, the transferred electron is effectively localised on one atom, and can be described by an atomic orbital, or, more particularly, by its asymptotic form. Magee (1940; 1952) and Berry (1957) applied this method to M + X systems, and Grice & Herschbach (1974) have extended the calculations to $M + X_2$. They published results only for the adiabatic splitting at the crossing $\Delta V(r_c)$ $(= 2|H_{12}(r_c)|)$, and fitted this to a form:

$$\Delta V(r_c) = \exp((r_c^{\,0} - r_c)/\Delta r) \qquad (1\text{-}6)$$

where the parameters $r_c^{\,0}$ and Δr depend on the halogen but not on the metal. They also fitted their results to an earlier empirical expression due to Olson et al (1971; see also Smirnov, 1965):

$$\Delta V^*(r_c) = r_c^* \exp(-0.86 r_c^*) \qquad (1\text{-}7)$$

(in atomic units)

with reduced variables:

$$\Delta V^* = \frac{\Delta V}{\sqrt{I_M E_{aX}}} \quad ; \qquad r_c^* = \tfrac{1}{2}(\sqrt{2I_M} + \sqrt{2E_{aX}})r_c .$$

The dependence of H_{12} on r for a particular system has attracted less attention. Evers & DeVries (1976) suggested an exponentially falling dependence on $(r - r_c)$.

Interest has also been shown in the reverse process of (1-1), i.e. mutual charge neutralisation:

$$M^+ + X^- \rightarrow M + X \qquad (1\text{-}8)$$

So far, molecular beam experiments, using the difficult technique

of merging beams, have, among alkali systems, only been used to investigate $M^+ + O^-$ collisions (Moseley et al, 1970; Weiner et al, 1971).

More complicated, but much more extensively studied, is the collision of an alkali metal atom with a halogen molecule. This has three principal types of non-elastic outgoing channel (ignoring electronic excitation of the M or X_2):

$$M + X_2 \longrightarrow \begin{cases} M + X_2^+ & \text{(i)} \\ M^+ + X_2^- & \text{(ii)} \\ MX + X & \text{(iii)} \end{cases} \qquad (1\text{-}9)$$

The first of these to be studied experimentally was the reactive channel (iii). Reviews have been given by Herschbach (1966), Kinsey (1972), Levine (1972), Toennies (1974), and Grice (1975). Alkali / halogen reactions have been very popular for molecular beam experiments (see e.g. Grosser & Bernstein, 1965; Birely & Herschbach, 1966; Birely et al, 1967; Gillen et al, 1971; Lin, Mascord & Grice, 1974; Van der Meulen et al, 1975; Sholeen et al, 1976). The observed characteristics of the scattering are typical of the behaviour called "stripping" (Wilson et al, 1964; Minturn, Datz & Becker, 1966): very large (~ 150 Å^2) total reactive cross sections at thermal collision energies; predominantly forward product scattering in the centre of mass frame; rapid fall-off, with angle, of elastically scattered M and no rainbow or glory effects; and appearance of the exothermicity of the reaction mainly in vibration of the MX. The accepted model for the reaction is as follows. The first step is an electron jump (Magee, 1940; see also Minturn, Datz & Becker, 1966; Davidovits & Maya, 1974), i.e. channel (ii). This occurs at a large distance, with high probability,

giving rise to the large cross section. The electron acts as a "harpoon" and the ions are rapidly drawn together by Coulomb attraction; in the subsequent reaction, the relative times for breakup of the X_2^- ion and approach of the M^+ are intermediate between those of the spectator stripping limit and the collision complex limit (Datz & Minturn, 1964; Minturn, Datz & Becker, 1966; Gover, 1975). The motion subsequent to the electron jump has been studied by classical trajectory calculations on assumed ionic potential energy surfaces of varying complexity (Godfrey & Karplus, 1968; Blais, 1968 & 1969; Kuntz, Nemeth & Polanyi, 1969; Gover, 1975; Evers & DeVries, 1976). The surfaces found are "attractive" or "early downhill", as the experimental results would suggest, and in agreement with less empirical surfaces (Nyeland & Ross, 1971; Balint-Kurti & Karplus, 1971 & 1973).

As the collision energy is increased above about 1 eV, the reactive cross section appears to drop off rapidly (Van der Meulen, Rulis & DeVries, 1975), but the total cross section for channel (ii) increases. It rises sharply after threshold to a maximum of tens of $Å^2$, then slowly decreases with increasing energy (Baede et al, 1969; Helbing & Rothe, 1969; Lacmann & Herschbach, 1970; Baede & Los, 1971; Auerbach et al, 1973; Hubers, Kleyn & Los, 1976). Similar cross sections are observed for other non-metal diatomics, e.g. O_2 (Moutinho, Baede & Los, 1971; Mochizuki & Lacmann, 1976), but are complicated by the fact that additional processes, e.g. dissociation, are more likely. Measurement of total cross sections has been followed by that of differential cross sections (Delvigne & Los, 1972; Young et al, 1974; Mochizuki & Lacmann, 1976; Aten, Lanting & Los, 1977; Evers, 1977; Aten, Evers, et al, 1977), and in both cases, observations and interpretations have been similar to

those for $M + X$.

Theoretical interest has been much concerned with vibrational energy distributions, of the X_2^- from (ii) and the X_2 from the inelastic channel (i). A start has recently been made on measuring such distributions (Kashihira et al, 1974; Groszer & Meyer, 1976; Mochizuki & Lacmann, 1976). When considering vibrations, three collisional energy regions can be distinguished (Hubers, Kleyn & Los, 1976):

(a) Threshold region: collision time $\gtrsim$ vibration time. The X_2^- formed is vibrationally excited, but it is subsequently quenched by the alkali ion;

(b) Post-threshold region: collision time $\sim$ vibration time. Effective quenching is no longer possible, but stretching of the X-X bond occurs. The crossing radius increases during the collision, which greatly increases the non-adiabatic transition probability on the outward crossing, giving considerable ion-pair formation;

(c) High-velocity region: collision time $\ll$ vibration time. Vibrational motion is frozen throughout the collision, the final distribution of X_2^- states being determined by the Franck-Condon principle.

There are several popular theoretical methods which enable vibrational energy distributions to be calculated, based on the classical path approximation, in which some of the motion is treated quantum mechanically, and the rest classically. Two methods are particularly appropriate to region (c) above, because X_2 bond stretching is not specifically allowed for; they treat only the relative motion as classical, and regard the vibrational levels of the diatomic as producing a network of curve crossings in one dimension. Appropriate at relatively low energies is the "diffusion"

model of Bauer, Fisher & Gilmore (1969). In this, adjacent crossings are assumed to be independent, being separated by more than the dynamic width. The system is allowed to diffuse through the network, branching as it reaches each crossing point. The branching at the crossing point r_{nm} between vibrational state n of the covalent channel and vibrational state m of the ionic channel is usually assumed to be governed by the Landau-Zener probability given in (1-2):

$$P_{nm} = \exp\left[\frac{-2\pi|H_{12}(r_{nm})|^2}{\hbar v\,|F_1(r_{nm}) - F_2(r_{nm})|}\right] \qquad (1\text{-}10)$$

where $H_{12}(r_{nm}) = H_{12}^{0}(r_{nm})\,\Omega_{nm}$

Here H_{12}^{0} is the electronic interaction integral, and Ω_{nm} is the Franck-Condon overlap integral. The increase of the crossing distance with the X-X separation ρ is included in that r_{nm} increases with the quantum number n, but no dependence of the potentials on ρ is included. Appropriate at relatively high collision energies is the Franck-Condon model (Kendall & Grice, 1972; Child, 1973). In this the dynamic width encompasses all the crossing points, and the system is described by a single electronic curve crossing, with final probabilities for the vibrational levels in the ionic channel after one traversal of the crossing region modulated by Franck-Condon factors $|\Omega_{nm}|^2$. Again, the Landau-Zener formula is often used, giving (assuming the system starts in the ground vibrational state of the covalent channel) an overall probability after one traversal of the crossing region:

$$P_{m\leftarrow 0} = P_{12}^{0}\,|\Omega_{0m}|^2 \qquad (1\text{-}11)$$

where $$P_{12}^{0} = 1 - \exp\left[\frac{-2\pi|H_{12}^{0}(r_c)|^2}{\hbar v\,|F_1(r_c) - F_2(r_c)|}\right]$$

where r_c is some nominal crossing radius. Both of these methods have been used fairly widely (see e.g. Fisher & Smith, 1971; Gislason & Sachs, 1975; Yuan & Micha, 1976, for low energy; Moutinho, Aten & Los, 1971, for high energy) and Child (1973) has given a validity criterion for the Franck-Condon approach.

Also popular is the surface hopping trajectory (SHT) method of Tully & Preston (1971), which is appropriate to all velocity regions in which the classical trajectory approximation is valid, although in practice it becomes very difficult to implement at low velocities. In this, only the electronic motion is treated quantally, the remainder classically. This is done by a full classical trajectory calculation in which all appropriate potential energy surfaces are considered. When a trajectory reaches a seam (intersection) between two diabatic surfaces, it is split into two branches, usually using the LZS formula. This method has been fairly widely used (see e.g. Düren, 1973; Aten et al, 1976; Evers, 1977), and it has been successful in calculating total and differential cross sections. It offers ready interpretation of the three peaks in the differential cross section (Evers, 1977): a covalent peak, due to trajectories which undergo a non-adiabatic transition during the ingoing part, and hence are scattered mainly under the influence of the covalent potential, at low $E\theta$; an ionic rainbow, due to trajectories which follow the lower, predominantly ionic, adiabatic surface on the way in, reaching the potential well, and hop on the way out, at high $E\theta$; and a broad peak, due to ionic trajectories which do not reach the adiabatic well, at intermediate $E\theta$. As the collision energy is increased, the ingoing crossing becomes more diabatic, and the covalent peak becomes stronger; the effect of A-X bond stretching decreases, and the outgoing crossing becomes more diabatic owing to increased

$H_{12}(r_c)$, so that the ionic peak becomes weaker. While the TSH method provides much physical insight of this kind, it has the disadvantage that it uses large amounts of computer time.

The present thesis is divided into three parts. In chapter III, the vibrational energy distribution from collisions of the type $M + X_2 \rightarrow M^+ + X_2^-$ is considered. The sequential Landau-Zener method of Bauer, Fisher & Gilmore (which we shall call the BFG method) and the Franck-Condon method are used extensively, yet their validity criteria would suggest that their use is limited. An "exact" formulation, within the framework of these two methods, but applicable at all energies, has been developed. It is used to test the effectiveness of the two approximations for a model system over a wide energy range.

In chapter IV, work on reactive collisions $M + X_2 \rightarrow MX + X$ is reported. The physical picture of the process is that after the electron jump the X-X bond is weakened by the electric field of the approaching M^+ ion, becoming weaker the closer it approaches. In an earlier work (Gover, 1975), this effect was modelled by a simple and transparent device in a crude potential energy surface, and it was discovered that the scattering is very sensitive to the one parameter used. Here an improvement to the dynamical part of the model, with no change in the simple surface, is described, and further comparison with experimental results is made.

In chapter V, calculations on the charge neutralisation collision $Na^+ + I^- \rightarrow Na + I$ are reported. It has been suggested (Gait & Berry, 1977) that because of the asymptotic near coincidence of the curves for $Na^+ + I^-$ and $Na(^2P\ 3p) + I(^2P_{\frac{3}{2}})$, it may be possible in such a collision to produce a population inversion of Na(3p) with respect to Na(3s). Calculations exploring

this, using the classical path approximation, are reported. Very little information is available on the variation of the interaction integrals with internuclear distance; calculations of these are also reported.

Non-adiabatic molecular collision theory, on which all of this relies, is outlined in chapter II (see also Child, 1974; Baede, 1975; Janev, 1976; Tully, 1976).

The units used for most of the calculations were those suggested by LaBudde (1973), which have the virtue of giving reasonably sized numbers for atomic systems while being less remote from SI units than are atomic units:

Mass: 1 ppg = 10^{-27} kg = 0.602 amu;

Length: 1 Å = 10^{-10} m;

Time: 1 dps = 10^{-13} s;

hence Energy: 1 cpe = 10^{-21} J

= 1.4393×10^{-1} kcal mol^{-1}

= 6.2415×10^{-3} eV.

Occasionally, atomic units were used; these are defined thus:

Mass: m_e = mass of electron = 9.109×10^{-4} ppg;

Length: a_0 = Bohr radius = 0.5292 Å;

Action: $\hbar = h/2\pi$ = 1.055 cpe dps;

Charge: e = charge of proton;

Hence:

Energy: Hartree = $e^2/4\pi\varepsilon_0 a_0$ = 4.358×10^3 cpe;

Time: $4\pi\varepsilon_0 a_0 / e^2$ = 2.42×10^{-4} dps.

CHAPTER II

NON-ADIABATIC MOLECULAR COLLISION THEORY

A Adiabatic states and the Born-Oppenheimer approximation.

Consider an inelastic collision between two species, with $\vec{r}$ representing the relative positions of the collision partners, and $\vec{\rho}$ representing internal (rotational, vibrational, electronic) degrees of freedom.

We can write the Hamiltonian for the system in the following form:

$$H^T(\vec{r},\vec{\rho}) = H_{int}(\vec{\rho}) - \frac{\hbar^2}{2m}\nabla_r^2 + V(\vec{r},\vec{\rho}) \qquad (2\text{-}1)$$

where H^T is the total Hamiltonian, H_{int} the internal Hamiltonian, unperturbed by the proximity of the collision partners, $-\frac{\hbar^2}{2m}\nabla_r^2$ the kinetic energy of relative translation, m being the appropriate reduced mass, and V is that part of the potential energy which involves an interaction between the partners; since there is no interaction when they are completely separated,

$$\lim_{r\to\infty} V(\vec{r},\vec{\rho}) = 0 \qquad (2\text{-}2)$$

The problem is to solve the Schrödinger equation for the wavefunction Φ of the system:

$$H^T(\vec{r},\vec{\rho})\,\Phi(\vec{r},\vec{\rho}) = E\,\Phi(\vec{r},\vec{\rho}) \qquad (2\text{-}3).$$

As usual, Φ is expanded in terms of a complete, orthonormal,

basis set, which consists of some set of internal eigenstates of the system. Writing the eigenstates $\{\psi_j(\vec{r},\vec{\rho})\}$ or $\{|j\rangle\}$, then putting the expansion

$$\Phi(\vec{r},\vec{\rho}) = \sum_n c_n(\vec{r})\,\psi_n(\vec{r},\vec{\rho}) \quad , \tag{2-4}$$

which is expected to be different at each value of $\vec{r}$, in (2-1),

$$\left[-\frac{\hbar^2}{2m}\nabla_r^2 + H_{ii} + \Lambda_{ii} - E\right]c_i(\vec{r}) = -\sum_{j\neq i}(H_{ij} + \Lambda_{ij})c_j(\vec{r}) \tag{2-5}$$

where $$H_{ij} = \langle i|H|j\rangle \quad ;$$

$$H(\vec{r},\vec{\rho}) = H_{int}(\vec{\rho}) + V(\vec{r},\vec{\rho}) \quad ;$$

and $$\Lambda_{ij} = \left\langle i\left|-\frac{\hbar^2}{2m}\nabla_r^2\right|j\right\rangle - \frac{\hbar^2}{m}\langle i|\vec{\nabla}_r|j\rangle\cdot\vec{\nabla}_r \tag{2-6}$$

The basis $\{|j\rangle\}$ can be chosen in various ways, according to the amount of V which is considered internal (Child, 1974). At one limit is the method which is most familiar and intuitively useful for reaction dynamics, the adiabatic (or kinetic) coupling scheme. This uses the eigenstates $\chi_j(\vec{r};\vec{\rho})$ of the full internal Hamiltonian $H(\vec{r},\vec{\rho}) = H_{int}(\vec{\rho}) + V(\vec{r},\vec{\rho})$:

$$\left[H_{int}(\vec{\rho}) + V(\vec{r},\vec{\rho})\right]\chi_j(\vec{r};\vec{\rho}) = W_j(\vec{r})\,\chi_j(\vec{r};\vec{\rho}) \tag{2-7}$$

This equation can be solved for any chosen value of $\vec{r}$, which is why the parameter $\vec{r}$ and argument $\vec{\rho}$ are separated by a semi-colon. If the expansion is written

$$\Phi(\vec{r},\vec{\rho}) = \sum_j \tilde{\psi}_j(\vec{r})\,\chi_j(\vec{r};\vec{\rho}) \quad , \tag{2-8}$$

then, as usual, we have a set of coupled equations for the coefficients $\tilde{\psi}_j(\vec{r})$:

$$\left[\frac{\hbar}{2m}^2\nabla_r^2 + E - W_i(\vec{r})\right]\tilde{\Psi}_i(\vec{r}) = -\sum_j\left[\vec{X}_{ij}(\vec{r})\cdot\vec{\nabla}_r + Y_{ij}(\vec{r})\right]\tilde{\Psi}_j(\vec{r}) \tag{2-9}$$

where the coupling terms are

$$\vec{X}_{ij}(\vec{r}) = 2\left\langle \chi_i\left|\frac{\hbar}{2m}^2\vec{\nabla}_r\right|\chi_j\right\rangle \;;\; Y_{ij}(\vec{r}) = \left\langle \chi_i\left|\frac{\hbar}{2m}^2\nabla_r^2\right|\chi_j\right\rangle \tag{2-10}$$

corresponding to the second and first terms respectively of Λ_{ij} given in (2-6).

Consider the Born-Oppenheimer (BO) approximation. As usually stated, this says that electronic and nuclear motion can be separated because of the large mass difference, with a corresponding difference in velocity, between electrons and nuclei. It can be extended to cover the difference in velocity between motion in $\vec{r}$ - type degrees of freedom and that in $\vec{\rho}$ - type degrees of freedom, in thermal energy collisions. The relative motion is assumed to be slow, so that terms in $\frac{\hbar}{2m}^2\vec{\nabla}_r$, i.e. $\vec{X}_{ij}$ and Y_{ij}, are negligable. Then the so-called adiabatic (nuclear) states $\tilde{\Psi}_i(\vec{r})$ are decoupled, and the wavefunction is a simple product:

$$\Phi_{mv}(\vec{r},\vec{\rho}) = \chi_m(\vec{r};\vec{\rho})\tilde{\Psi}_{mv}(\vec{r}) \tag{2-11}$$

The system stays in one adiabatic state, and transitions to another, as a result of nuclear motion, are not expected. In this product, χ_m is obtained, at a given value of $\vec{r}$, by solving the Schrödinger equation (2-7) in which nuclear motion is "clamped", and $\tilde{\Psi}_{mv}$ is given by:

$$\left[-\frac{\hbar}{2m}^2\nabla_r^2 + W_m(\vec{r})\right]\tilde{\Psi}_{mv}(\vec{r}) = E_{mv}\tilde{\Psi}_{mv}(\vec{r}) \tag{2-12}$$

$W_m(\vec{r})$ has the effect of a potential energy term, and, as a function of $\vec{r}$, it defines a potential energy surface (PES) on which the relative motion takes place. Solving this motion, often using classical mechanics, is the basis for trajectory studies of reactions using a PES, e.g. those in chapter IV.

When X and Y have appreciable values, the BO approximation will be expected to break down, and transitions will occur between adiabatic states, so that trajectories cease to follow a unique PES. It can be shown (Child, 1974) that X is usually the dominant term, and has non-zero off-diagonal elements given by:

$$\vec{X}_{ij} \ (i \neq j) = - \frac{\hbar^2}{m} \frac{\langle \chi_i | \vec{\nabla}_r V | \chi_j \rangle}{W_i(\vec{r}) - W_j(\vec{r})} \quad . \qquad (2\text{-}13)$$

Similar expressions can be derived for the Y_{ij}'s:

$$Y_{ii} = - \frac{\hbar^2}{2m} \sum_{k \neq i} \frac{\langle \chi_i | \vec{\nabla}_r V | \chi_k \rangle \cdot \langle \chi_k | \vec{\nabla}_r V | \chi_i \rangle}{(W_i - W_k)^2} \quad ;$$

$$Y_{ij} \ (i \neq j) = \frac{\hbar}{2m}^2 \left\{ 2 \sum_{k \neq i,j} \frac{\langle \chi_i | \vec{\nabla}_r V | \chi_k \rangle \cdot \langle \chi_k | \vec{\nabla}_r V | \chi_j \rangle}{(W_i - W_k)(W_k - W_j)} \right.$$

$$\left. + 2 \ (\vec{\nabla}_r W_i - \vec{\nabla}_r W_j) \cdot \frac{\langle \chi_i | \vec{\nabla}_r V | \chi_j \rangle}{(W_i - W_j)^2} - \frac{\langle \chi_i | \nabla_r^2 V | \chi_j \rangle}{W_i - W_j} \right\}$$

Since $\vec{X}$ is multiplied by $\vec{\nabla}_r$ in the coupling element, we see that breakdown of the BO approximation is expected when:

(i) The relative momentum ($\sim \vec{\nabla}_r$) is large; this is expected from the qualitative description of the BO approximation, and can arise in molecular collisions;

(ii) $W_i(\vec{r}) - W_j(\vec{r})$ is small or $\vec{\nabla}_r V$ is large; there are two important situations in which this is found. Firstly, $W_i(\vec{r}) - W_j(\vec{r})$

small occurs at crossings or weakly avoided crossings (pseudocrossings) of two adiabatic levels i and j. Avoided crossings are more common, and a typical example in one dimension is shown in fig. 2.

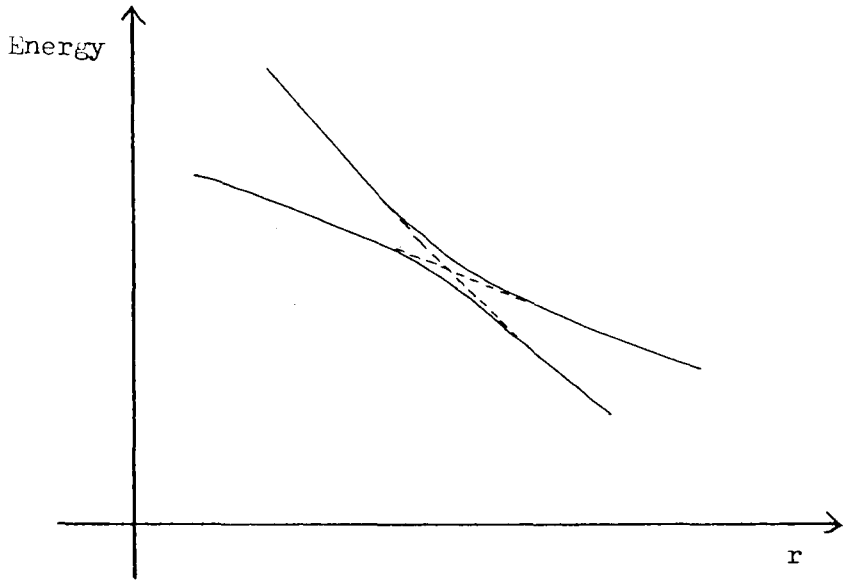

Fig. 2

In such a situation, $W_i(\vec{r}) - W_j(\vec{r})$ is small over a localised region. This type of breakdown is found in alkali / halogen systems of the type under consideration, and can often be well described by the LZS theory. Secondly, $W_i(\vec{r}) - W_j(\vec{r})$ can be small over a large asymptotic region; this occurs in the perturbed symmetric resonance or Demkov coupling case (Demkov, 1964; Olson, 1972), and the dominant region of breakdown is when $\vec{\nabla}_r V$ is large and $W_i(\vec{r}) - W_j(\vec{r})$ is still small. this effect is found in alkali-ion / alkali-atom charge exchange collisions.

From the expression for ∇_r^2 in polar coordinates:

$$\nabla_r^2 = \frac{1}{r^2}\frac{\partial}{\partial r}\left(r^2\frac{\partial}{\partial r}\right) + \frac{1}{r^2\sin\theta}\left\{\frac{\partial}{\partial\theta}\left(\sin\theta\,\frac{\partial}{\partial\theta}\right) + \frac{1}{\sin\theta}\,\frac{\partial^2}{\partial\phi^2}\right\}$$

it can be seen that $\vec{X}$ and Y contain radial and angular terms; both

of these may be important, giving rise to radial and rotational (or angular, or Coriolis) coupling. The radial contributions are generally the most important, and rotational coupling can be ignored (Thorson, 1969), except in certain high energy short range processes when the angular velocity may become high (Thorson, 1963).

B Diabatic states.

Transitions between adiabatic states arising from breakdown of the BO approximation over a localised region are called non-adiabatic transitions. When they occur, it is often preferable to use the simpler basis which gives rise to the "diabatic" (or potential) coupling scheme. This basis is the eigenstates of a Hamiltonian consisting of the internal Hamiltonian $H(\vec{r},\vec{\rho})$ (eqn. (2-6)) with some part of V excluded. Although the adiabatic representation is quite well characterised, a firm mathematical basis for the diabatic representation has been lacking. Physical intuition suggests something giving rise to the dashed curves shown in fig. 2, which run smoothly through the crossing region (Lichten, 1963). Smith (1969) suggested the following classification: the adiabatic states are diagonal in the full internal Hamiltonian H, and coupled by the nuclear kinematic operator Λ (eqn. (2-6)) (hence the alternative title "kinetic"); the diabatic states are then defined as being diagonal in the radial or angular part of Λ and coupled by H and the remainder of Λ. Lichten's choice corresponds to taking the diabatic states as diagonal in the whole of Λ, and coupled by H (hence giving a "potential" coupling scheme), and we shall use this definition here. This is equivalent to excluding all of V from H, so that the diabatic basis is defined thus:

$$H_{int}(\vec{\rho})\,\phi_j(\vec{\rho}) = E_j\,\phi_j(\vec{\rho}) \qquad (2\text{-}14)$$

With this definition, the diabatic states can be seen to be zero-order approximations of the adiabatic ones, and the two representations occupy opposite limits, in that in the adiabatic case none of V is excluded from the defining Hamiltonian whereas in the diabatic case all of it is excluded.

Writing the expansion

$$\Phi(\vec{r},\vec{\rho}) = \sum_j \Psi_j(\vec{r})\,\varphi_j(\vec{\rho}) \qquad (2\text{-}15)$$

then the diabatic nuclear states are the solutions of the coupled equations

$$\left[\frac{\hbar^2}{2m}\nabla_r^2 + E - E_i\right]\Psi_i(\vec{r}) = \sum_j V_{ij}(\vec{r})\,\Psi_j(\vec{r}) \qquad (2\text{-}16)$$

$$\text{where} \qquad V_{ij}(\vec{r}) = \int \varphi_i^*(\vec{\rho})\,V(\vec{r},\vec{\rho})\,\phi_j(\vec{\rho})\,d\vec{\rho} \qquad (2\text{-}17)$$

It can be seen that the diabatic states become decoupled, i.e. a good description of the possible states of the system, in the limit of high collision energy, when V_{ij} becomes negligable compared with $\frac{\hbar^2}{2m}\nabla_r^2$.

The nuclear states are then given by:

$$\left[-\frac{\hbar^2}{2m}\nabla_r^2 + H_{ii}(\vec{r})\right]\Psi_i(\vec{r}) = E\,\Psi_i(\vec{r}) \qquad (2\text{-}18)$$

Note that, from (2-2),

$$\varphi_j(\vec{\rho}) = \lim_{r\to\infty} \chi_j(\vec{r};\vec{\rho}) \quad ;$$

$$E_j = \lim_{r\to\infty} W_j(\vec{r}) = \lim_{r\to\infty} H_{ii}(\vec{r}) \qquad (2\text{-}19)$$

The diabatic and adiabatic nuclear potential energy curves,

in the limits in which they become decoupled (which we shall call the diabatic and adiabatic limits respectively), for the ground covalent and ionic states of an alkali halide molecule MX are sketched in fig. 3.

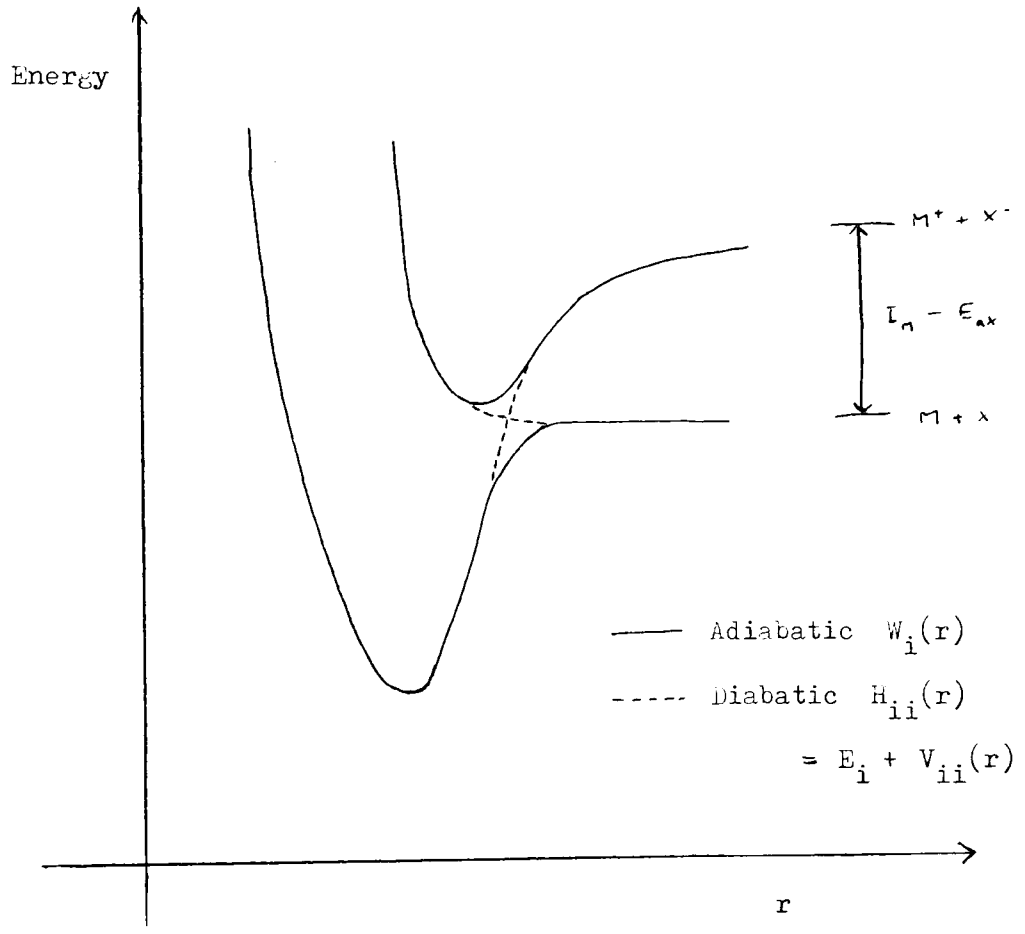

Fig. 3

C Classical path approximation.

The set of coupled differential equations for the nuclear wavefunctions can be more easily solved by making use of a semiclassical approach, the classical path (or trajectory) approximation, in which we assume a classical path $\vec{r}(t)$ for

the relative motion, and replace the coefficients $\Psi_i(\vec{r})$ in the diabatic coupling scheme by time-dependent coefficients $c_i(t)$ (see e.g. Delos, Thorson & Knudson, 1972; Bates & Crothers, 1970). The approach, first suggested by Mott (1931), is very much a hybrid, in which the relative motion of the collision partners is treated classically, while the internal motion is treated quantum mechanically (Child, 1974). The classical path may be calculated by integration of the motion over some PES, which may not be easy to find if non-adiabatic transitions are occurring. As a further approximation, however, it is often assumed that the trajectory is a straight line with a constant speed. This is called the impact parameter method, and if the speed is v and the impact parameter b, then the magnitude of r is clearly given by $r(t) = \sqrt{b^2 + v^2t^2}$, with the zero of time at the point of closest approach.

Consider an expansion

$$\Phi(\vec{r},\vec{\rho},t) = \sum_j \phi_j(\vec{r},\vec{\rho})\,\Psi_j(\vec{r},t) \qquad (2\text{-}20)$$

and substitute it in the time-dependent Schrödinger equation

$$H^T \Phi = i\hbar \frac{\partial}{\partial t} \Phi \qquad (2\text{-}21)$$

After multiplying both sides by $\phi_i^*(\vec{r},\vec{\rho})$ and integrating over $\vec{\rho}$ we get the coupled equations:

$$\sum_j H^T_{ij}\,\Psi_j(\vec{r},t) = i\hbar \frac{\partial}{\partial t} \Psi_i(\vec{r},t) \qquad (2\text{-}22)$$

Delos et al (1972) showed that if the diabatic basis is used in (2-20), and H is the internal Hamiltonian (eqn. (2-6)), then (2-22) can be reduced to

$$\sum_j H_{ij} c_j(t) = i\hbar \frac{d}{dt} c_i(t) \qquad (2\text{-}23)$$

where $$\Phi(\vec{r}(t),\vec{\rho}) = \sum_j c_j(t)\,\varphi_j(\vec{\rho}) \qquad (2\text{-}24)$$

Their first derivation of this involved a classical wavepacket description of the collision, and assumed that the packet could, in principle, actually be observed moving along the classical trajectory. A subsequent derivation, based on an extension of the semiclassical WKB approximation, showed, however, that the equations are more generally valid than this. The classical wavepacket validity criterion is $(\lambda\!\!\!^{-}/a_0)^{\frac{1}{2}} \ll 1$, where $\lambda\!\!\!^{-}$ is the De Broglie wavelength $\hbar/p$ and a_0 is a nominal interaction region. The criteria for the semiclassical derivation are (a): $(\lambda\!\!\!^{-}/a_0) \ll 1$; (b): $|H_{ii}(\vec{r}) - H_{jj}(\vec{r})| \ll$ kinetic energy in regions where coupling due to $H_{ij}(\vec{r})$ is important; (c): coupling must be negligable near classical turning-points. Under the more stringent classical conditions, the coefficients $c_i(t)$ have meaning as probability amplitudes at all times, but under semiclassical conditions, they only have such meaning at $t = \pm\infty$. The criterion (c) was shown not to be necessary in a third derivation (Delos & Thorson, 1972a) which involved a momentum space formulation.

The equations (2-23) can be derived in the following simple way, which makes no attempt to justify the classical trajectory, analogous to the method of "variation of constants" in time-dependent perturbation theory:

Assume that the less tightly bound relative motion can be treated classically, then write a wavefunction for the remaining quantum motion

$$\Phi(\vec{\rho},t) = \sum_j c_j(t)\,\varphi_j(\vec{\rho}) \qquad (2\text{-}25)$$

and substitute this in the time-dependent Schrodinger equation

$$H(\vec{\rho},t)\,\Phi(\vec{\rho},t) = i\hbar\frac{\partial}{\partial t}\Phi(\vec{\rho},t) \qquad (2\text{-}26)$$

where $H(\vec{\rho},t) = H_{int}(\vec{\rho}) + V(\vec{\rho},t)$

i.e. the relative motion is not included in the Hamiltonian, but merely provides a relationship between $\vec{r}$ and t. Then multiply by $\varphi_i^*(\vec{\rho})$, integrate over $\vec{\rho}$, and use the orthonormality of the basis $\{\varphi_i(\vec{\rho})\}$ to obtain (2-23) directly.

Note that using the classical path approximation has enabled a set of coupled second order differential equations to be replaced by a set of first order equations, without doubling the size of the set, thus decreasing the effort involved in solving them.

D Two-state curve-crossing approximation.

Usually, we know that there are more than two adiabatic states for a given system, but it is often a useful approximation to consider only two of these (Baede, 1975), since the regions of non-adiabatic coupling are localised, and often only two states are appreciably involved in any one such region. If in addition $\vec{r}$ has only one dimension, as in a collision between two atoms, then the situation, the two-state curve-crossing problem, is one which has been well studied. A typical pseudocrossing in this approximation is shown in fig. 4.

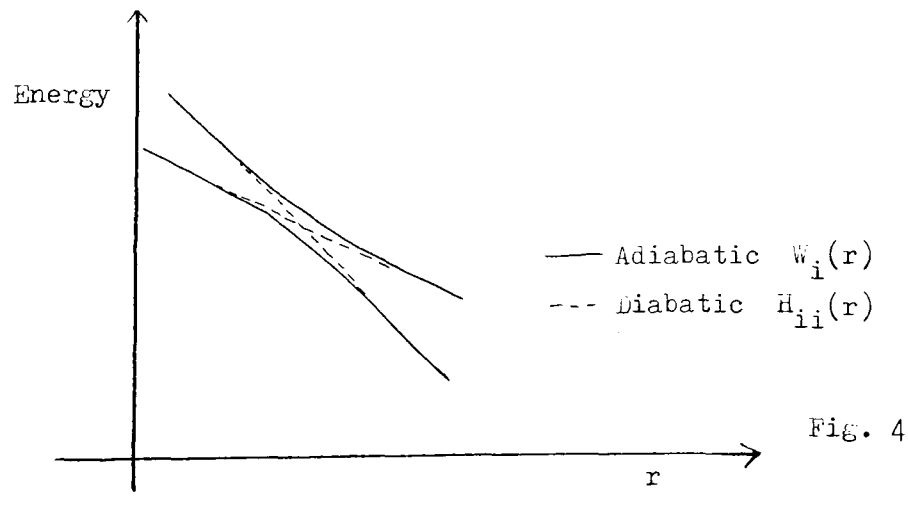

Fig. 4

The adiabatic curves are shown as having an avoided crossing in accordance with the theorem (Landau & Lifshitz, 1958) which asserts that adiabatic states of the same symmetry cannot cross. For the two-state curve-crossing problem the relations between diabatic and adiabatic states can be readily explored and some aspects of this are outlined below.

(i) Relation between the potential energy curves in the diabatic and adiabatic representations.

The adiabatic eigenstates $\{\chi_i\}$, whose eigenvalues are the $W_i(r)$, can be calculated from the diabatic eigenstates $\{\phi_i\}$ by diagonalisation of the full internal Hamiltonian matrix, in the diabatic representation, $\mathbb{H}$. Thus the W_i's are given by the eigenvalues $E^{\pm}$ of this matrix:

$$\begin{vmatrix} H_{11} - E & H_{12} - ES \\ H_{12} - ES & H_{22} - E \end{vmatrix} = 0$$

where $S = \langle \phi_1 | \phi_2 \rangle$

$$\Rightarrow E^{\pm} = \frac{H_{11} + H_{22} - 2H_{12}S \pm \sqrt{(H_{11}-H_{22})^2 + 4\{H_{11}H_{22}S^2 + H_{12}^2 - H_{12}S(H_{11}+H_{22})\}}}{2(1-S^2)}$$

$$\Rightarrow \Delta E = E^{+} - E^{-} = \frac{1}{(1-S^2)}\sqrt{(H_{11}-H_{22})^2 + 4\{H_{11}H_{22}S^2 + H_{12}^2 - H_{12}S(H_{11}+H_{22})}$$

(2-27)

At the crossing point r_c of the two diabatic curves, given by $H_{11}(r_c) = H_{22}(r_c)$, this is usually denoted $\Delta V(r_c)$:

$$\Delta V(r_c) = \left| \frac{2(H_{11}S - H_{12})}{1 - S^2} \right|_{r=r_c} \qquad (2\text{-}28)$$

If exact diabatic states have been used, then $S = 0$, and

$$E^{\pm} = \tfrac{1}{2}(H_{11} + H_{22}) \pm \tfrac{1}{2}\sqrt{(H_{11} - H_{22})^2 \quad 4H_{12}^2}$$

$$= \tfrac{1}{2}(H_{11} + H_{22}) \pm \tfrac{1}{2}(H_{11} - H_{22}) \sqrt{1 + 4\left(\frac{H_{12}}{H_{11} - H_{22}}\right)^2} \qquad (2\text{-}29)$$

Far from the crossing point r_c, $(H_{11} - H_{22})$ is large, and (2-29) can be expanded to give

$$E^{\pm} \doteq \tfrac{1}{2}(H_{11} + H_{22}) \pm \tfrac{1}{2}(H_{11} - H_{22})$$

$$= H_{11} \quad \text{or} \quad H_{22}$$

i.e. as expected the adiabatic states approach the diabatic ones.

Eqn. (2-27) becomes:

$$\Delta E = E^{+} - E^{-} = \sqrt{(H_{11} - H_{22})^2 + 4H_{12}^2}$$

and (2-28) becomes

$$\Delta V(r_c) = 2\,|H_{12}(r_c)| \qquad (2\text{-}30)$$

Further discussion of this much-used relation can be found in chapter V.

Note that if the adiabatic states are to cross at some point r_x, then

$$\left(H_{11}(r_x) - H_{22}(r_x)\right)^2 + 4\left(H_{12}(r_x)\right)^2 = 0$$

If ΔE is zero, it is at a minimum, since $\Delta E \geq 0$ always, in accordance with the well-known principle that the eigenvalues of a diagonal matrix move apart when Hermitian off-diagonal terms are

introduced. Also, both $(H_{11} - H_{22})^2$ and $H_{12}^2 \geq 0$, so the adiabatic curves only "cross" (i.e. meet) when $\Delta E = (H_{11} - H_{22})^2 = H_{12}^2 = 0$, and this will only occur at a particular r if H_{12} is zero for all r, i.e. the diabatic states are of different symmetry. This is the basis of the non-crossing rule (Landau & Lifshitz, 1958) in one dimension.

(ii) Relation between the diabatic and adiabatic wavefunctions.

It can be shown that the adiabatic and diabatic eigenstates are related by the orthogonal transformation:

$$\chi^+ = \varphi_1 \cos\theta(r) - \varphi_2 \sin\theta(r) \quad ;$$

$$\chi^- = \varphi_1 \sin\theta(r) + \varphi_2 \cos\theta(r) \qquad (2\text{-}31)$$

where $$\tan\theta(r) = -\frac{2H_{12}(r)}{H_{11}(r) - H_{22}(r)} \qquad (2\text{-}32)$$

Hence at $r = r_c$, $\chi^{\pm} = \frac{1}{\sqrt{2}}(\varphi_1 \pm \varphi_2)$;

and at $r = \pm\infty$, $\chi^{\pm} = \varphi_1$ or φ_2

and it is readily verified that $\langle \chi^+ | H | \chi^- \rangle = 0$.

(iii) The coupling in the diabatic and adiabatic representations.

We see from (ii) above that the adiabatic states differ appreciably from the diabatic ones at the diabatic crossing r_c, but approach them as we move away from r_c. Since non-adiabatic effects are expected only when the diabatic and adiabatic states differ appreciably, we see that they are localised to the all-important "crossing region" around r_c in which $H_{12}/(H_{11} - H_{22})$ is non-negligable. This accounts for the success of the two-state approximation, since if a third adiabatic state is present, its

localised region of interaction probably doesn't intersect with the one under consideration. As described in section B, the diabatic states are coupled by H_{12}; this is usually a smoothly varying function of r through the crossing region, which is fairly easy to deal with numerically. Most of the coupling between adiabatic states is usually due to $\vec{X}_{12}.\vec{\nabla}_r = \dfrac{\langle \chi^+ | \vec{\nabla}_r V | \chi^- \rangle}{E^+ - E^-}.\vec{\nabla}_r$ and this peaks fairly sharply around r_c, because $E^+ - E^-$ has a minimum there. This is less easy to deal with numerically, but demonstrates again the localisation of non-adiabaticity to the crossing region.

(iv) Coupled equations in the classical path approximation.

With just two states, eqn. (2-23) becomes:

$$i\hbar \frac{d}{dt} \begin{pmatrix} c_1(t) \\ c_2(t) \end{pmatrix} = \begin{pmatrix} H_{11}(t) & H_{12}(t) \\ H_{12}(t) & H_{22}(t) \end{pmatrix} \begin{pmatrix} c_1(t) \\ c_2(t) \end{pmatrix} \qquad (2\text{-}33)$$

where $\Phi(\vec{\rho},t) = c_1(t)\phi_1(\vec{\rho}) + c_2(t)\phi_2(\vec{\rho})$

We employ a common device to "remove" terms from the diagonal in (2-33) and display the equations in a somewhat clearer form: multiply the coefficients by phase factors as follows:

$$\text{Let} \quad c_1(t) = \gamma_1(t) \exp\left[-\frac{i}{\hbar} \int_0^t H_{11}(t')dt' \right] ;$$

$$c_2(t) = \gamma_1(t) \exp\left[-\frac{i}{\hbar} \int_0^t H_{22}(t')dt' \right] \qquad (2\text{-}34)$$

Then

$$i\hbar \frac{dc_1}{dt} = \exp\left[-\frac{i}{\hbar} \int_0^t H_{11}dt \right] i\hbar \frac{d\gamma_1}{dt} + \gamma_1 H_{11} \exp\left[-\frac{i}{\hbar} \int_0^t H_{11}dt \right]$$

Hence the first equation of (2-33) becomes

$$i\hbar \frac{d\gamma_1}{dt} \exp\left[-\frac{i}{\hbar}\int_0^t H_{11}dt \right] + \gamma_1 H_{11} \exp\left[-\frac{i}{\hbar}\int_0^t H_{11}dt \right]$$

$$= \gamma_1 H_{11} \exp\left[-\frac{i}{\hbar}\int_0^t H_{11}dt \right] + H_{12}\gamma_2 \exp\left[-\frac{i}{\hbar}\int_0^t H_{22}dt \right]$$

The terms in γ_1 now cancel, to give

$$i\hbar \frac{d}{dt}\gamma_1 = H_{12} \exp\left[\frac{i}{\hbar}\int_0^t (H_{11} - H_{22})dt \right] \gamma_2 \qquad (2\text{-}35)$$

Similarly, the second equation in (2-33) gives

$$i\hbar \frac{d}{dt}\gamma_2 = H_{12} \exp\left[-\frac{i}{\hbar}\int_0^t (H_{11} - H_{22})dt \right] \gamma_1 \qquad (2\text{-}36)$$

Equations (2-35) & (2-36), in the diabatic representation, can be transformed to the adiabatic representation using (2-31):

$$\text{Let } \Phi(\vec{\rho},t) = c_+(t)\chi^+(\vec{\rho},t) + c_-(t)\chi^-(\vec{\rho},t)$$

and apply a transformation similar to that of (2-34):

$$c_\pm(t) = \gamma_\pm(t) \exp\left[-\frac{i}{\hbar}\int_0^t E^\pm(t')dt' \right]$$

Then (Delos & Thorson, 1972a),

$$i\hbar \frac{d}{dt}\gamma_+ = -\frac{d\theta}{dt} \exp\left[\frac{i}{\hbar}\int_0^t (E^+ - E^-)dt \right] \gamma_- \qquad (2\text{-}37)$$

$$i\hbar \frac{d}{dt}\gamma_- = \frac{d\theta}{dt} \exp\left[-\frac{i}{\hbar}\int_0^t (E^+ - E^-)dt \right] \gamma_+ \qquad (2\text{-}38)$$

A disadvantage of using the adiabatic representation in the classical path approximation is now apparent; $E^+ - E^-$ is always greater

than $H_{11} - H_{22}$, so that the equations in the adiabatic representation oscillate more rapidly.

(v) Non-adiabatic transition probability.

On traversing the crossing region, the system follows one of the adiabatic curves in the limit of low velocity, and one of the diabatic curves in the limit of high velocity. At intermediate velocities, the coupled equations must be solved. It is usual to approximate the diabatic curves by straight lines in the crossing region, and using this approximation, together with those of constant $H_{12}(r)$ and constant velocity, the non-adiabatic transition probability was worked out in 1932. Landau and Zener each used the classical path method, described here, and Stückelberg used a phase integral method (see also Crothers, 1971).

With the assumptions

$$\text{(i)} \qquad H_{ii}(r) = E_c - F_i(r - r_c) \qquad (i = 1,2)$$

where E_c is the energy at the crossing;

$$\text{(ii)} \qquad H_{12}(r) = H_{12} \quad \text{(constant)};$$

$$\text{(iii)} \qquad \frac{dr}{dt} = v = \text{constant}$$

and the definition

$$x = r - r_c = v(t - t_c),$$

then eqns. (2-35) & (2-36) are readily transformed back to time-independent equations (the time dependence being in v):

$$\frac{d\gamma_1}{dx} = -i\beta \exp(-i\alpha x^2/2)\gamma_2 \qquad (2\text{-}39)$$

$$\frac{d\gamma_2}{dx} = -i\beta \exp(i\alpha x^2/2)\,\gamma_1 \qquad (2\text{-}40)$$

where $\alpha = \dfrac{F_1 - F_2}{\hbar v}$; $\beta = \dfrac{H_{12}}{\hbar v}$

Eliminating $\gamma_2(x)$ and putting

$$a_1(x) = \gamma_1(x)\exp(\tfrac{1}{4}\alpha x^2)$$

gives the second order equation

$$\left[\frac{d^2}{dx^2} + \beta^2 - \frac{i\alpha}{2} + \frac{\alpha^2 x^2}{4}\right] a_1(x) = 0$$

i.e. the curve-crossing problem is formally equivalent to that of motion through a quadratic potential barrier $-\frac{1}{4}\alpha^2 x^2$ with complex energy $\left(\beta^2 - \dfrac{i\alpha}{2}\right)$ (Child, 1972).

By substituting

$$z = \sqrt{\alpha}\, e^{i\pi/4} x \quad ; \qquad \nu = \frac{\beta^2}{\alpha} = \frac{H_{12}^2}{\hbar v(F_1 - F_2)}$$

we get the standard form of Weber's equation:

$$\frac{d^2 a_1}{dz^2} + (n + \tfrac{1}{2} - \tfrac{1}{4}z^2)a_1 = 0 \qquad (2\text{-}41)$$

where $n = i\nu$

The solutions of this are given in terms of the parabolic cylinder functions $D_n(z)$ by

$$a_1 = A\,D_n(z) + B\,D_n(-z)$$

where the $D_n(z)$ have the following asymptotic forms as $|z| \to \infty$:

$$D_n(z) \sim z^n \exp(-\tfrac{1}{4}z^2) \qquad \text{for} \quad -\tfrac{3}{4}\pi < \arg z < \tfrac{3}{4}\pi$$

(includes real + ve x)

$$D_n(z) \sim z^n \exp(-\tfrac{1}{4}z^2) - \frac{\sqrt{2\pi}}{\Gamma(-n)} e^{i\pi n} z^{-(n+1)} \exp(+\tfrac{1}{4}z^2) \qquad \text{for} \quad \tfrac{1}{4}\pi < \arg z < \tfrac{5}{4}\pi$$

(includes real -ve x)

Using these asymptotic forms, with the boundary condition $c_1(-\infty) = 1$; $c_2(-\infty) = 0$,

$$|c_2(\infty)|^2 = 1 - e^{-2\pi\nu}$$

and the probability of remaining in diabatic state 1 on a single passage through the crossing region is

$$P = |c_1(\infty)|^2 = 1 - |c_2(\infty)|^2$$

$$= \exp(-2\gamma) \qquad (2\text{-}42)$$

where $$\gamma = \frac{\pi |H_{12}|^2}{\hbar v |F_1 - F_2|}$$

This is the famous Landau-Zener-Stuckelberg (LZS) formula. Note that in the limit of high velocity v, $P \to 1$, giving diabatic behaviour, while in the limit of low velocity, $P \to 0$, giving adiabatic behaviour, as expected.

It can further be shown that the probability of crossing from state 1 to state 2 or vice versa during a double passage of the crossing region is given by

$$P_{12} = 4P(1 - P)\cos^2(\tau + \tfrac{\pi}{4}) \qquad (2\text{-}43)$$

where $$\tau = \frac{1}{\hbar}\int_0^{t_c}\{E^+(t) - E^-(t)\}\,dt$$

and this is zero in both the diabatic and adiabatic limits, as expected. The average of P_{12} over τ is $2P(1 - P)$, which is the result expected from classical probability theory.

As described in section (iii) above, non-adiabatic effects occur over a localised region, and for the LZS model to be valid, its assumptions must be true over this region. Hence we need an estimate of the size of the region. The simplest method is to use the analogy with the barrier penetration problem (Child, 1972). Equating the width of the barrier to that of the transition region, the extremities of the region are given by:

$$\left|\frac{\alpha^2 x^2}{4}\right| = \left|\beta^2 - \frac{i\alpha}{2}\right|$$

$$x_\pm = \pm\frac{2}{\alpha}\left[\beta^4 + \frac{\alpha^2}{4}\right]^{\frac{1}{4}} \qquad (2\text{-}44)$$

The width is then given by

$$\Delta x = x_+ - x_- \qquad (2\text{-}45)$$

The condition $|x| < x_+$ is equivalent to requiring that the second term in Weber's equation (2-41) be non-negligable. At low v, β^4 will dominate the bracket in (2-44) and, using (2-45), the width is:

$$\Delta x_s = \frac{4\beta}{\alpha} = \frac{4H_{12}}{F_1 - F_2} \qquad (2\text{-}46)$$

This is called the static width.

At high v, $\alpha^2/4$ will dominate, and the width is

$$\Delta x_d = 2\sqrt{\frac{2}{\alpha}} = \sqrt{\frac{8\hbar v}{F_1 - F_2}} \qquad (2\text{-}47)$$

This is the velocity dependent dynamic width.

Physically the significance of these widths is: the static width is the range over which H_{12} is significant compared with the diabatic energy separation, i.e. the adiabatic curves differ significantly from the diabatic ones; the dynamic width can be shown (Child, 1974) to be the distance range which is consistent with the uncertainty principle with the classical momentum uncertainty between motion on the two diabatic curves. Alternatively (Child, 1973), it can be seen to correspond roughly to the range outside which rapid oscillations in (2-39) & (2-40) start to damp out the transition probability.

Note that x being outside the range given by (2-44) is sufficient for the validity criterion (Child, 1974) on an asymptotic form to be satisfied:

$$\left|\frac{d}{dr}\left(\frac{\hbar}{p(r)}\right)\right| \ll 1$$

$$\Rightarrow \quad \frac{2\alpha^{-1}x^{-2}}{\left\{1 + x^{-2}(4\beta^2/\alpha^2 - 2i/\alpha)\right\}^{3/2}} \ll 1$$

which is satisfied by $x^2 \gg \left|4\beta^2/\alpha^2 - 2i/\alpha\right| > 2/\alpha$, because then the numerator is $\ll 1$ and the denominator ~ 1.

Thus the width of the transition zone over which the assumptions of the model must apply is seen to be the larger of the static and dynamic widths given by (2-46) & (2-47). In practice, the static width is only important at fairly low velocities, below that given by:

$$\Delta x_s = \Delta x_d$$

$$\Rightarrow \quad v = \frac{2 H_{12}^2}{\hbar(F_1 - F_2)} \qquad (2\text{-}48)$$

The dynamic width is usually more important, and it is useful to define a "dynamic time" t_0:

$$t_0 = \frac{\Delta x_d}{v} = \sqrt{\frac{8\hbar}{v(F_1 - F_2)}} \qquad (2\text{-}49)$$

Although the LZS formula predicts the correct qualitative behaviour at high and low velocities, it is in these regions that the results become dubious, because the assumptions become difficult to accommodate. At low velocities, the potentials governing the motion will have a marked effect on the velocity, so that assumption (iii) is no longer valid; at high velocities, the dynamic width increases without limit, so that eventually assumptions (i) & (ii) become unacceptable. Modifications to deal with the high velocity limit have been examined (Coulson & Zalewski, 1962; Dubrovskii, 1964; Child, 1971).

E Multi-curve crossing approach to atom / diatom systems.

The two-state curve-crossing model is readily applicable to atom / atom collisions, and the LZS formula has been extensively used for such systems. Now consider an atom / diatom system, and in perticular the electron transfer between an alkali atom and a halogen molecule:

$$M + X_2 \rightarrow M^+ + (X_2^-)^\dagger \qquad (2\text{-}50)$$

where the product halogen molecule ion may be vibrationally and

rotationally excited. Although the LZS model is often associated with theoretical considerations of this type of system, there are clearly two ways in which it is more complicated than the two-state curve-crossing problem:

(i) There are three atoms present; the coordinates used to define the positions of these are shown in fig. 5;

(ii) More than two states must necessarily be considered if the internal energy of the X_2^- is to be studied.

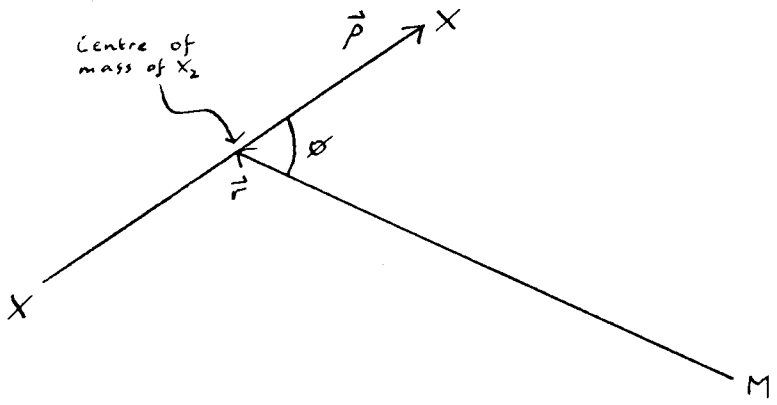

Fig. 5. The coordinates used to describe the positions of the atoms in M/X_2 collisions.

Complication (i) is often dealt with by applying the two-particle approximation (Baede, 1975), in which the molecule is treated as a single particle with more internal structure than an atom. Thus the three-dimensional potential energy surfaces are reduced to potential curves. There are two objections to doing this. Firstly the surfaces may be sensitive to the X-X separation ρ, and this may change considerably during a collision. Secondly, although in one dimension adiabatic states either cross or pseudocross depending on their relative symmetries, in more than one dimension

the relative symmetries are variable, and a conical crossing is expected.

Within the classical path approximation, there are two approaches to (i) &(ii), the multi-curve crossing approach, and the surface hopping trajectory approach, described in section H.

In the multi-curve crossing approach (Bauer, Fisher & Gilmore, 1969; Child, 1973), which has been applied to vibrational energy transfer, all internal motion is treated quantum mechanically, and only relative motion classically. The two-particle approximation is used, but conical crossings are allowed for by a dependence of $H_{12}(\vec{r})$ on the angle φ (see chapter III, B(i)). Having reduced the problem

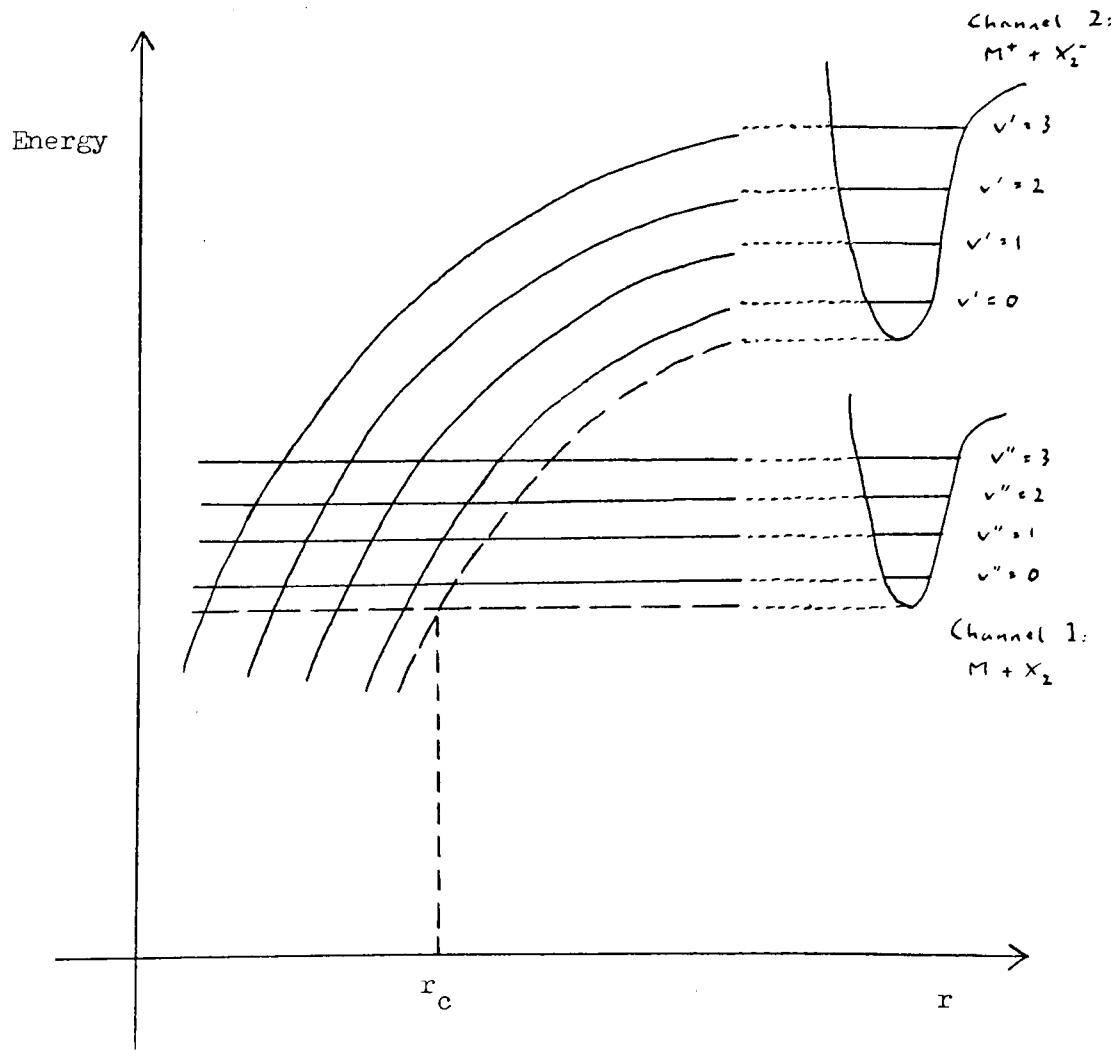

Fig. 6.

to one dimension, there remains (ii) to deal with. By ignoring rotation, and treating vibration as internal, this is achieved by introducing the idea of a network of curve crossings between the states arising from the various vibrational levels of X_2 and X_2^-, as shown, in the diabatic limit, in fig. 6.

Following the treatment of equations (2-25) & (2-26), and ignoring rotational motion, write the wavefunction for the system thus (Child, 1973):

$$\Phi(\vec{q},\vec{\rho},t) = \xi_1(\vec{q}) \sum_{n'} c_{1n'}(t)\, \varphi_{1n'}(\vec{\rho}) + \xi_2(\vec{q}) \sum_{m'} c_{2m'}(t)\, \varphi_{2m'}(\vec{\rho}) \qquad (2\text{-}51)$$

where $\vec{q}$ = electronic coordinates;

$\vec{\rho}$ = vibrational coordinates;

and channel 1 is the covalent channel, 2 the ionic channel, and substitute it in the time-dependent equation

$$H\Phi = i\hbar \frac{\partial}{\partial t} \Phi .$$

Multiplying by $\xi_1^*(\vec{q})\varphi_{1n}^*(\vec{\rho})$ and integrating over $\vec{q}$ & $\vec{\rho}$:

$$\sum_{n'} H_{1n1n'} c_{1n'}(t) + \sum_{m'} H_{1n2m'} c_{2m'}(t) = i\hbar \frac{dc_{1n}(t)}{dt} \qquad (2\text{-}52)$$

Now, $H = H_{int}(\vec{q},\vec{\rho}) + V(\vec{q},\vec{\rho},\vec{r}(t))$

i.e. non-adiabatic transitions are induced by relative motion only. But by the two-particle approximation, V is independent of $\vec{\rho}$, i.e. the internal states remain unperturbed, hence

$$H_{1n1n'} = \int \xi_1^*(\vec{q})\,\phi_{1n}^*(\vec{\rho})\,(H_{int}(\vec{q},\vec{\rho}) + V(\vec{q},t))\,\xi_1(\vec{q})\,\phi_{1n'}(\vec{\rho})\,d\vec{q}d\vec{\rho}$$

$$= (E_{1n} + V_{11}(t))\,\delta_{nn'}$$

and

$$H_{1n2m'} = \int \xi_1^*(\vec{q})\,\phi_{1n}^*(\vec{\rho})\,(H_{int} + V)\,\xi_2(\vec{q})\,\phi_{2m'}(\vec{\rho})\,d\vec{q}d\vec{\rho}$$

$$= V_{12}(t)\Omega_{nm'}$$

where Ω_{nm} (element of overlap matrix Ω) is given by:

$$\Omega_{nm} = \int \phi_{1n}^*\phi_{2m}\,d\vec{\rho} \qquad (2\text{-}53)$$

Hence, substituting in (2-52) and rearranging,

$$\left[i\hbar\frac{d}{dt} - E_{1n} - V_{11}(t) \right] c_{1n}(t) = V_{12}(t)\sum_{m'}\Omega_{nm'}c_{2m'}(t) \qquad (2\text{-}54)$$

Similarly, multiplying through by $\xi_2^*(\vec{q})\,\phi_{2m}^*(\vec{\rho})$ and integrating over $\vec{q}$ & $\vec{\rho}$:

$$\Rightarrow \left[i\hbar\frac{d}{dt} - E_{2m} - V_{22}(t) \right] c_{2m}(t) = V_{21}(t)\sum_{n'}\Omega'_{mn'}c_{1n'}(t) \qquad (2\text{-}55)$$

where $\Omega'_{mn} = \int \phi_{2m}^*\phi_{1n}\,d\vec{\rho}$

Assuming the ϕ's are real, $\Omega'_{mn} = \Omega_{nm}$, i.e.

$$\Omega' = \tilde{\Omega} \qquad (2\text{-}56)$$

Consider the product $\Omega'\Omega$:

$$(\Omega'\Omega)_{ik} = \sum_j \Omega'_{ij}\Omega_{jk}$$

$$= \sum_j \langle 2i|1j\rangle\langle 1j|2k\rangle$$

$$= \langle 2i|2k\rangle \quad \text{by completeness of} \quad \{\varphi_{1i}\}$$

$$= \delta_{ik} \quad \text{by completeness of} \quad \{\varphi_{2i}\}$$

$$\Rightarrow \quad \Omega'\Omega = \mathbb{I} \qquad \text{(unit matrix)}$$

Similarly, $\Omega\,\Omega' = \mathbb{I}$

Hence, comparing (2-56),

$$\widetilde{\Omega} = \Omega^{-1} \tag{2-57}$$

i.e. Ω is orthogonal, and so is Ω'.

Hence, with the assumption that $V_{12}(t) = V_{21}(t)$, the equations (2-55) may be rewritten:

$$\left[i\hbar \frac{d}{dt} - E_{2m} - V_{22}(t) \right] c_{2m}(t) = V_{12}(t) \sum_{n'} \Omega^{-1}_{mn'} c_{1n'}(t) \tag{2-58}$$

where A^{-1}_{ij} will throughout be understood to mean $(A^{-1})_{ij}$.

Equations (2-54) & (2-58) are the basic sets of coupled equations for multi-curve crossing theory. Before considering the methods for solving them, a transformation due to Child (1973), which makes them more physically transparent, will be outlined.

Prepare non-stationary vibrational states in the ionic channel by the orthogonal transformation

$$\Psi_{2n}(\vec{\rho}) = \sum_m \Omega_{nm} \varphi_{2m}(\vec{\rho}).$$

These overlap exactly with the covalent vibrational states:

$$\langle \Psi_{2n} | \varphi_{1n'} \rangle = \sum_m \Omega_{nm} \langle \varphi_{2m} | \varphi_{1n'} \rangle$$

$$= \sum_m \Omega_{nm} \Omega_{mn}$$

$$= \delta_{nn'}$$

i.e. n denotes the channel 1 level to which the transformed channel 2 level is coupled. Then, if we define "a-coefficients" by

$$\sum_m c_{2m}(t)\varphi_{2m} = \sum_n a_{2n}(t)\Psi_{2n}$$

then
$$a_{2n}(t) = \sum_{m'} \Omega_{nm'} c_{2m'}(t) \qquad (2\text{-}59)$$

and
$$c_{2m}(t) = \sum_{n'} \Omega^{-1}_{mn'} a_{2n'}(t) \qquad (2\text{-}60)$$

$$= \sum_{n'} \Omega'_{mn'} a_{2n'}(t)$$

Substituting (2-59) in (2-54),

$$\Rightarrow \left[i\hbar \frac{d}{dt} - E_{1n} - V_{11}(t) \right] c_{1n}(t) = V_{12}(t)\, a_{2n}(t) \qquad (2\text{-}61)$$

and (2-60) in (2-58)

$$\Rightarrow \left[i\hbar \frac{d}{dt} - E_{2m} - V_{22}(t) \right] \sum_{n'} \Omega^{-1}_{mn'} a_{2n'}(t) = V_{12}(t) \sum_{n'} \Omega^{-1}_{mn'} c_{1n'}(t).$$

Now add $(E_{2m} - \bar{E}_{2n}) \sum_{n'} \Omega^{-1}_{mn'} a_{2n'}(t)$ to both sides, then multiply by Ω_{nm}, and sum over m

$$\Rightarrow \left[i\hbar \frac{d}{dt} - \bar{E}_{2n} - V_{22}(t) \right] a_{2n}(t) = \sum_{n'} X_{nn'} a_{2n'}(t) + V_{12}(t) c_{1n}(t)$$

$$\text{where} \quad X_{nn'} = \sum_m \Omega_{nm} (E_{2m} - \bar{E}_{2n}) \Omega^{-1}_{mn} \qquad (2\text{-}62)$$

Now, if we choose for $\bar{E}_{2n}$

$$\bar{E}_{2n} = \sum_m \Omega_{nm} E_{2m} \Omega^{-1}_{mn} \qquad (2\text{-}63)$$

i.e. the expectation value for the energy of the transformed state Ψ_{2n},

then $$X_{nn} = \sum_m \Omega_{nm}(E_{2m} - \bar{E}_{2n})\,\Omega^{-1}_{mn}$$

$$= 0$$

With this definition, for $i \neq j$,

$$X_{ij} = \sum_m \Omega_{im}(E_{2m} - \bar{E}_{2i})\,\Omega^{-1}_{mj}$$

$$= \sum_m \Omega_{im}E_{2m}\Omega^{-1}_{mj} - \sum_m \Omega_{im}\Omega^{-1}_{mj}\bar{E}_{2i}$$

$$= \sum_m \Omega_{im}E_{2m}\Omega^{-1}_{mj}$$

$$= \sum_m \Omega_{jm}E_{2m}\Omega^{-1}_{mi}$$

$$= X_{ji}$$

$\therefore$ the matrix $\mathbb{X}$ is symmetric.

Since $X_{nn} = 0$, we can write

$$\left[i\hbar\frac{d}{dt} - \bar{E}_{2n} - V_{22}(t) \right] a_{2n}(t) = \sum_{n' \neq n} X_{nn'}\, a_{2n'}(t) + V_{12}(t)\, c_{1n}(t) \qquad (2\text{-}64)$$

Consider the new sets of coupled equations (2-61) & (2-64). If it weren't for the coupling terms involving $X_{nn'}$, they would represent a single crossing between just two states, i.e. some chosen vibrational level in the covalent channel:

$$W_{1n}(t) = E_{1n} + V_{11}(t) \qquad (2\text{-}65)$$

and the appropriate transformed mean level in the ionic channel:

$$\bar{W}_{2n}(t) = \bar{E}_{2n} + V_{22}(t) \qquad (2\text{-}66)$$

This is shown in section F to correspond to the high energy Franck-

Condon model, the relative size of $X_{nn'}$ determining the validity of the model.

We shall call equations (2-61) & (2-64) the a-coefficient equations, and (2-54) & (2-58) the c-coefficient equations.

Now check the asymptotic behaviour of (2-61) & (2-64). At large distances, corresponding to very early or late times, $V \to 0$, so put $V_{ab}(t) = 0$ for all a & b in these equations. Then (2-61) becomes

$$\left[i\hbar \frac{d}{dt} - E_{1n} \right] c_{1n}(t) = 0$$

$$\Rightarrow \quad c_{1n}(t) = c_{1n}(0)\, e^{-iE_{1n}t/\hbar} \qquad (2\text{-}67)$$

which is the correct free behaviour, while (2-64) becomes

$$\left[i\hbar \frac{d}{dt} - \bar{E}_{2n} \right] a_{2n}(t) = \sum_{n' \neq n} X_{nn'}\, a_{2n'}(t)$$

Returning $X_{nn} = 0$ to the sum,

$$i\hbar \frac{d}{dt} a_{2n}(t) = \sum_{n'} X_{nn'}\, a_{2n'}(t) + \sum_{n'} \bar{E}_{2n'}\, \delta_{nn'}\, a_{2n'}(t)$$

$$\Rightarrow \quad i\hbar \frac{d}{dt} \underset{\sim}{a}(t) = \mathbb{A}\, \underset{\sim}{a}(t) \qquad (2\text{-}68)$$

where $A_{ij} = X_{ij} + \bar{E}_{2i}\, \delta_{ij}$

and $\underset{\sim}{a}$ is a column vector of the a-coefficients.

Since $\mathbb{A}$ is independent of t, the matrix equation (2-68) is readily solved (Mirsky, 1971) to give

$$\underset{\sim}{a}(t) = \exp\left\{ \frac{t}{i\hbar} \mathbb{A} \right\} \underset{\sim}{a}(0) \qquad (2\text{-}69)$$

where $\exp \mathbb{B} = \mathbb{I} + \mathbb{B} + \frac{1}{2!} \mathbb{B}^2 + \cdots\cdots$

is defined for all square matrices $\mathbb{B}$; however, it is not readily evaluated for a general matrix such as $\frac{t}{i\hbar}\mathbb{A}$.

Now, for any matrix U,

$$\exp \mathbb{B} = U U^{-1} \{\exp \mathbb{B}\} U U^{-1}$$

and by expanding the series it is readily shown that this is equal to

$$U \{\exp (U^{-1} \mathbb{B} U)\} U^{-1}$$

But suppose U diagonalises $\mathbb{B}$; then $\exp(U^{-1}\mathbb{B}U)$ is easily evaluated, since clearly for $\mathbb{M}$ diagonal,

$$(\exp \mathbb{M})_{ij} = \exp (\mathbb{M}_{ij}) \delta_{ij}$$

and suppose we calculate $Q = \Omega^{-1} \mathbb{A} \Omega$.

Then $$Q_{il} = \sum_j \sum_k \Omega^{-1}_{ij} (X_{jk} + \bar{E}_{2j} \delta_{jk}) \Omega_{kl}$$

$$= \sum_j \sum_k \Omega^{-1}_{ij} X_{jk} \Omega_{kl} + \sum_j \Omega^{-1}_{ij} \bar{E}_{2j} \Omega_{jl}$$

$$= \sum_j \sum_k \sum_p \Omega^{-1}_{ij} \Omega_{jp} (E_{2p} - \bar{E}_{2j}) \Omega^{-1}_{pk} \Omega_{kl} + \sum_j \Omega^{-1}_{ij} \bar{E}_{2j} \Omega_{jl}$$

$$= \sum_j \Omega^{-1}_{ij} (E_{2l} - \bar{E}_{2j}) \Omega_{jl} + \sum_j \Omega^{-1}_{ij} \bar{E}_{2j} \Omega_{jl}$$

$$= E_{2l} \delta_{il}$$

and it can be seen that Ω diagonalises $\mathbb{A}$ and (2-69) can be rewritten

$$\underset{\sim}{a}(t) = \Omega \exp \left\{ \frac{t}{i\hbar} \Omega^{-1} \mathbb{A} \Omega \right\} \Omega^{-1} \underset{\sim}{a}(0)$$

$$\Rightarrow a_{2n}(t) = \sum_m \sum_j \Omega_{nj} e^{-iE_j t/\hbar} \Omega^{-1}_{jm} a_{2m}(0) \qquad (2\text{-}70)$$

Note that the modulus of a_{2n} varies with time even a long time after the collision, so it is not possible to talk of the probability of transition to one of these non-stationary states. However, we can now derive the behaviour of the stationary states described by the c-coefficients, and see that the modulus does not vary with time asymptotically:

$$\begin{aligned} c_{2n}(t) &= \sum_{n'} \Omega^{-1}_{nn'} a_{2n'}(t) \\ &= \sum_{n'} \sum_{m} \sum_{j} \Omega^{-1}_{nn'} \Omega_{n'j} e^{-iE_{2j}t/\hbar} \Omega^{-1}_{jm} a_{2m}(0) \\ &= \sum_{m} \Omega^{-1}_{nm} e^{-iE_{2n}t/\hbar} a_{2m}(0) \\ &= c_{2n}(0)\, e^{-iE_{2n}t/\hbar} \end{aligned} \qquad (2\text{-}71)$$

which is as expected.

F High energy limit - the Franck-Condon method.

Consider equations (2-61) & (2-64) again:

$$\left[i\hbar \frac{d}{dt} - E_{1n} - V_{11}(t) \right] c_{1n}(t) = V_{12}(t)\, a_{2n}(t) \qquad (2\text{-}61)$$

$$\left[i\hbar \frac{d}{dt} - \bar{E}_{2n} - V_{22}(t) \right] a_{2n}(t) = \sum_{n' \neq n} X_{nn'}\, a_{2n'}(t) + V_{12}(t)\, c_{1n}(t) \qquad (2\text{-}64)$$

The coupling terms in $X_{nn'}$ can be regarded as responsible for spontaneous decay of the non-stationary ionic states. In order that the system may be approximated by a single crossing between $W_{1n} = E_{1n} + V_{11}$ and the averaged curve $\bar{W}_{2n} = \bar{E}_{2n} + V_{22}$, as described in section E, the time-constant for this decay must be large compared with some interaction time t_0. That this should occur in the limit of high velocity was suggested by Child (1973); while the

dynamic width for a particular crossing increases without limit as the velocity is increased, until it encompasses all the crossing points of the network, the interaction time, given roughly by the dynamic time (2-49), dependent on $v^{-\frac{1}{2}}$, decreases and eventually becomes small compared with the spontaneous decay time-constant. This argument was expressed more quantitatively as follows:

First "remove" the diagonal zeroth order E terms and first order V terms from (2-61) & (2-64) by a transformation analogous to that of (2-34):

Let
$$c_{1n}(t) = \gamma_n(t) \exp\left\{ -\frac{i}{\hbar} \int W_{1n}(t)\, dt \right\} \qquad (2\text{-}72)$$

and
$$a_{2n}(t) = \alpha_n(t) \exp\left\{ -\frac{i}{\hbar} \int \overline{W}_{2n}(t)\, dt \right\} \qquad (2\text{-}73)$$

Then
$$\left[i\hbar \frac{d}{dt} - E_{1n} - V_{11}(t) \right] c_{1n}(t)$$

$$= \exp\left\{ -\frac{i}{\hbar} \int W_{1n}(t)dt \right\} \left[i\hbar \frac{d}{dt} + i\hbar \frac{d}{dt} \left(-\frac{i}{\hbar} \int W_{1n}(t)dt \right) - W_{1n}(t) \right] \gamma_n(t)$$

$$= \exp\left\{ -\frac{i}{\hbar} \int W_{1n}(t)dt \right\} \left[i\hbar \frac{d}{dt} + W_{1n}(t) - W_{1n}(t) \right] \gamma_n(t)$$

$$= e^{-\Gamma_n(t)}\, i\hbar \frac{d}{dt} \gamma_n(t)$$

where
$$\Gamma_n(t) = \frac{i}{\hbar} \int W_{1n}(t)\, dt$$

Similarly,
$$\left[i\hbar \frac{d}{dt} - \overline{E}_{2n} - V_{22}(t) \right] a_{2n}(t)$$

$$= e^{-A_n(t)}\, i\hbar \frac{d}{dt} \alpha_n(t)$$

where $A_n(t) = \frac{i}{\hbar}\int \overline{W}_{2n}(t)\,dt$

Hence eqns. (2-61) & (2-64) become

$$i\hbar\frac{d}{dt}\gamma_n(t) = V_{12}(t)\,e^{(\Gamma_n - A_n)}\alpha_n(t) \qquad (2\text{-}74)$$

$$i\hbar\frac{d}{dt}\alpha_n(t) = \sum_{n'\neq n} X_{nn'}\,e^{(A_n - A_{n'})}\alpha_{n'}(t) + V_{12}(t)\,e^{(A_n - \Gamma_n)}\gamma_n(t) \qquad (2\text{-}75)$$

where $A_n - A_{n'} = \frac{i}{\hbar}\int(\overline{W}_{2n} - \overline{W}_{2n'})dt$

$$= \frac{i}{\hbar}\int(\overline{E}_{2n} + V_{22}(t) - \overline{E}_{2n'} - V_{22}(t))dt$$

$$= \frac{i}{\hbar}(\overline{E}_{2n} - \overline{E}_{2n'})\,t$$

Now introduce a dimensionless time variable $\tau = (t-t_x)/t_0$, where t_x is the time at the crossing point $W_{1n}(t_x) = \overline{W}_{2n}(t_x)$, and t_0 is some interaction time. Equations (2-74) & (2-75) now become

$$i\frac{d\alpha_n(\tau)}{d\tau} = \frac{t_0 V_{12}}{\hbar}\exp(i\beta(\tau))\,\alpha_n(\tau) \qquad (2\text{-}76)$$

$$i\frac{d\alpha_n(\tau)}{d\tau} = \frac{t_0 V_{12}}{\hbar}\exp(-i\beta(\tau))\,\alpha_n(\tau) + \sum_{n\neq n'}\frac{t_0 X_{nn'}}{\hbar}\exp\left(\frac{it_0(\overline{E}_{2n} - \overline{E}_{2n'})\tau}{\hbar}\right)\alpha_{n'}(\tau) \qquad (2\text{-}77)$$

where $\beta(\tau) = \frac{t_0}{\hbar}\int_0^\tau\{W_{1n}(t_0\tau) - \overline{W}_{2n}(t_0\tau)\}\,d\tau$

The condition for neglect of the second term in (2-77), for moderate V_{12}'s, is

$$\frac{t_0 X_{nn'}}{\hbar} \ll 1 \qquad (2\text{-}78)$$

We now need an estimate for t_0. Most of the contribution to the first term in (2-77) comes from $|\beta(\tau)| < \pi$, and for t_0 to represent some interaction time, we require this to happen at $|t - t_x| = t_0$, i.e. $\tau = \pm 1$. Now, β can be estimated using the constant velocity, constant potential slope approximation, giving

$$\beta(\tau) \simeq -\frac{t_0^2 (F_1 - F_2) v \tau^2}{2\hbar}$$

$$\therefore \quad \frac{t_0^2 (F_1 - F_2) v}{2\hbar} = \pi$$

$$\Rightarrow \quad t_0 = \sqrt{\frac{2\pi\hbar}{v(F_1 - F_2)}} \qquad (2\text{-}79)$$

Comparing (2-79) with (2-34), we see that this is of the same order of magnitude as the dynamic time. Hence the condition for neglect of the coupling is

$$A = X_{nn'} \sqrt{\frac{2\pi}{\hbar v (F_1 - F_2)}} \ll 1 \qquad (2\text{-}80)$$

Under these conditions, the equations represent a single crossing between one vibrational level in the covalent channel and the appropriate transformed level in the ionic. The case when $t_0 V_{12}/\hbar \ll 1$ can be shown by first order perturbation theory to give the same result (Child, 1973).

Now, in all collisions under consideration, initially only the ground vibrational level in the covalent channel is populated, hence only the appropriate level ψ_{20} is ever populated in one pass of the

crossing region, so a_{20} is some non-zero number, while all other a-coefficients are zero. Hence, after a pass of the crossing region,

$$c_{2m} = \sum_n \Omega^{-1}_{mn} a_{2n}$$

$$= \Omega^{-1}_{m0} a_{20}$$

$$= \Omega_{0m} a_{20} \qquad (2\text{-}81)$$

i.e. the final coefficients in the ionic channel have a distribution

$$c_{2m} \propto \Omega_{0m}$$

and the probabilities a distribution

$$|c_{2m}|^2 \propto |\Omega_{0m}|^2,$$

which is the so-called Franck-Condon factor. The constant of proportionality a_{20} can be obtained e.g. by the LZS formula. The result is that, at high collision energies, sufficient that condition (2-80) holds, the system can be described as a single crossing, with final probabilities in the ionic channel modulated by Franck-Condon factors. This is the Franck-Condon model, described by Kendall & Grice (1972) and Child (1973).

In the type of collision being considered, the crossing region is traversed twice, and a transition can occur at 0, 1, or 2 of these crossings.

Consider the case when two transitions occur:

Let there be a transition at $r = r_x$, followed by evolution in time, and then a transition back when $r = r_x$ again, both transitions being governed by the Franck-Condon principle.

Let $r = r_x$ for the first time at $t = -t_f$. Then the ionic part

of the wavefunction is given by

$$\Psi^{\text{ionic}}(\rho, -t_f) = \sum_m a_{20}\Omega_{0m}\phi_{2m}(\rho) \qquad \text{by} \qquad (2\text{-}81)$$

$$= |T_{12}| \sum_m \Omega_{0m}\phi_{2m}(\rho)$$

where T_{12} = transition amplitude between the effective pair of levels.

Assuming the ionic states each evolve freely until the next transition, at $t = +t_f$,

$$\Psi^{\text{ionic}}(\rho, +t_f) = |T_{12}| \sum_m \Omega_{0m}\phi_{2m}(\rho)\, e^{-2iE_{2m}t_f/\hbar}.$$

At this point there is a transition back to the covalent channel. Assuming the Franck-Condon principle holds again,

$$\Psi^{\text{cov}}(\rho, t_f) = |T_{12}| \sum_n \Omega_{nI}(t_f)\phi_{1n}(\rho)$$

where Ω_{nI} is the overlap between the nth level of the covalent channel, and the overall ionic state:

$$\Omega_{nI}(t_f) = \int \phi^*_{1n}(\rho)\Psi^{\text{ionic}}(\rho, t_f)\, d\rho$$

$$= \int \phi^*_{1n}(\rho)\, |T_{12}| \sum_m (\Omega_{0m}\phi_{2m}(\rho)\, e^{-2iE_{2m}t_f/\hbar})\, d\rho$$

$$= |T_{12}| \sum_m \Omega_{0m}\Omega_{nm}\, e^{-2iE_{2m}t_f/\hbar}$$

$\therefore$ amplitude $c_{1n}(t_f) = |T_{12}|\, \Omega_{nI}(t_f)$

$$= |T_{12}|^2 \sum_m \Omega_{0m}\Omega_{nm}\, e^{-2iE_{2m}t_f/\hbar} \qquad (2\text{-}82)$$

This expression has been derived from a fairly physical picture of

the process; a shorter derivation which does not invoke the Franck-Condon principle with Ω_{nI} is as follows:

$$a_{2n}(-t_f) = \delta_{n0} \; |T_{12}|$$

$$\Rightarrow a_{2n}(t_f) = \sum_m \sum_j \Omega_{nj} \, e^{-2iE_{1j}t_f/\hbar} \, \Omega^{-1}_{jm} \, \delta_{m0} \; |T_{12}| \qquad \text{using (2-70)}$$

$$= |T_{12}| \sum_j \Omega_{nj} \, e^{-2iE_{1j}t_f/\hbar} \, \Omega^{-1}_{j0}$$

$$\therefore \; c_{1n}(t_f) = |T_{12}| \; a_{2n}(t_f)$$

$$= |T_{12}|^2 \sum_m \Omega_{0m}\Omega_{nm} \, e^{-2iE_{1m}t_f/\hbar}$$

as before.

Let $|T_{12}|^2 = P$ = probability of changing diabatic curves during one passage of the transition region.

Then the probability of ending up in state 1n after two crossings is

$$P_2 = |c_{1n}(t_f)|^2 = P^2 Q_n \qquad (2\text{-}83)$$

where $$Q_n = \left| \sum_m \Omega_{0m}\Omega_{nm} \, e^{-2iE_{1m}t_f/\hbar} \right|^2$$

$$\left(\sum_m \Omega_{0m}\Omega_{nm} \cos q_m \right)^2 + \left(\sum_m \Omega_{0m}\Omega_{nm} \sin q_m \right)^2$$

where $$q_m = 2 E_{2m} t_f/\hbar$$

This probability Q_n, within the covalent manifold, is seen to be dependent on the collision energy, since this determines the time $2t_f$ during which evolution takes place. The total probability of two transitions is

$$\sum_n P^2 \, Q_n$$

$$= P^2 \sum_n Q_n$$

But
$$\sum_n Q_n = \sum_n \left\{ \left(\sum_m \Omega_{0m}\Omega_{nm} \cos q_m \right)^2 + \left(\sum_m \Omega_{0m}\Omega_{nm} \sin q_m \right)^2 \right\}$$

$$= \sum_n \left\{ \sum_m \left[(\Omega_{0m}\Omega_{nm} \cos q_m)^2 + (\Omega_{0m}\Omega_{nm} \sin q_m)^2 \right] \right.$$

$$\left. + \sum_{\substack{m,j \\ m \neq j}} \left[\Omega_{0m}\Omega_{nm} \cos(q_m)\Omega_{0j}\Omega_{nj} \cos(q_j) + \Omega_{0m}\Omega_{nm} \sin(q_m)\Omega_{0j}\Omega_{nj} \sin(q_j) \right] \right\}$$

$$= \sum_n \left\{ \sum_m (\Omega_{0m}\Omega_{nm})^2 + \sum_{\substack{m,j \\ m \neq j}} \Omega_{0m}\Omega_{nm}\Omega_{0j}\Omega_{nj} \cos(q_m - q_j) \right\}$$

$$= \sum_m \Omega_{0m}^2 + \sum_{\substack{m,j \\ m \neq j}} \delta_{mj}\Omega_{0m}\Omega_{0j} \cos(q_m - q_j)$$

$$= 1$$

i.e. the total probability of two transitions $= P^2$, which is as expected.

When less than two transitions occur, the situation is easier to deal with, as there is no time evolution to consider. If no transitions occur, then we end up in the initial ground vibrational state of the covalent channel, with probability P_0:

$$P_0 = (1 - P)^2 \qquad (2\text{-}84)$$

If one transition occurs, then, regardless of the crossing at which it occurs, the distribution of the ionic states is according to the Franck-Condon factors $(\Omega_{0m})^2$

$$\Rightarrow \text{probability of emerging in ionic state m} = P_1 \Omega_{0m}^2 \qquad (2\text{-}85)$$

Note that here the distribution within the ionic manifold is independent of the collision energy. P_1 is the probability of only

one electronic transition occuring, and this is equal to the sum of probabilities $\sum_m P_1 \Omega_{Om}^2$ because of the orthogonality of Ω. According to classical probability theory,

$$P_1 = 2\,P(1 - P) \qquad (2\text{-}86)$$

Aside from the fundamental limitation imposed by (2-78), the Franck-Condon method is subject to inaccuracy arising from the choice of a method for calculating P, e.g. the LZS method, and also from the use of the classical formula (2-86), which ignores interference effects between ingoing and outgoing trajectories. However, within its validity range, it should successfully predict the distribution among vibrational levels within the ionic channel, since this is independent of the method used for calculating P.

G Low energy limit - the sequential Landau-Zener BFG method.

Consider the network of crossings, shown again in fig. 7, where the covalent and ionic states are now numbered consecutively.

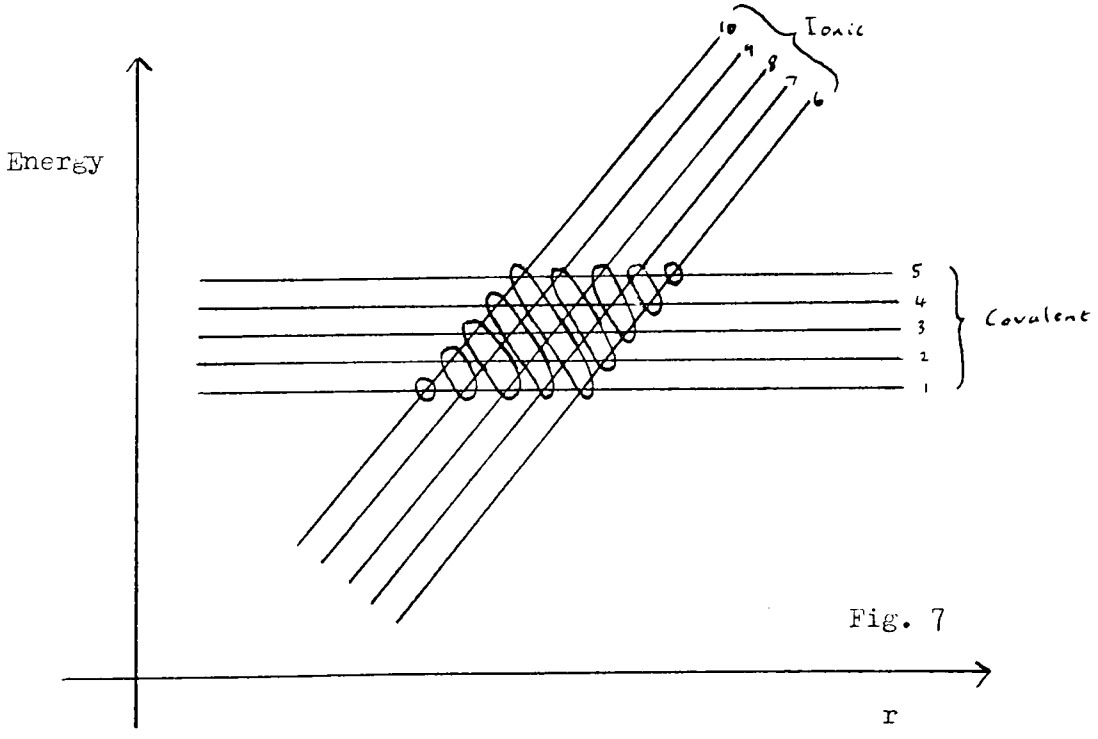

Fig. 7

If adjacent crossings are further apart than the dynamic width, it would be reasonable to treat each one independently, and move through the crossings in order, branching appropriately as each one is encountered. This is the "diffusion" method described by Bauer, Fisher & Gilmore (1969) for the system $Na + N_2$; it has since been applied to alkali / halogen collisions by Gislason & Sachs (1975). The individual crossings are usually dealt with by the LZS method. We shall call this approach the BFG method. Since the dynamic width is proportional to $v^{\frac{1}{2}}$, the method will be expected to be valid only at low collision energies.

Consider the validity criteria for this low energy approach. The condition required is:

$$\text{Dynamic width} \ll \text{spacing of crossings}$$

Now, an estimate of the spacing of the crossings is given by $\Delta E/|F_1 - F_2|$, where ΔE is a nominal energy level spacing.

Hence, using (2-47),

$$\sqrt{\frac{8\hbar v}{|F_1 - F_2|}} \ll \frac{\Delta E}{|F_1 - F_2|}$$

$$\sqrt{\frac{8\hbar v |F_1 - F_2|}{(\Delta E)^2}} \ll 1 \qquad (2\text{-}87)$$

So, using the dynamic width criterion, the BFG method will be expected to approach validity for v below a value v_{BFG}:

$$v_{BFG} = \frac{(\Delta E)^2}{8\hbar |F_1 - F_2|} \qquad (2\text{-}88)$$

However, there is still the static width to consider. At low v, this eventually becomes larger than the dynamic width, and is the

important interaction width. The cross-over occurs at (2-48)

$$v = \frac{2 H_{12}^2}{\hbar |F_1 - F_2|} \qquad (2\text{-}89)$$

This must come in at a velocity lower than v_{BFG}, otherwise the static width will always be too big

$$\Rightarrow \quad \frac{2 H_{12}^2}{\hbar |F_1 - F_2|} < \frac{(\Delta E)^2}{8 \hbar |F_1 - F_2|}$$

$$\Rightarrow \quad |H_{12}| < \tfrac{1}{4} \Delta E \qquad (2\text{-}90)$$

which is the same as saying that the static width must be less than the spacing of the crossings, as an essential precondition for the method to be valid.

Consider the progress through the network of crossings. At the crossing point $r = r_{pq}$ between covalent state p ($= n + 1$) and ionic state q ($= m + 1 + N$, where N is the number of covalent states considered), the amplitudes (or probabilities) for these two states will be transformed by some matrix $\begin{pmatrix} a & b \\ c & d \end{pmatrix}$, and the total scattering matrix accumulated so far will be multiplied by

$$A_{pq} = \begin{pmatrix} 1 & & & & & & & & & & \\ & \ddots & & & & & & & & & \\ & & 1 & & & & & & & & \\ & & & a & 0 & \cdots & 0 & b & & & \\ & & & 0 & 1 & & & 0 & & & \\ & & & \vdots & & \ddots & & \vdots & & & \\ & & & 0 & & & 1 & 0 & & & \\ & & & c & 0 & \cdots & 0 & d & & & \\ & & & & & & & & 1 & & \\ & & & & & & & & & \ddots & \\ & & & & & & & & & & 1 \end{pmatrix}$$

(Column: p, q; Row: p, q)

Since for $p \neq p'$, $q \neq q'$, $\mathcal{A}_{pq}\mathcal{A}_{p'q'} = \mathcal{A}_{p'q'}\mathcal{A}_{pq}$, then on the inward (or outward) trajectory it is sufficient to take the sets of crossings grouped together in fig. 7 in order from right to left (or from left to right), but within each group the order of taking the crossings is arbitrary.

Let S^{in} be the total scattering matrix obtained going inwards, and S^{out} that obtained going out again. Then, ignoring bond stretching in the X_2,

$$\text{if} \qquad S^{in} = A\ B\ C\ \ldots\ldots\ X\ Y\ Z \qquad \text{say}$$

$$\text{then} \qquad S^{out} = Z\ Y\ X\ \ldots\ldots\ C\ B\ A\ .$$

But for all $\mathcal{A}_{pq}$, $b = c \Rightarrow \mathcal{A}_{pq} = \tilde{\mathcal{A}}_{pq}$

$$\Rightarrow S^{out} = \tilde{Z}\ \tilde{Y}\ \tilde{X}\ \ldots\ldots\ \tilde{C}\ \tilde{B}\ \tilde{A}$$

$$= \tilde{S}^{in}$$

$$\therefore \text{total } \mathcal{S} = S^{out}\, S^{in}$$

$$= \tilde{S}^{in}\, S^{in} \qquad (2\text{-}91)$$

If each crossing is governed by the LZS formula, then

$$a = d = P_{pq} \ ;$$

$$b = c = 1 - P_{pq} \qquad (2\text{-}92)$$

$$\text{where} \qquad P_{pq} = \exp\left(\frac{-2\pi \left| H_{1n2m}(r_{pq}) \right|^2}{\hbar v_R \left| F_1(r_{pq}) - F_2(r_{pq}) \right|} \right) \qquad (2\text{-}93)$$

where v_R = radial velocity

$$= \frac{d}{dt}\sqrt{v^2t^2 + b^2}\Big|_{r=r_{pq}} \quad \text{in the impact parameter approximation}$$

$$= \frac{v\sqrt{r_{pq}^2 - b^2}}{r_{pq}}$$

Note that in (2-93), the interaction element between the actual wavefunctions involved in the crossing is used, and, from section E,

$$H_{1n2m} = V_{12}\Omega_{nm}$$

Thus the Franck-Condon factor appears again, this time in the LZS formula for each individual crossing:

$$P_{pq} = \exp\left(-\frac{2\pi(V_{12}(r_{pq}))^2(\Omega_{nm})^2}{\hbar v_R|F_1 - F_2|}\right)$$

Again, sources of unreliability in this method over and above the restrictions imposed by (2-87) & (2-90) lie in the choice of the LZS method for each crossing probability, and the neglect of interference between ingoing and outgoing trajectories.

H Surface hopping trajectory approach to atom / diatom systems.

An alternative approach to the complications of atom / diatom systems described in section E is the surface hopping trajectory (SHT) method (Tully & Preston, 1971). In this, only electronic motion is considered internal, the rest being external and treated classically. A trajectory is started on the appropriate surface, and integrated until a crossing seam in the diabatic surfaces is reached, when it is split into branches, with weights equal to the transition probabilities to each surface. Each branch is continued, and may meet further seams. The probabilities are calculated using the LZS

formula, or by a more general classical path method; it is assumed that over the region of strong coupling the surfaces are similar enough that the choice of path is not critical. A large number of trajectories, with a distribution of starting conditions, is calculated, as in adiabatic trajectory work, and the results are calculated by considering all the final branches from every trajectory, weighted appropriately. Alternatively, at each seam, a weighted decision is made on whether to hop or not, so that for each trajectory only one particular branch is followed. These two methods have been called the "ants" and "anteater" methods respectively. The calculation of the classical trajectory can be done using diabatic or adiabatic surfaces; in the latter case a velocity correction must be made at each hop to conserve energy and angular momentum.

Interference between branching trajectories is not taken into account; this is done in the Miller & George (1972) method, in which a semiclassical phase is accumulated by calculating the classical action along the trajectory. The trajectory goes into the complex plane to reach transition points where the adiabatic surfaces intersect, thereby conserving energy and angular momentum. However, there are considerable computational difficulties in calculating the trajectory and finding the crossing points in the complex time plane, and an intermediate scheme has been proposed (Komornicki, George & Morokuma, 1976). Although the simpler TSH method is predominantly classical and allows much physical interpretation, it still uses large amounts of computer time, and is particularly troublesome at low energies, when the trajectory can cross the seam many times.

CHAPTER III

COMPARISON OF METHODS FOR CALCULATING VIBRATIONAL ENERGY DISTRIBUTIONS IN ELECTRON TRANSFER COLLISIONS $M + X_2 \rightarrow M^+ + X_2^-$

A Introduction.

If an alkali metal atom and a halogen molecule in their respective ground states collide, at a sufficiently high velocity, there is a chance that an electron will be transferred from the metal to the halogen to give ions in their ground electronic states. The states involved (Baede, 1975) are known to be:

$$M\,(^2S) + X_2\,(^1\Sigma_g^+) \rightarrow M^+(^1S) + X_2^-(^2\Sigma_u^+) \qquad (3\text{-}1)$$

The X_2^- ions produced are vibrationally excited, and some work has been done towards measuring vibrational energy distributions resulting from these collisions (see Kashihira et al, 1974; Groszer & Meyer, 1976; Mochizuki & Lacmann, 1976 (for $K + O_2$); Aten, Lanting & Los, 1977). Two methods are available within the classical path approximation for calculating such distributions, the multi-curve crossing approach, and the surface hopping trajectory approach (see sections E & H of chapter II). The multi-curve crossing approach has only been used in the form of two approximations, the low energy sequential Landau-Zener BFG model and the high energy Franck-Condon model (see sections G & F of chapter II), in spite of the limitations on the validity of these methods. The primary aim of this chapter is to test the validity of these two approximations by comparison of results obtained from them with those obtained

from solution of the coupled differential equations of the general multi-curve crossing approach.

B Description of the model system.

To emphasise the comparison of different approximations being made, a model system M / X_2 was invented, with parameters appropriate to a typical alkali / halogen system. These parameters, with associated assumptions, are given below.

(i) Parameters and assumptions.

Diatom potentials:

The ground states of X_2 and X_2^- were represented by Morse potentials:

$$V(\rho) = D\left\{1 - \exp\left(\beta(\rho_e - \rho)\right)\right\}^2 \qquad (3\text{-}2)$$

where $$\beta = \pi\nu\sqrt{\frac{2\mu}{D}}$$

and ρ = internuclear distance

The Morse potential is commonly used to describe covalent bonds of this type. It has the correct qualitative behaviour: an infinite repulsive wall at low ρ (although $V \to \infty$ as $\rho \to -\infty$ rather than as $\rho \to 0$), a minimum at the equilibrium distance ρ_e, and a finite value as $\rho \to \infty$, higher than the minimum by the dissociation energy D. If the Morse oscillator potential is expanded about $\rho = \rho_e$, then the first term is in $(\rho_e - \rho)^2$, and taken alone this corresponds to a harmonic oscillator of frequency ν. The parameters used were:

Reduced mass μ = 12 ppg (corr. to A.W. of X ~ 15)

X_2: ν = 1500 cm^{-1} = 4.5 dps^{-1} ;

$$\rho_e = 1.2 \text{ Å} ;$$

$$D = 500 \text{ cpe} \quad (\sim 3 \text{ eV}) ;$$

$$\Rightarrow \beta = 3.10 \text{ Å}^{-1}$$

X_2^-: $\nu = 1000 \text{ cm}^{-1} = 3.0 \text{ dps}^{-1}$;

$$\rho_e = 1.25 \text{ Å} ;$$

Electron affinity of X $= E_{aX} = 275$ cpe ;

Adiabatic electron affinity of X_2 $= E^a_{aX_2} = 250$ cpe ;

$$\Rightarrow D_{X_2^-} = D_{X_2} + E^a_{aX_2} - E_{aX}$$

$$= 475 \text{ cpe} ;$$

$$\Rightarrow \beta = 2.12 \text{ Å}^{-1}$$

These potentials are in agreement with the observation that the X_2^- is generally less tightly bound than X_2, with a larger equilibrium distance and smaller dissociation energy. They are chosen to be somewhat more similar than is found in practice, so that the overlap matrix Ω is not too different from the unit matrix, so that only a fairly small number of vibrational states need be included in the calculation.

M / X_2 potentials:

For the covalent diabatic potential, a Lennard-Jones 6-12 potential was used:

$$V_{11}(r) = \varepsilon \left\{ \left(\frac{\sigma}{r}\right)^{12} - 2\left(\frac{\sigma}{r}\right)^{6} \right\} \qquad (3\text{-}3)$$

This has the same qualitative shape as a Morse potential, but the repulsive wall is at $r = 0$, and the long range behaviour is the observed Van der Waals C_6 attraction. The parameters were chosen to give loose binding:

$\sigma = 3$ Å ; $\varepsilon = 50$ cpe (~ 0.3 eV)

The zero of energy is seen to be infinitely separated $M + X_2$ with no vibrational energy.

For the ionic diabatic potential, a simplefied Kittner (1951) potential was used:

$$V_{22}(r) = -\frac{e^2}{4\pi\varepsilon_0 r} - \frac{e^2(\alpha_1 + \alpha_2)}{8\pi\varepsilon_0 r^4} + Ae^{-r/k} + I_M - E^a_{aX_2} \qquad (3\text{-}4)$$

with I_M = 1st ionisation potential of M = 500 cpe ;

α_1 = polarisability of M = 0.2 Å^3;

α_2 = " " X_2^- = 5 Å^3;

$A = 1.5 \times 10^6$ cpe ; $k = 0.2$ Å.

This potential becomes infinitely attractive at the origin, but this can be ignored because the exponential repulsion $Ae^{-r/k}$ produces a high wall between this and the potential well. Note that the inclusion of the asymptotic difference $I_M - E^a_{aX_2}$ means that the energies E_{1n} and E_{2m} (see section E of chapter II) should be measured relative to the bottoms of the respective wells.

Before finding an expression for $V_{12}(r)$, it is necessary to consider the conical crossing which is expected between the adiabatic surfaces in two dimensions. It is easy to see how this arises by examining the symmetries of the quasimolecular groups arising from (3-1) as a function of the orientation φ, defined in fig. 5.

The possible symmetry point groups for the system are:

$\varphi = 0$	$C_{\infty v}$
$\pi/2$	C_{2v}
other	C_s

and the symmetries of the two electronic states are (Baede, 1975):

	C_{2v}	$C_{\infty v}$	C_s
$M + X_2$	$^2A_1$	$^2\Sigma^+$	$^2A'$
$M^+ + X_2^-$	$^2B_2$	$^2\Sigma^+$	$^2A'$

For $\varphi = \pi/2$, $H_{12}(r_c) = H_{12}(r) = 0$, and the adiabatic states cross. This dependence of $H_{12}(r)$ on φ is readily modelled in the two-particle approximation by inclusion of a factor $\cos\varphi$ (see Anderson & Herschbach, 1975). This approximate angular dependence was confirmed by the ab initio calculations of Balint-Kurti & Karplus (1971; 1973) and similar angular dependences for other symmetries of M / X_2 systems were estimated by Gislason & Sachs (1975).

The expression used for the interaction potential was that suggested by Evers & DeVries (1976), which includes the $\cos\phi$ factor:

$$V_{12}(r) = \xi\sqrt{I_M E^a_{aX_2}}\; r_c\; e^{-0.86\xi r_c}\cos\phi\; \exp\{-c\,\xi(r - r_c)\} \qquad (3\text{-}5)$$

where $$\xi = \tfrac{1}{2}\left\{\sqrt{2\,I_M} \quad \sqrt{2\,E^a_{aX_2}}\right\}$$

in atomic units, with $c = 0.6$

This consists of the Olson et al (1971) expression for $V_{12}(r_c)$ multiplied by the $\cos\varphi$ factor and an exponentially falling dependence on $(r - r_c)$. This expression was later multiplied by a factor f, chosen in such a way that the LZS probability $P \sim 0.5$ for a particular energy region, to allow comparison of the approximations with transition probabilities reasonably different from 0 or 1. To convert from atomic units, the two constants 0.86 and c must be multiplied by 2.86×10^{-2}; and the whole expression must also be multiplied by this factor (which is $(a_0)^{-1}(\text{Hartree})^{-\frac{1}{2}}$, as required

by dimensional analysis). r_c is the nominal crossing radius, given by

$$r_c = \frac{e^2}{4\pi\varepsilon_0(I_M - E^a_{aX_2})} \qquad (3\text{-}6)$$

$$= 9.21 \text{ Å} \quad \text{in this case.}$$

Classical path:

The impact parameter approximation was used throughout, with a fixed impact parameter, and with the X_2 axis parallel to the direction of motion. Referring to fig. 8, with time t running from $-\infty$ to $+\infty$ with $t = 0$ at the point of closest approach:

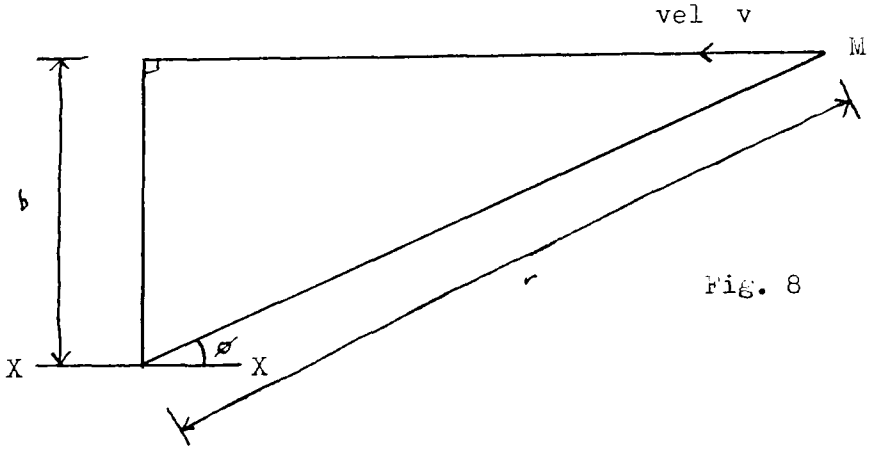

Fig. 8

At time t,

$$r = \sqrt{b^2 + v^2t^2} \qquad (3\text{-}7)$$

and $$\cos\varphi = \frac{vt}{r} = \frac{vt}{\sqrt{b^2 + v^2t^2}} \qquad (3\text{-}8)$$

If the collision energy is E, then

$$v = \sqrt{\frac{2E}{\mu_{M,X_2}}}$$

The following values were used for the impact parameter and M / X_2 reduced mass:

$$b = 5 \text{ Å} \; ; \qquad \mu_{H,X_2} = 20 \text{ ppg.}$$

Before solving the multi-curve crossing equations (2-61) & (2-64), it now remains to calculate the energies E_{1n} & E_{2m}, and the overlap matrix Ω.

(ii) Morse oscillator wavefunctions and energies.

Consider the Morse oscillator. The solution of $H\psi_n = E_n \psi_n$ with $V(\rho)$ given by (3-2) is (Shore, 1973b):

$$\psi_n(\rho) = \frac{1}{\sqrt{N_n}} \frac{1}{\sqrt{2Ke^{\beta(\rho_e - \rho)}}} M_{K,K-n-\frac{1}{2}}\left(2 K e^{\beta(\rho_e-\rho)}\right) \qquad (3\text{-}9)$$

where M is whittaker's function, expressible in terms of a confluent hypergeometric function (see Abramowitz & Stegun, 1964, and chapter V below),

and $$K = \frac{\sqrt{2\mu D}}{\beta\hbar} \; ; \quad N_n = \frac{\Gamma(n+1)\Gamma(2K-2n-1)}{\beta\,\Gamma(2K-n)}$$

These eigenvectors are not easy to calculate (see chapter V), but in contrast the eigenvalues have a simple form, which is not dependent on ρ_e:

$$E_n = Ax - \frac{A^2x^2}{4D} \qquad (3\text{-}10)$$

where $$A = \hbar\omega \; (= h\nu) \; ; \quad x = n + \tfrac{1}{2}.$$

Here the second term is an anharmonicity term, and ω is the angular frequency of the harmonic oscillator which fits the potential at the bottom of the well (see part (i) above). The energy levels are

relative to the bottom of the well as zero.

The highest level in the well is found by putting $E = D$

$$\Rightarrow \quad x = \frac{2D}{A} \qquad (= K)$$

and at this point, $\frac{\partial E}{\partial x} = 0$

Equation (3-10) was used to calculate some energy levels for X_2 and X_2^-, and the results are shown in table 2.

(iii) Harmonic oscillator overlap integrals.

Some idea of the form of the overlap matrix Ω can be gained by replacing the wavefunctions (3-9) by harmonic oscillator wavefunctions:

$$\psi_n^p(\rho) = N_n H_n(p) e^{-p^2/2}$$

where $p = P(\rho - p_0)$;

$N_n = \sqrt{\frac{P}{2^n\, n!\sqrt{\pi}}}$, a normalising constant,

and $H_n(x)$ is a Hermite polynomial.

Using the generating function for the Hermite polynomials (Abramowitz & Stegun, 1964), expanding the exponential, and equating coefficients, it is possible to derive an expression for overlap integrals between these wavefunctions, as suggested by Schrödinger (1926; see also Hutchisson, 1930). The result is:

$$\Omega_{nm} = \langle \psi_n^p | \psi_m^q \rangle$$

$$= e^F \sqrt{\frac{2PQ}{P^2 + Q^2}} \sqrt{\frac{n!\, m!}{2^{n+m}}}\, K_{nm} \qquad (3\text{-}11)$$

where

$$K_{nm} = \sum_{a=0}^{\mathrm{int}(\frac{1}{2}n)} \sum_{b=0}^{\mathrm{int}(\frac{1}{2}m)} \sum_{c=0}^{\min(n-2a,m-2b)} \frac{A^a B^b C^c D^{n-2a-c} E^{m-2b-c}}{a!b!c!(n-2a-c)!(m-2b-c)!}$$

where $\mathrm{int}(x)$ = largest integer $< x$

$\min(x,y)$ = smaller of x and y

and $$A = \frac{2P^2}{P^2+Q^2} - 1 \; ; \quad B = -A \; ; \quad C = \frac{4PQ}{P^2+Q^2} \; ;$$

$$D = \frac{2P(P^2p_0 + Q^2q_0)}{P^2+Q^2} - 2Pp_0 \; ; \quad E = \frac{2Q(P^2p_0 + Q^2q_0)}{P^2+Q^2} - 2Qq_0 \; ;$$

$$F = \frac{(P^2p_0 + Q^2q_0)^2}{2(P^2+Q^2)} - \tfrac{1}{2}(P^2p_0^2 + Q^2q_0^2)$$

It is readily verified that this gives $\Omega_{nm} = \delta_{nm}$ if $P = Q$ and $p_0 = q_0$. Using (3-11), the top left hand corner of Ω for X_2/X_2^- is as given in (3-25).

(iv) Solution of Morse oscillator by finite element method.

As already mentioned, it is not easy to work out the Morse oscillator wavefunctions (3-9), and overlap integrals between them. Numerical solution of the one-dimensional Schrödinger equation was therefore indicated, and since a fairly large number of wavefunctions was required, a global method, the finite element method using cubic splines, studied in particular by Shore (1973a; 1973c), was investigated.

Writing the Schrödinger equation in 1-D:

$$\mathcal{L}\,\psi(\rho) = 0 \quad \text{where} \quad \mathcal{L} = \frac{\hbar^2}{2m}\frac{d^2}{d\rho^2} + E - V(\rho) \qquad (3\text{-}12)$$

consider an approximation $\tilde{\psi}(\rho)$ of the true bound state ($E < 0$)

solution $\psi(\rho)$, given by a linear combination of basis functions ϕ, which in general do not form a complete set:

$$\tilde{\psi}(\rho) = \sum_{n=1}^{\tilde{N}} c_n \phi_n(\rho) \qquad (3\text{-}13)$$

with an outer boundary condition $\phi_n(\rho) = 0$ for $\rho \geq \rho_{max}$.

In the finite element method, each basis function $\phi_n(\rho)$ is non-zero over a limited range of ρ. Particularly popular for this is a cubic spline, which is a piecewise continuous function, with continuous first and second derivatives, expressible as a cubic polynomial in any subinterval of its domain. The cubic splines used are:

$$\phi_n(\rho) = \phi_0(\rho - nh)$$

$$\left.\begin{array}{lll} \text{where } \phi_0(\rho) = 0 & & |\rho| \geq 2h \\ \text{or } = f_1 = \tfrac{1}{4}(2 - |\rho/h|)^3 & & 2h \geq |\rho| \geq h \\ \text{or } = f_2 = \tfrac{1}{4}(2 - |\rho/h|)^3 - (1 - |\rho/h|)^3 & & h \geq |\rho| \end{array}\right\} \qquad (3\text{-}14)$$

These are B splines (Schoenberg, 1946), with knots (indicated in fig. 9) equidistant with spacing h.

The simplest method for obtaining the coefficients in (3-13) is the collocation method (see Collatz, 1966), which requires that $\tilde{\psi}(\rho)$ satisfy (3-12) exactly at various collocation points ρ_i. N such collocation points produce an $N \times N$ generalised matrix eigenvalue equation:

$$(\mathbb{A} - E\mathbb{B})\,\underset{\sim}{c} = 0$$

$$\text{where} \qquad A_{in} = -\frac{\hbar^2}{2m}\phi_n''(\rho_i) + V(\rho_i)\phi_n(\rho_i) \quad ;$$

$$B_{in} = \phi_n(\rho_i)$$

Spline knots shown thus •

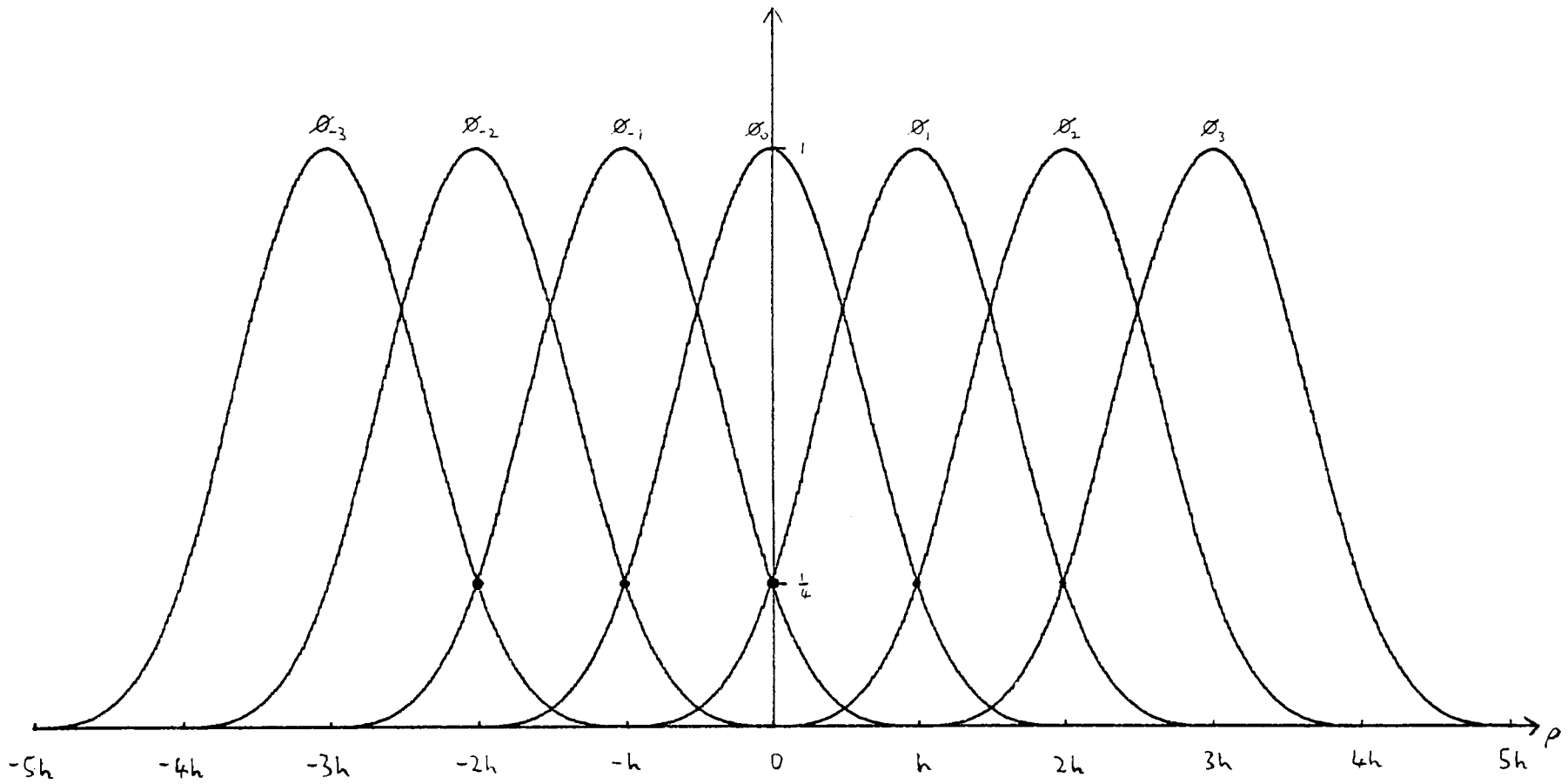

Fig. 9. "B" cubic splines.

The collocation points were placed, as suggested by Shore (1973a), at the spline knots, and the values of φ_n and φ_n'' at these are:

$\rho =$	ρ_{n-2}, ρ_{n-3} etc.	ρ_{n-1}	ρ_n	ρ_{n+1}	ρ_{n+2}, ρ_{n+3} etc.
$\varphi_n(\rho) =$	0	$\frac{1}{4}$	1	$\frac{1}{4}$	0
$\varphi_n''(\rho) =$	0	$\frac{1}{4}$	1	$\frac{1}{4}$	0

where ρ_n is the collocation point at the knot $\rho = nh$. As a result of the choice of collocation points, the matrices $\mathbb{A}$ and $\mathbb{B}$ are seen to be tridiagonal; production of banded matrices is one of the main advantages of the finite element method. However, there remains the important problem of boundary conditions, and in particular the form of the top left hand corners of the matrices. The right hand boundary condition

$$\sum_n c_n \varphi_n(\rho_{max}) = 0 \qquad (3\text{-}16)$$

is accommodated by using a finite basis set, with the collocation points ranging from some lower bound to $\rho_N = \rho_{max} - 2h$. Writing $V(\rho_i) = V_i$ and $\frac{3\hbar^2}{2m} = q$, the collocation equations are:

$$\left(\frac{q}{2h^2} + \frac{1}{4}(E - V_i)\right) c_{i-1} + \left(\frac{-q}{h^2} + (E - V_i)\right) c_i + \left(\frac{q}{2h^2} + \frac{1}{4}(E - V_i)\right) c_{i+1} = 0 \qquad (3\text{-}17)$$

From the left hand boundary condition

$$\sum_n c_n \varphi_n(0) \quad 0 \qquad (3\text{-}18)$$

it is clear that $\varphi_{-1}(\rho)$ must be included; (3-18) can be rewritten

$$c_{-1} = -(4c_0 + c_1) \qquad (3\text{-}19)$$

Putting $i = 0$ in (3-17) and combining with (3-19)

$$\Rightarrow c_0 = 0 \quad \text{and hence} \quad c_{-1} = -c_1$$

$$\therefore \tilde{\Psi}(\rho) = -c_1 \phi_{-1}(\rho) + \sum_{n=1}^{\tilde{N}} c_n \phi_n(\rho) \qquad (3\text{-}20)$$

where the coefficients in the summation are determined from

$$(\mathbb{A} - E\mathbb{B})\,\underset{\sim}{c} = 0$$

with

$$A_{ii} = \frac{q}{h^2} + V_i \;;$$

$$A_{i,i\pm1} = -\frac{q}{2h^2} + \frac{V_i}{4} \;;$$

$$B_{ii} = 1 \;; \qquad B_{i,i\pm1} = \tfrac{1}{4} \;;$$

$$A_{ij} = B_{ij} = 0 \quad \text{for } |i-j| \geq 2$$

The simple collocation method has been described mainly to illustrate manipulations with cubic splines. However, as reported by Shore (1973a), the eigenvalues it gives are rather poor. For an $O_2(X\,^3\Sigma_g^-)$ Morse potential (using $\omega = 1580.361\ cm^{-1}$; $\rho_e = 1.20739$ Å; $D = 5.080$ eV (Herzberg, 1950)), collocation with $h = 0.04$ Å; $N = 100$ (hence over the range 0-4 Å) gave the results shown in table 1 (note that all eigenvalues given are relative to the separated atoms).

Substantial improvement is obtained by recognising that collocation is just a special case of the general Galerkin method, in which (3-13) is substituted in (3-12) and various equations obtained by taking the scalar products of various functions $f_i(\rho)$ with the resulting equation:

$$\sum_n c_n \langle f_i(\rho) | \mathcal{L} \phi_n(\rho) \rangle = 0 \qquad (3\text{-}21)$$

The collocation method corresponds to $f_i(\rho) = \delta(\rho - \rho_i)$, and an improved method can be obtained by using projection functions $f_i(\rho)$ which are more delocalised than delta functions. The famous Rayleigh-Ritz-Galerkin (RRG) method uses $f_i(\rho) = \phi_i(\rho)$, and much of chapter II depends on this. Shore suggested using the RRG method applied to cubic splines with a 3-point Gaussian quadrature to evaluate the integrals:

$$\sum_p w_p \phi_i(\rho_p) \sum_n c_n \mathcal{L} \phi_n(\rho_p) = 0$$

with 12 abscissae ρ_p distributed about ρ_i, and weights w_p. Because of the limited domains of the splines, only ten of these abscissae give non-zero contributions. Also, $\phi_n(\rho_p) = 0$ for $|n - i| \geq 4$, with the result that the matrices $\mathbf{A}$ and $\mathbf{B}$ in the generalised eigenvalue equation produced are banded, with bandwidth 7:

$$A_{in} = \sum_{p=-5}^{+5} w_p \phi_i(\rho_p) \left(V(\rho_p)\phi_n(\rho_p) - \beta\phi_n''(\rho_p)\right);$$

$$B_{in} = \sum_{p=-5}^{+5} w_p \phi_i(\rho_p)\phi_n(\rho_p)$$

where $\beta = \hbar^2/2m$.

There is still the left hand boundary condition to consider, and much the simplest way to do this is to introduce a slightly modified basis $\bar{\phi}_i(\rho)$ $(i = 0, 1, 2, \ldots\ldots N)$, defined thus:

$$\left.\begin{aligned} \bar{\phi}_0(\rho) &= \phi_0(\ ) - 4\phi_{-1}(\rho); \\ \bar{\phi}_1(\rho) &= \phi_1(\rho) - \phi_{-1}(\rho); \\ \bar{\phi}_i(\rho) &= \phi_i(\rho) \quad \text{for } i \geq 2 \end{aligned}\right\} \qquad (3\text{-}22)$$

Then it can be seen that $\bar{\phi}_i(0) = 0$ for all i, hence

$$\tilde{\psi}(0) = \sum_{n=0}^{\tilde{}} c_n \bar{\varphi}_n(0) = 0$$

and the inner boundary condition is automatically satisfied.

Thus a 7-bandwidth generalised eigenvalue problem $(\mathbb{A} - E\mathbb{B})\underset{\sim}{c} = 0$ has to be solved, with

$$A_{ij} = \sum_{p=-5}^{+5} w_p \bar{\varphi}_i(\rho_p)\,(V(\rho_p)\bar{\varphi}_j(\rho_p) - \beta\,\bar{\varphi}_j''(\rho_p));$$

$$B_{ij} = \sum_{p=-5}^{+5} w_p \bar{\varphi}_i(\rho_p)\bar{\varphi}_j(\rho_p) \quad ;$$

$$A_{ij} = B_{ij} = 0 \qquad \text{for } |i-j| \geq 4 \qquad (3\text{-}23)$$

In table 1, results are given for a Morse approximation to O_2 $(X\,^3\Sigma_g^-)$ using the RRG method with various values of h, and N = 100 in each case. These are compared with exact results using (3-10) and results from a collocation calculation. It can be seen that the RRG results are much better than the collocation ones, also that the finite element results tend to give lower energies than the exact ones at low n, and higher energies at high n. Adjusting h can then be used to obtain a "best fit" over a given range of n.

With X_2 and X_2^-, it was necessary to use the same value of h for both calculations, to facilitate calculation of the overlap matrix (see (v) below). An optimum value of h = 0.04 Å was arrived at. Using this, the eigenvalues calculated were as shown in table 2.

(v) Morse oscillator overlap integrals.

The lowest 16 eigenvectors for X_2 and X_2^- corresponding to the eigenvalues given in table 2 were calculated, and from them a 16×16 truncated overlap matrix was calculated.

An element of the overlap matrix is given by:

$$\Omega_{mn} = \int_{-\infty}^{\infty} \Psi_m^{(1)}(\rho)\Psi_n^{(2)}(\rho)\,d\rho$$

n	|Eigenvalue| /cpe (relative to separated atoms)				
	Exact	Collocation h = 0.04 Å	RRG h = 0.04 Å	RRG h = 0.03 Å	RRG h = 0.02 Å
0	798.3	797.4	798.5	798.4	798.3
1	767.5	763.6	768.5	768.0	767.7
2	737.3	728.4	739.9	738.7	737.8
3	707.7	693.2	712.6	710.4	708.8
4	678.7	655.9	685.7	683.1	680.5
5	650.3	627.0	659.6	656.8	652.9
6	622.5	600.6	633.9	631.4	626.1
7	595.4	551.7	602.0	606.7	600.0
8	568.8	505.8	575.0	582.5	574.7
9	542.8	499.0	554.9	558.6	550.0
10	517.5	446.7	516.5	534.6	526.1
20	297.3	118.3	227.1	300.3	338.1
30	137.8	7.3	49.1	125.8	174.4

Table 1. O_2 ($X\ ^3\Sigma_g^-$) Morse eigenvalues

by finite element method with cubic splines

n	|Eigenvalue|/cpe							
	X_2				X_2^-			
	Morse		Harmonic		Morse		Harmonic	
	Exact	RRG	Exact	RRG	Exact	RRG	Exact	RRG
0	485.2	485.4	485.1	485.1	465.1	465.2	465.1	465.1
1	456.3	457.0	455.3	455.3	445.7	446.0	445.2	445.2
2	428.2	430.2	425.4	425.7	426.6	427.5	425.3	425.4
3	401.1	404.8	395.6	396.2	408.0	409.7	405.4	405.6
4	374.8	380.6	365.8	366.7	389.8	392.6	385.5	385.9
5	349.5	357.4	335.9	337.4	372.0	376.1	365.6	366.3
6	325.0	334.7	306.1	308.2	354.6	360.1	345.7	346.7
7	301.4	310.9	276.3	279.2	337.6	344.7	325.9	327.1
8	278.7	288.6	246.4	250.2	321.1	329.6	306.0	307.6
9	256.9	270.0	216.6	221.4	304.9	314.7	286.1	288.0
10	235.9	247.0	186.8	192.7	289.2	299.7	266.2	268.4
11	215.9	221.1	157.0	164.2	273.9	284.9	246.3	248.7
12	196.8	195.7	127.1	135.8	259.0	271.0	226.4	228.5
13	178.5	181.2	97.3	107.5	244.6	257.0	206.5	208.0
14	161.1	169.1	67.5	79.3	230.5	241.1	186.6	187.0
15	144.7	146.8	37.6	51.3	216.9	225.2	166.8	165.6

Table 2. X_2 & X_2^- Morse and Harmonic oscillator eigenvalues

The RRG results are with h = 0.04 Å (Morse) and h = 0.016 Å (Harmonic)

$$= \int_{-\infty}^{\infty} \left(\sum_{i=0}^{\tilde{N}} c_i^{(1)} \bar{\varphi}_i(\rho) \right) \left(\sum_{j=0}^{\tilde{N}} c_j^{(2)} \bar{\varphi}_j(\rho) \right) d\rho$$

$$= \sum_i \sum_j c_i^{(1)} c_j^{(2)} \int_{-\infty}^{\infty} \bar{\varphi}_i(\rho)\, \bar{\varphi}_j(\rho)\, d\rho \qquad (3\text{-}24)$$

Consider the integral in (3-24). For $|i - j| \geq 4$, the contribution to the sum will be zero, since the domains of the two basis splines do not intersect. For the remainder, the integral will take one of a few values; these were all worked out analytically in advance. Thus, provided the sets of eigenvectors have both been calculated using the same spline basis, calculation of the overlap integrals is now very easy. The non-zero contributions to the sum are given below.

If i & $j > 2$, then

$$\int_{-\infty}^{\infty} \bar{\varphi}_i(\rho)\, \bar{\varphi}_j(\rho)\, d\rho = \int_{-\infty}^{\infty} \varphi_i(\rho)\, \varphi_j(\rho)\, d\rho = hQ_{ij}$$

where Q_{ij} can take the following values:

$|i - j| \geq 4$: $\quad Q_{ij} = 0$

$|i - j| = 3$: $\quad Q_{ij} = \frac{1}{h} \int_0^h \varphi_{-1}(\rho)\, \varphi_2(\rho)\, d\rho = \frac{1}{2240} = 4.464 \times 10^{-4}$

$|i - j| = 2$: $\quad Q_{ij} = \frac{1}{h} \int_0^{2h} \varphi_0(\rho)\, \varphi_2(\rho)\, d\rho = \frac{3}{56} = 5.357 \times 10^{-2}$

$|i - j| = 1$: $\quad Q_{ij} = \frac{1}{h} \int_{-h}^{2h} \varphi_0(\rho)\, \varphi_1(\rho)\, d\rho = \frac{1191}{2240} = 5.317 \times 10^{-1}$

$i = j$: $\quad Q_{ij} = \frac{1}{h} \int_{-2h}^{2h} \{\varphi_0(\rho)\}^2\, d\rho = \frac{151}{140} = 1.079$

If i or $j \leq 2$, we require the following additional Q_{ij}'s:

$$\bar{Q}_{00} = \frac{1}{h}\int_{-\infty}^{\infty}\left[\phi_0(\rho) - 4\phi_{-1}(\rho)\right]^2 d\rho$$

$$= Q_{00} + 16Q_{-1,-1} - 8Q_{-1,0}$$

$$= \frac{3943}{280} = 14.08$$

$$\bar{Q}_{10} = \bar{Q}_{01} = \frac{1}{h}\int_{-\infty}^{\infty}\left[\phi_0(\rho) - 4\phi_{-1}(\rho)\right]\left[\phi_1(\rho) - \phi_{-1}(\rho)\right]d\rho$$

$$= 4.1 \quad \text{exactly}$$

$$\bar{Q}_{11} = \frac{1}{h}\int_{-\infty}^{\infty}\left[\phi_1(\rho) - \phi_{-1}(\rho)\right]^2 d\rho$$

$$= 2.05 \quad \text{exactly}$$

$$\bar{Q}_{20} = \bar{Q}_{02} = \frac{1}{h}\int_{-\infty}^{\infty}\left[\phi_0(\rho) - 4\phi_{-1}(\rho)\right]\phi_2(\rho)\, d\rho$$

$$= \frac{29}{560} = 5.179 \times 10^{-2}$$

$$\bar{Q}_{12} = \bar{Q}_{21} = \frac{1}{h}\int_{-\infty}^{\infty}\left[\phi_1(\rho) - \phi_{-1}(\rho)\right]\phi_2(\rho)\, d\rho$$

$$= \frac{17}{32} = 0.53125$$

Using these relations, the overlap of each vibrational state with itself was first calculated. The coefficients c_n were then divided by the square root of this overlap to normalise the wavefunction. The elements of the overlap matrix were then calculated in the same way.

The calculation was first performed using harmonic oscillator

wavefunctions for X_2 and X_2^-. The eigenvalues calculated with the chosen value of $h = 0.016$ Å are given in table 2. For these calculations, the origin was shifted 1.5 Å to the right, i.e. the domain of the wavefunctions was from $\rho = 1.5$ Å to $\rho = 3.1$ Å with $N = 100$. It is intuitively clear that such a shift of the origin should not affect values of the energy levels or the overlap integrals, but a large region in which the wavefunctions are effectively zero is removed from the calculation. In other words, the overlap integrals are dependent only on the difference between the two equilibrium distances, and this is confirmed by examination of (3-11), when it can be readily shown that replacing p_0 by $(p_0 - q_0)$ and q_0 by zero does not alter the expression. The top left hand corner of the full 16×16 harmonic oscillator matrix calculated in this way is as follows:

$$\Omega^{h.o.} = \begin{array}{c} \\ n: \\ 0 \\ 1 \\ 2 \\ 3 \\ 4 \\ 5 \\ 6 \\ \vdots \end{array} \begin{array}{c} \begin{array}{ccccccc} m: 0 & 1 & 2 & 3 & 4 & 5 & 6 \end{array} \\ \begin{pmatrix} .8423 & .5243 & .1115 & -.0455 & .0336 & .0014 & .0057 \\ .4277 & -.5582 & -.6703 & -.2132 & -.0720 & -.0731 & .0064 \\ .2729 & -.4226 & .3203 & .7214 & -.3179 & .0851 & -.1214 \\ -.1502 & .3697 & -.3219 & .1352 & -.7106 & -.4162 & -.0828 \\ -.0861 & .2412 & -.3934 & .1813 & .0051 & .6566 & -.5007 \\ -.0470 & .1597 & -.2966 & .3635 & .0313 & .0713 & .5740 \\ -.0259 & .0969 & -.2248 & .3136 & .2972 & .1085 & .0984 \\ \vdots & & & & & & \end{pmatrix} \end{array} \quad \ldots$$

(3-25)

This should be compared with the exact matrix calculated using (3-11):

$\Omega^{h.o.}$ (exact)

$$= \begin{pmatrix} .8429 & -.5234 & .1106 & .0458 & -.0334 & .0011 & .0058 & \cdots \\ .4274 & .5606 & -.6692 & .2109 & .0729 & -.0726 & .0055 & \\ .2724 & .4230 & .3250 & -.7209 & .3137 & .0870 & -.1204 & \\ .1495 & .3695 & .3243 & .1418 & -.7119 & .4104 & .0862 & \\ .0851 & .2402 & .3945 & .1862 & .0128 & -.6608 & .4935 & \\ .0460 & .1578 & .2963 & .3670 & .0388 & -.0638 & -.5819 & \\ .0251 & .0949 & .2226 & .3152 & .3039 & -.0992 & -.0929 & \\ \vdots & & & & & & & \end{pmatrix} \qquad (3\text{-}26)$$

and it can be seen that, apart from the arbitrary appearance of phase factors of -1 applied to some eigenvectors, there is quite good agreement.

The calculation was then performed using Morse oscillators, and the result, corresponding to the eigenvalues given in table 2, is as follows:

$$\Omega = \begin{pmatrix} -.8454 & .5010 & -.1804 & -.0256 & .0200 & .0210 & .0118 & \cdots \\ .4687 & .5570 & -.6070 & -.3058 & -.0707 & -.0278 & .0429 & \\ -.2370 & -.5264 & -.3094 & -.6160 & -.4099 & .1329 & .0235 & \\ .0853 & .3596 & .4924 & -.1072 & -.5673 & .4864 & -.2047 & \\ ..0300 & .1533 & .4397 & -.4142 & -.0454 & -.4861 & .5315 & \\ .0062 & .0613 & .2137 & -.4830 & .3162 & -.1518 & -.3880 & \\ -.0018 & -.0135 & -.0957 & .2675 & -.5101 & -.2379 & .2243 & \\ \vdots & & & & & & & \end{pmatrix} \qquad (3\text{-}27)$$

This is fairly similar to the harmonic oscillator result, the difference becoming greater further from the top left hand corner. Using the 16×16 version of Ω, the following matrices were calculated:

$$\Omega^{-1} = \begin{pmatrix} -.8458 & .4690 & -.2393 & .0875 & .0305 & .0064 & -.0019 & \cdots \\ .5006 & .5585 & -.5271 & .3668 & .1604 & .0642 & -.0145 & \\ -.1802 & -.6060 & -.3136 & .4933 & .4550 & .2307 & -.1033 & \\ -.0268 & -.3039 & -.6149 & -.1159 & -.4136 & .5113 & .2999 & \\ .0180 & -.0727 & -.4040 & -.5683 & -.0305 & .3122 & -.5555 & \\ -.0197 & -.0219 & .1334 & .4744 & -.4925 & .1285 & -.2264 & \\ .0120 & .0374 & .0125 & -.1992 & .5125 & .4059 & .1920 & \\ \vdots & & & & & & & \end{pmatrix}$$

(3-28)

$$\mathcal{K}/\text{cpe} = \begin{pmatrix} 2.03\times10^{-4} & 10.13 & -2.88 & -1.83 & 0.805 & -0.253 & 7.05\times10^{-3} & \cdots \\ 10.13 & -1.74\times10^{-2} & 14.57 & -4.60 & 3.58 & -1.78 & -0.490 & \\ -2.80 & 14.56 & -0.135 & 18.15 & 6.02 & -5.80 & -3.23 & \\ -1.71 & -4.33 & 18.08 & -0.530 & -21.16 & -7.31 & -8.31 & \\ 0.835 & 3.15 & 5.42 & -20.97 & -1.36 & -23.92 & 7.19 & \\ -0.426 & -1.74 & -4.65 & -6.09 & -23.49 & -3.20 & 27.58 & \\ -0.195 & -0.919 & -2.79 & -5.87 & 5.41 & 26.54 & -6.98 & \\ \vdots & & & & & & & \end{pmatrix}$$

(3-29)

Note that, ideally,

$$\Omega^{-1} = \widetilde{\Omega} ;$$

$$X_{ij} = X_{ji} ;$$

$$X_{ii} = 0 .$$

A slight discrepency is expected because only 16 vibrational states in each channel have been used, instead of a complete set. In calculations below which use $\mathcal{K}$, the diagonal elements were set to zero.

Calculation of 256 (16×16) elements of Ω took $\sim$900 seconds of computer time (including calculation of the eigenvectors), i.e. < 4 sec for one integral on average, achieving an absolute accuracy indicated by the harmonic oscillator calculation of about ± 0.001. One important advantage of the finite element method is the production of banded matrices; unfortunately this was not made use of since the only generalised eigenvalue routine available was for general matrices. Use of a routine for banded matrices would be expected to speed up the calculation, also to free much of the core, so that a larger N could be used.

C The Magnus approximation.

One approach to the solution of the differential equations arising from the multi-curve crossing theory is to propagate the solution in matrix form from one time to another using a method due to Magnus (1954). This remained fairly unknown until the work of Pechukas & Light (1966), which is that usually referred to.

Consider the a-coefficient differential equations (2-61) & (2-64):

$$\left[i\hbar \frac{d}{dt} - E_{1n} - V_{11}(t) \right] c_{1n}(t) = V_{12}(t)\, a_{2n}(t) \qquad (2\text{-}61)$$

$$\left[i\hbar \frac{d}{dt} - \bar{E}_{2n} - V_{22}(t) \right] a_{2n}(t) = \sum_{n' \neq n} X_{nn'}\, a_{2n'}(t) + V_{12}(t)\, c_{1n}(t) \qquad (2\text{-}64)$$

These can be rewritten in matrix form:

$$(2\text{-}61): \quad i\hbar \frac{d}{dt} \underset{\sim}{c}_1(t) = \mathbb{W}_1(t)\, \underset{\sim}{c}_1(t) + V_{12}(t)\, \mathbb{I}\, \underset{\sim}{a}_2(t) \qquad (3\text{-}30)$$

$$\text{where} \qquad (\mathbb{W}_1)_{ij} = (E_{1i} + V_{11}(t))\, \delta_{ij}$$

and $\underset{\sim}{c}_1$ and $\underset{\sim}{a}_2$ are column vectors of the c- and a-coefficients respectively;

(2-64): $$i\hbar \frac{d}{dt} \underset{\sim}{a}_2(t) = V_{12}(t)\,\mathbb{I}\,\underset{\sim}{c}_1(t) + (\bar{W}_2 + \mathbb{K})\,\underset{\sim}{a}_2(t) \qquad (3\text{-}31)$$

where $$(\bar{W}_2)_{ij} = (\bar{E}_{2i} + V_{22}(t))\,\delta_{ij}$$

Equations (3-30) & (3-31) can be combined by a direct summation:

$$i\hbar \frac{d}{dt} \underset{\sim}{v}(t) = \mathbb{H}(t)\,\underset{\sim}{v}(t) \qquad (3\text{-}32)$$

This is the important final form for the matrix formulation of the problem. If the ionic and covalent basis sets are truncated to N elements, $\underset{\sim}{v}$ is a 2N-dimensional column vector:

$$\underset{\sim}{v}(t) = \begin{pmatrix} c_{11}(t) \\ \vdots \\ c_{1N}(t) \\ a_{21}(t) \\ \vdots \\ a_{2N}(t) \end{pmatrix}$$

and $\mathbb{H}(t)$ is a $2N \times 2N$ matrix:

$$\mathbb{H}(t) = \begin{pmatrix} W_1(t) & V_{12}(t)\mathbb{I} \\ V_{12}(t)\mathbb{I} & \bar{W}_2(t) + \mathbb{K} \end{pmatrix}$$

Equation (3-32) is superficially similar to (2-68), and the solution is written formally:

$$\underset{\sim}{v}(t) = \left\{ \exp\left[-\frac{i}{\hbar} \int_0^t \mathbb{H}(t')\,dt' \right] \right\} \underset{\sim}{v}(0) \qquad (3\text{-}33)$$

but care must be taken in evaluating it, because $\mathbb{H}$ is a function of t, and its value at one time does not generally commute with that at

another. It is usual first to convert (3-32) to an operator equation (Child, 1974) by introducing the time evolution matrix U:

$$\underset{\sim}{v}(t) = U(t,t_0)\,\underset{\sim}{v}(t_0)$$

$$\Rightarrow \quad i\hbar \frac{d}{dt} U(t,t_0) = \mathcal{H}(t)\,U(t,t_0) \qquad (3\text{-}34)$$

with the boundary condition $U(t_0,t_0) = \mathbb{I}$

$$\Rightarrow \quad U(t,t_0) = \left\{ \exp\left[-\frac{i}{\hbar} \int_{t_0}^{t} \mathcal{H}(t')\,dt' \right] \right\} \qquad (3\text{-}35)$$

Hence the scattering matrix S, which describes the only evolution physically measurable, is written formally

$$S = U(\infty,-\infty) = \left\{ \exp\left[-\frac{i}{\hbar} \int_{-\infty}^{\infty} \mathcal{H}(t)\,dt \right] \right\} \qquad (3\text{-}36))$$

One method for giving meaning to this expression is to turn the differential equation (3-34) into an integral equation, and iterate the right hand side, giving a series analogous to the Born series (Child, 1974):

$$U(t,t_0) = \mathbb{I} - \frac{i}{\hbar} \int_{t_0}^{t} \mathcal{H}(t_1)\,dt_1 + \left(\frac{i}{\hbar}\right)^2 \int_{t_0}^{t} \left[\int_{t_0}^{t_1} \mathcal{H}(t_1)\mathcal{H}(t_2)\,dt_2 \right] dt_1 + \ldots \qquad (3\text{-}37)$$

A disadvantage of this series is that if it is truncated, the unitarity of U, necessary for conservation of probability, is destroyed. More useful computationally is the Magnus form for (3-35) (Pechukas & Light, 1966):

$$U(t,t_0) = \exp\left[\mathbb{A}(t,t_0)\right] = \mathbb{I} + \mathbb{A}(t,t_0) + \tfrac{1}{2}\mathbb{A}^2(t,t_0) + \ldots \qquad (3\text{-}38)$$

where $$\mathbb{A}(t,t_0) = \mathbb{A}^{(1)}(t,t_0) + \mathbb{A}^{(2)}(t,t_0) + \ldots \qquad (3\text{-}39)$$

where $$\mathbb{A}^{(1)}(t,t_0) = -\frac{i}{\hbar}\int_{t_0}^{t} \mathbb{H}(t_1)\,dt_1 \quad ;$$

$$\mathbb{A}^{(2)}(t,t_0) = \frac{1}{2}\left(\frac{i}{\hbar}\right)^2 \int_{t_0}^{t}\left[\int_{t_0}^{t_1}\left[\mathbb{H}(t_1),\mathbb{H}(t_2)\right]dt_2\right]dt_1 \quad ;$$

$$\mathbb{A}^{(3)}(t,t_0) = -\frac{1}{6}\left(\frac{i}{\hbar}\right)^3 \int_{t_0}^{t}\left\{\int_{t_0}^{t_1}\left[\int_{t_0}^{t_2}\left(\left[\mathbb{H}(t_3),\left[\mathbb{H}(t_2),\mathbb{H}(t_1)\right]\right] + \left[\left[\mathbb{H}(t_3),\mathbb{H}(t_2)\right],\mathbb{H}(t_1)\right]\right)dt_3\right]dt_2\right\}dt_1$$

and so on. Note the appearance of the non-zero commutators in the second and higher order terms. Now, if $\mathbb{H}$ is Hermitian, it can be shown that $\mathbb{A}$ is anti-Hermitian, no matter where the series for it is truncated, using the fact that the commutator of two non-commuting Hermitian matrices is anti-Hermitian. Hence U is always unitary, being the exponential of an anti-Hermitian matrix (provided the exponential series is worked out in full).

Before considering the evaluation of the two series (3-38) & (3-39), consider the various possibilities for the basis $\underset{\sim}{v}(t)$:

(i) Basis A:

$$\underset{\sim}{v} = \begin{pmatrix} \underset{\sim}{c}_1 \\ \underset{\sim}{a}_2 \end{pmatrix} \quad ; \qquad \mathbb{H} = \begin{pmatrix} \mathbb{W}_1 & V_{12}\mathbb{I} \\ V_{12}\mathbb{I} & \bar{\mathbb{W}}_2 + \mathbb{X} \end{pmatrix}$$

This is the basis discussed in the introduction to the Magnus method above, i.e. it corresponds to the basic a-coefficient equations (2-61) & (2-64). Notice that, as required, $\mathbb{H}(t)$ is Hermitian, because $\mathbb{W}_1$ and $\bar{\mathbb{W}}_2$ are diagonal, and $\mathbb{X}$ is symmetric.

(ii) The series (3-38) will converge very slowly for the matrix corresponding to basis A, because of the very large terms on the

diagonal. The situation can be improved by "removing" the zeroth order E terms from the diagonal into phase factors, as in the transformation of (2-34), i.e. define

$$c_{1n}(t) = \gamma'_n(t) \exp\left\{ -\frac{i}{\hbar} E_{1n}\, t \right\}$$

and $$a_{2n}(t) = \alpha'_n(t) \exp\left\{ -\frac{i}{\hbar} \bar{E}_{2n}\, t \right\}$$

Then, with $\Gamma_n(t) = \frac{i}{\hbar} E_{1n}\, t$; $A_n(t) = \frac{i}{\hbar} \bar{E}_{2n}\, t$,

(2-61) becomes

$$\left[i\hbar \frac{d}{dt} - V_{11}(t) \right] \gamma'_n(t) = V_{12}(t) \exp(\Gamma_n - A_n)\, \alpha'_n(t) \qquad (3\text{-}40)$$

and (2-64) becomes

$$\left[i\hbar \frac{d}{dt} - V_{22}(t) \right] \alpha'_n(t) = \sum_{n' \neq n} X_{nn'} \exp(A_n - A_{n'})\, \alpha'_{n'}(t) + V_{12}(t) \exp(A_n - \Gamma_n)\, \gamma'_n(t) \qquad (3\text{-}41)$$

Combining (3-40) & (3-41) in matrix form, we again get

$$i\hbar \frac{d}{dt} \underset{\sim}{v}(t) = \mathbb{H}(t)\, \underset{\sim}{v}(t)$$

where now we are using

Basis B: ("interaction picture")

$$\underset{\sim}{v} = \begin{pmatrix} \underset{\sim}{\gamma}'(t) \\ \underset{\sim}{\alpha}'(t) \end{pmatrix} \quad ; \qquad \mathbb{H} = \begin{pmatrix} V_{11}\mathbb{I} & \mathbb{K}_{12} \\ \mathbb{K}_{21} & V_{22}\mathbb{I} + \bar{\mathbb{X}} \end{pmatrix}$$

where $$\gamma'_n(t) = c_{1n}(t) \exp\left\{ \frac{i}{\hbar} E_{1n}\, t \right\} ;$$

$$\alpha'_n(t) = a_{2n}(t) \exp\left\{\frac{i}{\hbar}\bar{E}_{2n}\, t\right\} \quad ;$$

$$(\mathbb{K}_{12})_{ij} = V_{12}(t)\,\delta_{ij} \exp\left\{\frac{i}{\hbar}(E_{1i} - \bar{E}_{2i})t\right\} \quad ;$$

$$(\mathbb{K}_{21})_{ij} = V_{12}(t)\,\delta_{ij} \exp\left\{\frac{i}{\hbar}(\bar{E}_{2i} - E_{1i})t\right\} \quad ;$$

$$(\bar{\mathbb{X}})_{ij} = 0 \qquad \text{for } i = j$$

$$\text{or} \quad X_{ij} \exp\left\{\frac{i}{\hbar}(\bar{E}_{2i} - \bar{E}_{2j})t\right\} \qquad \text{for } i \neq j$$

$\mathbb{K}_{12}$ and $\mathbb{K}_{21}$ are diagonal, with corresponding elements complex conjugates of each other, and $\mathbb{X}$ is symmetric $\Rightarrow \bar{\mathbb{X}}$ is Hermitian, hence $\mathbb{H}(t)$ is Hermitian once again.

(iii) Further improvement in rate of convergence of (3-38) will clearly be obtained by removing the first order V terms from the diagonal as well. This has already been discussed in the treatment leading up to equations (2-74) & (2-75), and conversion of these to matrix form gives

Basis C:

$$\underset{\sim}{v}(t) = \begin{pmatrix} \underset{\sim}{\gamma}(t) \\ \underset{\sim}{\alpha}(t) \end{pmatrix} \quad ; \quad \mathbb{H} = \begin{pmatrix} 0 & \mathbb{K}_{12} \\ \mathbb{K}_{21} & \bar{\mathbb{X}} \end{pmatrix} \qquad (3\text{-}42)$$

$$\text{where} \quad \gamma_n(t) = c_{1n}(t) \exp\left\{\frac{i}{\hbar}\int_0^t W_{1n}(t')\,dt'\right\} \quad ; \quad (3\text{-}43)$$

$$\alpha_n(t) = a_{2n}(t) \exp\left\{\frac{i}{\hbar}\int_0^t \bar{W}_{2n}(t')\,dt'\right\} \quad ; \quad (3\text{-}44)$$

$$W_{1n}(t) = E_{1n} + V_{11}(t) \quad ; \qquad (2\text{-}65)$$

$$\bar{W}_{2n}(t) = \bar{E}_{2n} + V_{22}(t) \qquad (2\text{-}66)$$

$$(\mathbb{K}_{12})_{ij} = V_{12}(t)\,\delta_{ij} \exp\left\{\frac{i}{\hbar}\int (W_{1i} - \bar{W}_{2i})\,dt\right\} ;$$

$$(\mathbb{K}_{21})_{ij} = V_{12}(t)\,\delta_{ij} \exp\left\{\frac{i}{\hbar}\int (\bar{W}_{2i} - W_{1i})\,dt\right\} ;$$

and $$(\bar{\mathbb{X}})_{ij} = 0 \qquad \text{for } i = j$$

or $$X_{ij} \exp\left\{\frac{i}{\hbar}\int (\bar{W}_{2i} - \bar{W}_{2j})\,dt\right\}$$

$$= X_{ij} \exp\left\{\frac{i}{\hbar}(\bar{E}_{2i} - \bar{E}_{2j})t\right\} \qquad \text{for } i \neq j.$$

(iv) So far, the basis sets have all been based on the a-coefficient approach. Two examples follow using the c-coefficient approach.

Basis D:

$$\underset{\sim}{v}(t) = \begin{pmatrix} \underset{\sim}{c}_1(t) \\ \underset{\sim}{c}_2(t) \end{pmatrix} ; \quad \mathbb{H} = \begin{pmatrix} \mathbb{W}_1 & V_{12}\Omega \\ V_{12}\Omega^{-1} & \mathbb{W}_2 \end{pmatrix}$$

where $$(\mathbb{W}_1)_{ij} = (E_{1i} + V_{11}(t))\,\delta_{ij} ;$$

$$(\mathbb{W}_2)_{ij} = (E_{2i} + V_{22}(t))_{ij}$$

This is the matrix form of the original coupled equations (2-54) & (2-58).

Basis E:

$$\underset{\sim}{v}(t) = \begin{pmatrix} \underset{\sim}{y}_1(t) \\ \underset{\sim}{y}_2(t) \end{pmatrix} ; \quad \mathbb{H} = \begin{pmatrix} 0 & \mathbb{K}_{12} \\ \mathbb{K}_{21} & 0 \end{pmatrix} \qquad (3\text{-}45)$$

where $$\gamma_{1n}(t) = c_{1n}(t) \exp\left\{\frac{i}{\hbar}\int W_{1n}(t)\,dt\right\} \quad ; \qquad (3\text{-}46)$$

$$\gamma_{2m}(t) = c_{2m}(t) \exp\left\{\frac{i}{\hbar}\int W_{2m}(t)\,dt\right\} \quad ; \qquad (3\text{-}47)$$

where $$W_{2m}(t) = E_{2m} + V_{22}(t)$$

i.e. this is a c-coefficient formulation with all terms removed from the diagonal of $\mathbb{H}$;

$$(\mathbb{K}_{12})_{ij} = V_{12}\Omega_{ij} \exp\left\{\frac{i}{\hbar}\int (W_{1i} - W_{2j})\,dt\right\} \quad ;$$

$$(\mathbb{K}_{21})_{ij} = V_{12}\Omega^{-1}_{ij} \exp\left\{\frac{i}{\hbar}\int (W_{2i} - W_{1j})\,dt\right\}$$

$$= (\mathbb{K}_{21})^{*}_{ji}$$

It is readily verified that $\mathbb{H}$ is Hermitian for the bases C, D & E. E can be derived from D in the same way as C from A. Alternatively, it can be derived from C directly, by matrix manipulation, as follows:

We need a transformation between (3-43) & (3-44) and (3-46) & (3-47). Comparing (3-43) & (3-46),

$$\gamma_n(t) = \gamma_{1n}(t)$$

Now, (3-47) $\Rightarrow$ $$c_{2m}(t) = \gamma_{2m}(t) \exp\left\{-\frac{i}{\hbar}\int W_{2m}(t)\,dt\right\}$$

$$\Rightarrow \quad a_{2n}(t) = \sum_{m'} \Omega_{nm'} c_{2m'}(t)$$

$$= \sum_{m'} \Omega_{nm'} \gamma_{2m'}(t) \exp\left\{-\frac{i}{\hbar}\int W_{2m'}(t)\,dt\right\}$$

$$\therefore \quad \alpha_n(t) = a_{2n}(t) \exp\left\{\frac{i}{\hbar}\int \overline{W}_{2n}(t)\,dt\right\}$$

$$= \sum_{m'} \Omega_{nm'}\,\gamma_{2m'}(t) \exp\left\{\frac{i}{\hbar}\int (\overline{W}_{2n} - W_{2m'})\,dt\right\}$$

$$\Rightarrow \quad \underset{\sim}{\alpha} = \overline{\Omega}\,\underset{\sim}{\gamma}_2$$

where $$(\overline{\Omega})_{ij} = \Omega_{ij} \exp\left\{\frac{i}{\hbar}\int (\overline{W}_{2i} - W_{2j})\,dt\right\}$$

$$\therefore \quad \underset{\sim}{v} = \begin{pmatrix} \underset{\sim}{\gamma} \\ \underset{\sim}{\alpha} \end{pmatrix} = \begin{pmatrix} \mathbb{I} & 0 \\ 0 & \overline{\Omega} \end{pmatrix} \begin{pmatrix} \underset{\sim}{\gamma}_1 \\ \underset{\sim}{\gamma}_2 \end{pmatrix}$$

$$= \mathbb{P}\,\underset{\sim}{x} \qquad \text{say.}$$

But, $$i\hbar \frac{d}{dt}\,\underset{\sim}{v} = \mathbb{H}\,\underset{\sim}{v} \qquad \text{with } \mathbb{H} \text{ given by (3-42)}$$

$$\Rightarrow \quad i\hbar \frac{d}{dt}(\mathbb{P}\,\underset{\sim}{x}) = \mathbb{H}\mathbb{P}\,\underset{\sim}{x}$$

$$\Rightarrow \quad \mathbb{P}\, i\hbar \frac{d}{dt}\,\underset{\sim}{x} + \left(i\hbar \frac{d}{dt}\mathbb{P}\right)\underset{\sim}{x} = \mathbb{H}\mathbb{P}\,\underset{\sim}{x}$$

$$i\hbar \frac{d}{dt}\,\underset{\sim}{x} = \mathbb{M}\,\underset{\sim}{x}$$

with $$\mathbb{M} = \mathbb{P}^{-1}\mathbb{H}\mathbb{P} - \mathbb{P}^{-1} i\hbar\, \dot{\mathbb{P}}$$

which is the required new $\mathbb{H}$ matrix.

Now, $$\mathbb{P} = \begin{pmatrix} \mathbb{I} & 0 \\ 0 & \overline{\Omega} \end{pmatrix}$$

$$\Rightarrow \quad \mathbb{P}^{-1} = \begin{pmatrix} \mathbb{I} & 0 \\ 0 & \overline{\Omega}^{-1} \end{pmatrix}$$

and $$i\hbar\, \dot{\mathbb{P}} = \begin{pmatrix} 0 & 0 \\ 0 & i\hbar\, \dot{\overline{\Omega}} \end{pmatrix}$$

$$\Rightarrow \mathbb{P}^{-1}\mathbb{H}\mathbb{P} = \begin{pmatrix} \mathbb{I} & 0 \\ 0 & \bar{\Omega}^{-1} \end{pmatrix} \begin{pmatrix} 0 & \mathbb{K}_{12} \\ \mathbb{K}_{21} & \bar{\mathbb{W}} \end{pmatrix} \begin{pmatrix} \mathbb{I} & 0 \\ 0 & \bar{\Omega} \end{pmatrix}$$

$$= \begin{pmatrix} 0 & \mathbb{K}_{12}\bar{\Omega} \\ \bar{\Omega}^{-1}\mathbb{K}_{21} & \bar{\Omega}^{-1}\mathbb{W}\bar{\Omega} \end{pmatrix}$$

and $$\mathbb{P}^{-1}\, i\hbar\, \dot{\mathbb{P}} = \begin{pmatrix} 0 & 0 \\ 0 & \bar{\Omega}^{-1}\, i\hbar\, \dot{\bar{\Omega}} \end{pmatrix}$$

$$\therefore \mathbb{M} = \begin{pmatrix} 0 & \mathbb{K}_{12}\bar{\Omega} \\ \bar{\Omega}^{-1}\mathbb{K}_{21} & \bar{\Omega}^{-1}\bar{\mathbb{W}}\bar{\Omega} - \bar{\Omega}^{-1}\, i\hbar\, \dot{\bar{\Omega}} \end{pmatrix}$$

Now $$(\bar{\Omega})_{ij} = \Omega_{ij} \exp\left\{\frac{i}{\hbar}\int (\bar{W}_{2i} - W_{2j})\, dt\right\}$$

$$\Rightarrow (\bar{\Omega}^{-1})_{ij} = \Omega^{-1}_{ij} \exp\left\{\frac{i}{\hbar}\int (W_{2i} - \bar{W}_{2j})\, dt\right\}$$

and $$(i\hbar\dot{\Omega})_{ij} = \Omega_{ij}(W_{2j} - \bar{W}_{2i}) \exp\left\{\frac{i}{\hbar}\int (\bar{W}_{2i} - W_{2j})dt\right\} \qquad (3\text{-}48)$$

But $$(\bar{\mathbb{W}}\bar{\Omega})_{ij} = \sum_p (\bar{\mathbb{W}})_{ip}(\bar{\Omega})_{pj}$$

$$= \sum_p X_{ip} \exp\left\{\frac{i}{\hbar}\int (\bar{W}_{2i} - \bar{W}_{2p})dt\right\} \Omega_{pj} \exp\left\{\frac{i}{\hbar}\int (\bar{W}_{2p} - W_{2j})dt\right\}$$

$$= \exp\left\{\frac{i}{\hbar}\int (\bar{W}_{2i} - W_{2j})\, dt\right\} (\mathbb{W}\Omega)_{ij}$$

and $$(\mathbb{W}\Omega)_{ij} = \sum_p \sum_m \Omega_{im}(E_{2m} - \bar{E}_{2i})\Omega^{-1}_{mp}\Omega_{pj}$$

$$= \Omega_{ij}(E_{2j} - \bar{E}_{2i})$$

$$= \Omega_{ij}(W_{2j} - \bar{W}_{2i})$$

Comparing this with (3-48), we see that $i\hbar\dot{\bar{\Omega}} = \bar{K}\bar{\Omega}$

$$\therefore M = \begin{pmatrix} 0 & K_{12}\bar{\Omega} \\ \bar{\Omega}^{-1}K_{21} & 0 \end{pmatrix}$$

with $(K_{12}\bar{\Omega})_{ij}$

$$= \sum_k V_{12}\,\delta_{ik} \exp\left\{\frac{i}{\hbar}\int (W_{1i} - \bar{W}_{2k})dt\right\} \Omega_{kj} \exp\left\{\frac{i}{\hbar}\int (\bar{W}_{2k} - W_{2j})dt\right\}$$

$$= V_{12}\,\Omega_{ij} \exp\left\{\frac{i}{\hbar}\int (W_{1i} - W_{2j})\,dt\right\}$$

and $(\bar{\Omega}^{-1}K_{21})_{ij}$

$$= \sum_k \Omega^{-1}_{ik} \exp\left\{\frac{i}{\hbar}\int (W_{2i} - \bar{W}_{2k})dt\right\} V_{12}\,\delta_{kj} \exp\left\{\frac{i}{\hbar}\int (\bar{W}_{2k} - W_{1j})dt\right\}$$

$$= V_{12}\,\Omega^{-1}_{ij} \exp\left\{\frac{i}{\hbar}\int (W_{2i} - W_{1j})\,dt\right\}$$

which is the result given in (3-45).

D Magnus solution to coupled equations.

Consider equation (3-32):

$$i\hbar\frac{d}{dt}\underset{\sim}{v}(t) = H(t)\,\underset{\sim}{v}(t) \qquad (3\text{-}32)$$

The problem is, given $\underset{\sim}{v}(-\infty)$, to find $\underset{\sim}{v}(+\infty)$, and in the Magnus method this is solved by calculating the scattering matrix S given by (3-36). In practice, the collision is defined to take place between large times $-t_f$ and t_f, large enough tnat $U(t_f,-t_f)$ does not differ significantly from S. Then the final vector of coefficients

is given by:

$$\underset{\sim}{y}(t_f) = U(t_f,-t_f)\,\underset{\sim}{y}(-t_f) \qquad (3\text{-}50)$$

The advantages of the Magnus method are:

(i) A complete scattering matrix is produced, so that once it is calculated the results of collisions with any starting conditions are readily calculated by a simple matrix multiplication (3-50);

(ii) The scattering matrix produced is unitary, provided series (3-38) is summed fully.

However, a disadvantage is that truncation of (3-39) still introduces errors, so that unitarity of the scattering matrix is no guarantee of its accuracy.

$U(t_f,-t_f)$ could be calculated directly by summing (3-38) & (3-39) for the entire time interval $[-t_f,t_f]$. However, in view of the disadvantage mentioned above, and the desirability of truncating both series to a few terms, an alternative implementation of the Magnus method was investigated:

Consider $U(t,t_0)$, where t and t_0 are very nearly equal. Then the commutators between H's at different times are small, and series (3-39) can be truncated to one term. This preserves the unitarity of U, although the results will be slightly different. However, A itself is small, so (3-38) can be truncated to two terms, although this does remove the unitarity of the matrix slightly. Bearing these properties of small time intervals in mind, the technique is to divide the time interval $[-t_f,t_f]$ into small segments δt; then

$$U(t+\delta t,-t_f) = U(t+\delta t,\,t)\,U(t,-t_f) \qquad (3\text{-}51)$$

$U(t_f,-t_f)$ is calculated by multiplying together successive increments $U(t+\delta t,t)$ until $t+\delta t = t_f$. For each increment, δt is

assumed sufficiently small that both series (3-38) & (3-39) may be truncated to first order. When this is done, it can be seen that it is equivalent to truncating the Born type series (3-37) to first order.

Now, if the system starts off in the ground vibrational state of the covalent channel, which we shall always assume, then the initial vector is

$$\underset{\sim}{v}(-t_f) = \begin{pmatrix} 1 \\ 0 \\ 0 \\ \vdots \\ \vdots \\ \vdots \\ \vdots \\ \vdots \end{pmatrix}$$

and substituting this in (3-50) gives

$$\underset{\sim}{v}(t_f) = \text{first column of } U(t_f,-t_f) \qquad (3\text{-}52)$$

The square modulus of each final c-coefficient then gives the probability of transition to the appropriate vibrational level from the initial ground state covalent level.

This method was tried with various bases $\underset{\sim}{v}(t)$, and non-unitarity of the scattering, gauged by comparing the sum of the transition probabilities with unity, was used as an indication of the poorness of the results, although, as described above, unitarity is not expected to be a completely reliable indication of goodness. After calculations in which a-coefficients were involved, i.e. based on the coupled equations (2-61) & (2-64), the coefficients at the end were transformed back to c-coefficients using (2-60) so that transition probabilities could be calculated. When using the interaction type bases B, C & E, the final c-coefficients are multiplied by some phase factor, but this was ignored as only square moduli were required.

All calculations were performed at the high collision energy of 10^5 cpe ($\sim$625 eV), at which the impact parameter approximation is good, and with an impact parameter of 5 Å and initial diatom orientation as described in section B(i) above. Initially, a value $t_f = 8 \times 10^{-2}$ dps (8×10^{-15} sec) was selected.

Table 3 shows results from the use of basis A, i.e. the a-coefficient method with no terms removed from the diagonal, using a time interval of $\delta t = 5 \times 10^{-3}$ dps. The sum of the transition probabilities is 2.49×10^4, representing a large departure from unitarity, and indicating that a much smaller δt is required. However, although the computation will take a little longer, using basis B, which differs in that the E terms have been removed from the diagonal of $\mathbb{H}$, will be expected to give better results with the same value of δt. This can be seen in table 4, in which the improvement with decreased δt can also be seen. However, the computation times are prohibitively high, and the improvement over use of basis A is slight.

Clearly, the only sensible basis is C or E, a-coefficient and c-coefficient methods respectively, in which all terms have been removed from the diagonal of $\mathbb{H}$. For a given δt, the computation time is considerably longer, because further integration is necessary in terms such as $\exp\left\{\frac{i}{\hbar}\int_0^t \left[W_{1i}(t') - W_{2j}(t')\right]dt'\right\}$, but the result is much improved, as can be seen in table 5, where results using the c-coefficient basis E are set out. Here transition probabilities into the bottom five states only of each channel are shown; the remainder are very small.

Since the more reliable calculations show that transitions into the higher vibrational states have low probability, the basis E calculation, with $\delta t = 1.6 \times 10^{-3}$ dps, was repeated with only the lowest five vibrational states in each channel considered, but with

$E = 10^5$ cpe; $b = 5$ Å; $t_f = 8 \times 10^{-2}$ dps; $\delta t = 5 \times 10^{-3}$ dps		
n	Final probabilities in vibrational level n of	
	Covalent channel	Ionic channel
0	5.43	2.49(2)
1	9.49(-1)	2.46(1)
2	1.61(-1)	1.26
3	2.24(-2)	1.90(-2)
4	2.45(-3)	4.56(-3)
5	1.38(-4)	1.37(-3)
6	2.27(-4)	1.27(-2)
7	1.23(-3)	8.26(-2)
8	2.18(-2)	1.23(-1)
9	5.14(-2)	1.12(-2)
10	5.30(-2)	9.78(-1)
11	2.96	1.48
12	4.01(1)	7.00
13	1.85(3)	5.36
14	4.18(3)	7.24(1)
15	1.85(4)	2.46(1)
Total probability = 2.49×10^4		

Table 3. Results for $M + X_2 \rightarrow M^+ + X_2^-$ using the Magnus method with basis A

The notation n(m) means $n \times 10^m$

n	$\delta t = 5 \times 10^{-3}$ dps		$\delta t = 5 \times 10^{-4}$ dps		$\delta t = 1 \times 10^{-4}$ dps	
	Covalent	Ionic	Covalent	Ionic	Covalent	Ionic
0	1.99(1)	3.84(2)	8.82(-1)	1.74(-1)	9.11(-1)	8.61(-2)
1	6.79	6.70(1)	1.96(-3)	1.43(-2)	9.08(-5)	8.18(-3)
2	1.18	3.72(1)	7.40(-4)	1.84(-3)	7.45(-5)	4.27(-3)
3	5.52(-1)	5.04	2.23(-4)	2.26(-4)	2.19(-5)	2.94(-4)
4	2.11(-1)	7.67(-1)	2.67(-4)	1.62(-4)	1.07(-5)	7.20(-5)
5	2.87(-2)	2.58(-1)	8.52(-5)	3.45(-6)	1.50(-7)	4.46(-5)
6	1.79(-3)	5.40(-2)	2.32(-5)	2.38(-5)	3.16(-7)	1.24(-4)
7	2.31(-4)	2.07(-2)	5.19(-6)	5.36(-6)	1.31(-7)	2.27(-5)
8	7.57(-5)	2.45(-2)	9.30(-7)	4.14(-6)	8.21(-8)	1.10(-7)
9	6.59(-6)	1.50(-2)	3.41(-7)	8.65(-6)	1.38(-8)	1.99(-7)
10	1.92(-6)	1.16(-2)	1.02(-7)	3.76(-6)	4.11(-9)	1.89(-8)
11	2.02(-6)	9.41(-3)	6.32(-8)	3.72(-6)	4.79(-10)	1.62(-9)
12	5.99(-7)	2.96(-3)	2.04(-8)	4.02(-6)	8.59(-12)	1.94(-11)
13	1.81(-5)	8.95(-3)	5.93(-8)	2.02(-6)	9.44(-11)	4.41(-9)
14	2.05(-6)	3.71(-3)	6.22(-9)	3.96(-6)	6.85(-12)	5.42(-9)
15	1.64(-6)	1.89(-2)	2.47(-9)	1.31(-5)	4.62(-12)	2.65(-9)
Total probability: 5.23(2)			1.076		1.011	
Computation time / sec: 320			997		6367	

Table 4. Results from use of basis B

n	$\delta t = 5 \times 10^{-3}$ dps		$\delta t = 2.5 \times 10^{-3}$ dps		$\delta t = 1.6 \times 10^{-3}$ dps	
	Covalent	Ionic	Covalent	Ionic	Covalent	Ionic
0	9.65(-1)	8.06(-2)	9.44(-1)	7.87(-2)	9.36(-1)	7.80(-2)
1	3.32(-5)	6.43(-4)	3.71(-5)	6.67(-4)	3.80(-5)	6.75(-4)
2	1.18(-3)	4.21(-4)	1.24(-3)	3.90(-4)	1.26(-3)	3.79(-4)
3	1.47(-5)	2.12(-5)	1.39(-5)	1.86(-5)	1.37(-5)	1.75(-5)
4	6.48(-5)	5.42(-6)	6.72(-5)	6.69(-6)	6.74(-5)	7.07(-6)
5	2.79(-7)	1.07(-6)	1.76(-7)	1.52(-6)	1.45(-7)	1.73(-6)
Total probability: 1.048			1.025		1.017	
Computation time / sec: 827			1557		2400	

Table 5. Results from use of basis E

$t_f = 1.6 \times 10^{-1}$ dps (at which $V_{12} \sim 0.1\ \% (V_{11} - V_{22})$). The results are shown in table 6, and in figs 10 & 11 the square moduli of the coefficients for $v = 0$ in the covalent channel, and $v = 0$ and 1 in the ionic channel are plotted as a function of time. The point labelled 0 is the time at which the crossing r_c, between the electronic diabatic curves without vibration, shown as dashed lines in fig. 6, is reached. Points 1, 2, 3, 4 show when the $v = 0$ vibrational curve of the covalent channel crosses the $v = 0$, 1, 2, 3 curves respectively of the ionic channel. In fig. 12, the sum $|c_{10}|^2 + |c_{20}|^2 + |c_{21}|^2$, which includes virtually all of the transition probability, is plotted as a function of time, and the progressive departure from

unitarity can be seen. Note that using $t_f = 8 \times 10^{-2}$ dps does not include all of the interaction, which is to be expected, as it corresponds to a point just outside the crossing point. This calculation took several hundred seconds of computer time to complete, and clearly an even smaller δt is desirable. It was decided that the computation time involved would be unacceptable, so a different approach, that of direct numerical integration of the coupled differential equations as an initial value problem by Krogh's method, was investigated.

$t_f = 1.6 \times 10^{-1}$ dps; $\delta t = 1.6 \times 10^{-3}$ dps		
n	Covalent	Ionic
0	8.90(-1)	1.37(-1)
1	2.83(-4)	1.28(-2)
2	1.66(-3)	2.91(-4)
3	5.42(-5)	1.29(-5)
4	5.24(-5)	3.84(-6)

Table 6. Results from E basis calculations

shown in figs 10, 11, 12

Sum of probabilities = 1.042

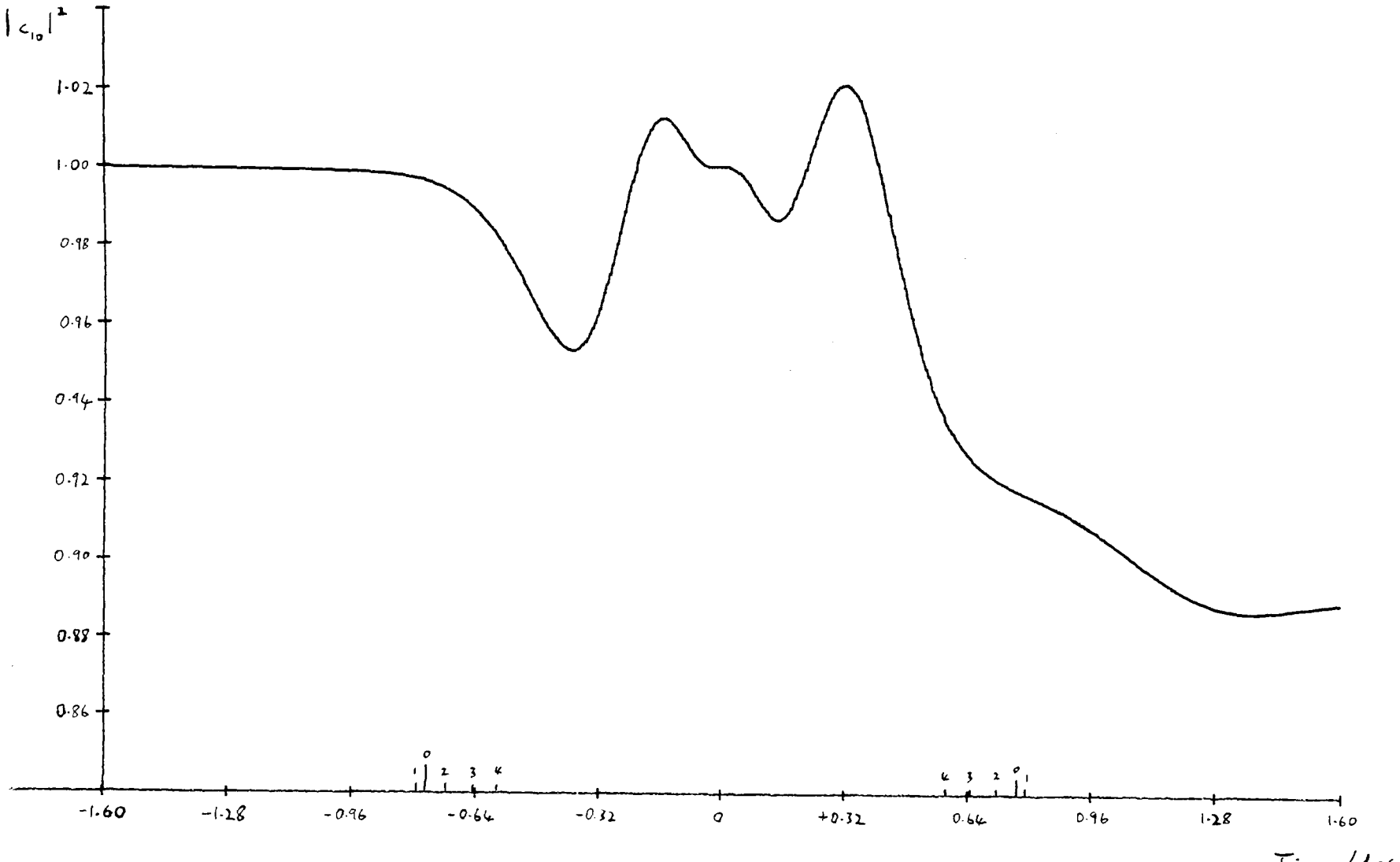

Fig. 10. M / X_2 collision ($E = 10^5$ cpe; $b = 5$ Å); change of $|c_{10}|^2$ with time, calculated by Magnus approximation with $\delta t = 1.6 \times 10^{-3}$ dps

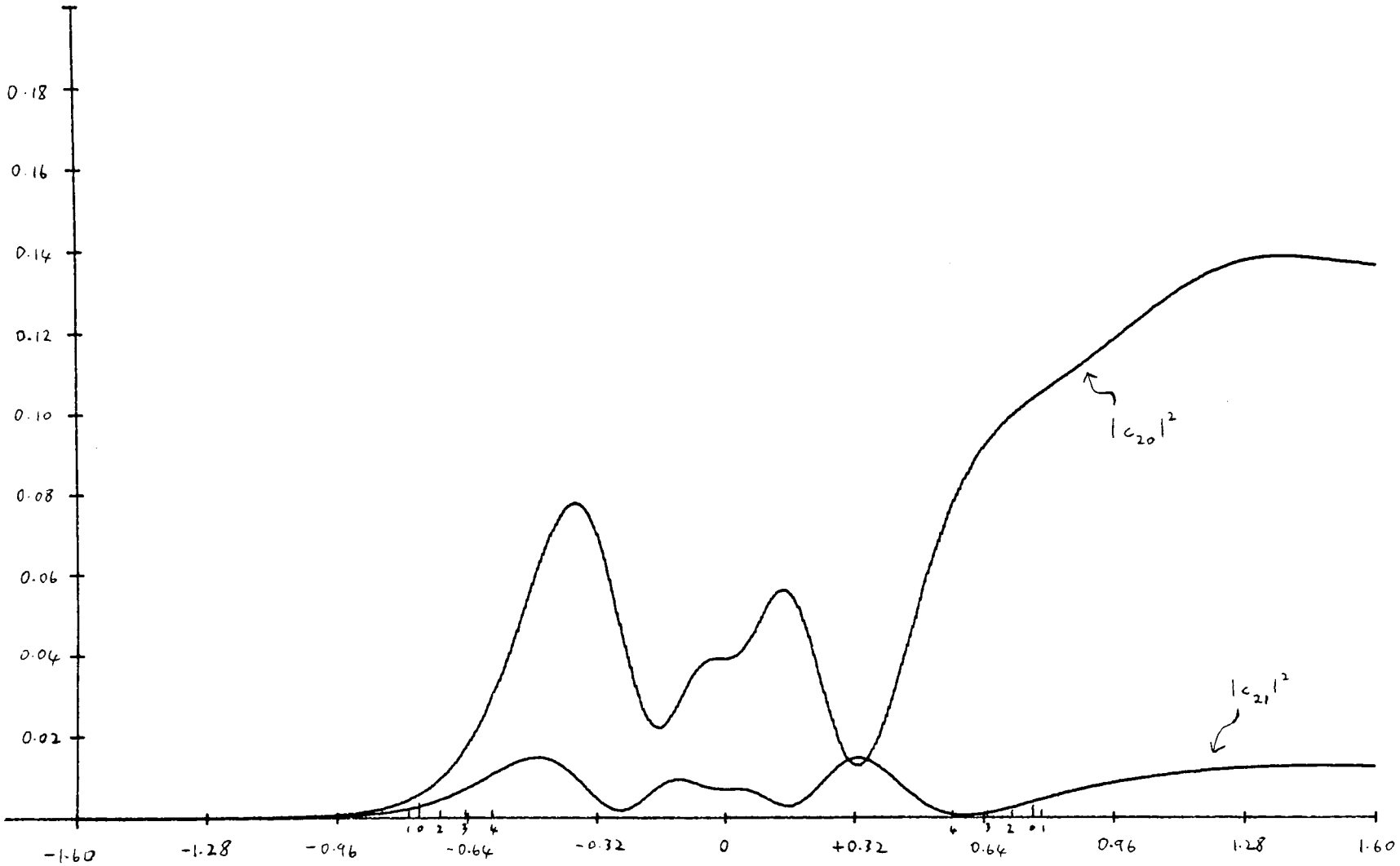

Fig. 11. M / X_2 collision ($E = 10^5$ cpe; $b = 5$ Å): evolution of ionic vibrational states by Magnus method

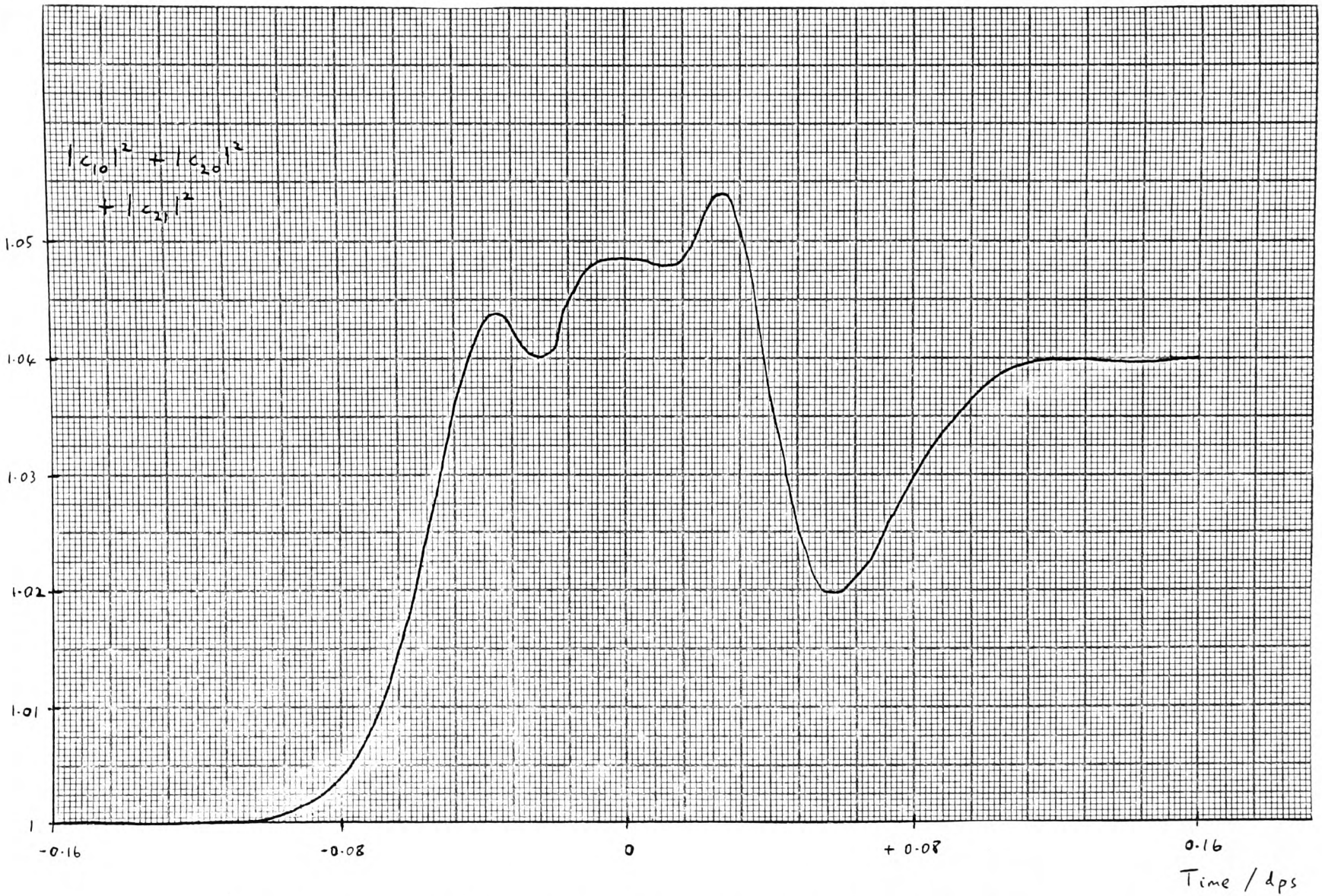

Fig. 12 Evolution of non-unitarity of collision shown in figs 10 & 11

E Krogh solution to coupled equations.

The original coupled differential equations in the c-coefficient method (2-54) & (2-58) were now solved using a variable order Adams method due to Krogh (1973), which is available in the NAG library, and was used in a previous work (Gover, 1975). Since this is designed to solve an initial value problem, the starting values of the coefficients must be specified each time the equations are solved. Using the same starting conditions as those described for the Magnus calculations, it can readily be seen that this method is hoped to be faster than the Magnus method simply because it gives only the first column of the scattering matrix rather than all of it. Krogh's method was applied to the problem in the following way:

The c-coefficients were split into real and imaginary parts:

$$\begin{aligned} c_{1n}(t) &= R_{1n}(t) + iI_{1n}(t) \ ; \\ c_{2m}(t) &= R_{2m}(t) + iI_{2m}(t) \end{aligned} \qquad (3\text{-}53)$$

If N vibrational states in each channel are considered, this gives rise to 4N simultaneous first order differential equations:

$$\begin{aligned} \hbar \frac{d}{dt} R_{1n} &= V_{12} \sum_m \Omega_{nm} I_{2m} + (E_{1n} + V_{11}) I_{1n} \ ; \\ \hbar \frac{d}{dt} I_{1n} &= -(V_{12} \sum_m \Omega_{nm} R_{2m} + (E_{1n} + V_{11}) R_{1n}) \ ; \\ \hbar \frac{d}{dt} R_{2m} &= V_{12} \sum_m \Omega_{nm} I_{1n} + (E_{2m} + V_{22}) I_{2m} \ ; \\ \hbar \frac{d}{dt} I_{2m} &= -(V_{12} \sum_m \Omega_{nm} R_{1n} + (E_{2m} + V_{22}) R_{2m}) \end{aligned} \qquad (3\text{-}54)$$

Before attempting any solutions, V_{12} was modified by the factor f described in section B(i) to give, for each energy range, interesting

results with which to compare the high and low energy calculations with the exact results. The factors used were: for high energy, $f = 3.5$ (increasing the interaction to make the system behave more adiabatically); for low energy, $f = 0.2$ (decreasing the interaction, to make the system behave less adiabatically).

A typical result from a high energy calculation is given in table 7.

$E = 10^5$ cpe; $b = 5$ Å; $t_f = 3 \times 10^{-1}$ dps; error bound (see Gover, 1975) $= 10^{-6}$		
n	Transition probability to level n of:	
	Covalent channel	Ionic channel
0	5.69(-1)	2.13(-2)
1	5.26(-2)	3.21(-1)
2	1.90(-2)	9.60(-3)
3	5.87(-3)	4.44(-4)
4	1.50(-4)	9.43(-4)
5	7.00(-6)	1.17(-4)
6	4.86(-7)	1.09(-4)
7	1.05(-6)	6.05(-5)
8	2.56(-7)	4.86(-7)
9	1.23(-7)	1.88(-6)
Total probability = 1.0000		

Table 7. $M + X_2 \rightarrow M^+ + X_2^-$ results from calculation using Krogh's method

This calculation took 57 sec of computer time. This is clearly a vast improvement on the Magnus approach, and Krogh's method was used for the remaining calculations. The progress of this collision is shown in fig. 13, and again the crossing point r_c of the dashed diabatic electronic curves in fig. 6 is indicated by the points labelled 0.

Attention was focussed on the $v = 0$ level of X_2 and the $v = 0$ and $v = 1$ levels of X_2^-. It was found that the results could be relied on to 3 figure accuracy with specified error $= 10^{-4}$ (see Gover, 1975), only five levels in each channel considered, and $t_f = 0.3$ dps for $E = 10^5$ cpe, corresponding to starting and finishing at $r \sim 40$ Å; refining the error to 10^{-5} or 10^{-6}, using 10 levels in each channel, or increasing the value of t_f by 50% had no effect to 3 significant figures in a number of test cases. With these conditions, calculations at $\sim 10^5$ cpe (~ 600 eV) took ~ 10 sec, and those at ~ 100 cpe (~ 0.6 eV) took ~ 300 sec; it can be seen that the computation time is roughly proportional to the real collision time, and this is reasonable since it is roughly proportional to the number of oscillations in the solution, which are roughly evenly spaced in time. The latter time was reckoned still too long, and a slight improvement was obtained by using Krogh's method with the equations corresponding to the basis E, i.e. all diagonal terms of $\mathbb{H}$ removed in a c-coefficient formulation, instead of the original equations (2-54) & (2-58). The equations are:

$$i\hbar \frac{d}{dt} \begin{pmatrix} \underset{\sim}{\gamma}_1 \\ \underset{\sim}{\gamma}_2 \end{pmatrix} = \begin{pmatrix} 0 & \mathbb{K}_{12} \\ \mathbb{K}_{21} & 0 \end{pmatrix} \begin{pmatrix} \underset{\sim}{\gamma}_1 \\ \underset{\sim}{\gamma}_2 \end{pmatrix}$$

$$\Rightarrow \quad i\hbar \frac{d}{dt} \underset{\sim}{\gamma}_1 = \mathbb{K}_{12} \underset{\sim}{\gamma}_2$$

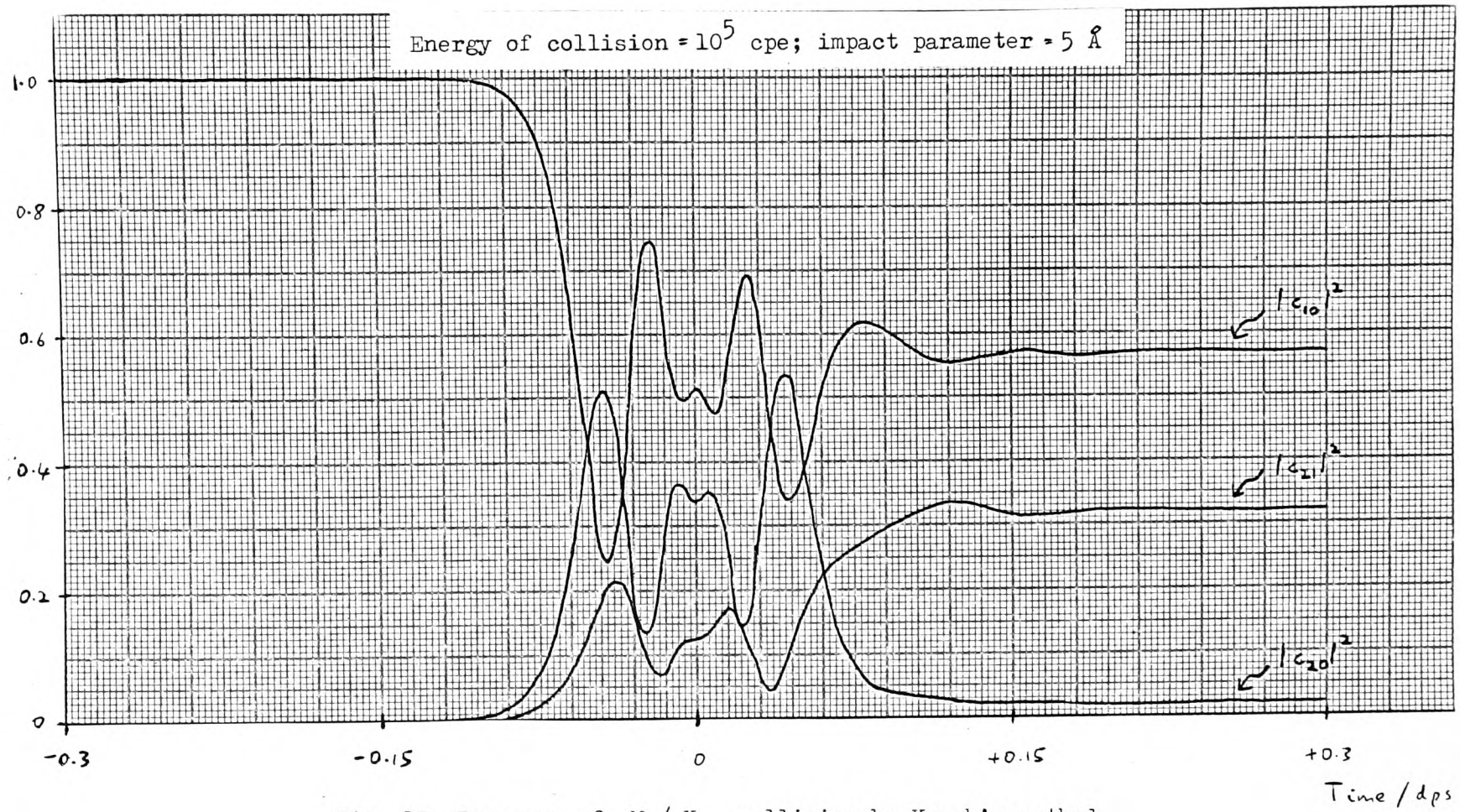

Fig. 13. Progress of M / X_2 collision by Krogh's method

$$\Rightarrow \quad i\hbar \frac{d}{dt} \gamma_{1n}(t) = \sum_m (\mathcal{H}_{12})_{nm} \gamma_{2m}(t)$$

$$= V_{12} \sum_m \Omega_{nm} \exp\left\{ \frac{i}{\hbar} \int (W_{1n} - W_{2m})\, dt \right\} \gamma_{2m}$$

$$= V_{12} \sum_m \Omega_{nm} (\cos p_{nm} + i \sin p_{nm}) \gamma_{2m}$$

$$= V_{12} \sum_m \Omega_{nm} (\cos p_{nm} + i \sin p_{nm})(R_{2m} + iI_{2m}) \qquad \text{say}$$

$$= i\hbar \frac{d}{dt} (R_{1n} + iI_{1n})$$

$$\Rightarrow \quad \hbar \frac{d}{dt} R_{1n} = V_{12} \sum_m \Omega_{nm} (I_{2m} \cos p_{nm} + R_{2m} \sin p_{nm})$$

and

$$\hbar \frac{d}{dt} I_{1n} = V_{12} \sum_m \Omega_{nm} (-R_{2m} \cos p_{nm} + I_{2m} \sin p_{nm})$$

$$\text{where} \qquad p_{nm} = \frac{1}{\hbar} \int_0^t (W_{1n} - W_{2m})\, dt$$

$$= (E_{1n} - E_{2m}) \frac{t}{\hbar} + \frac{1}{\hbar} \int_0^t (V_{11} - V_{22})\, dt$$

Similarly, $$i\hbar \frac{d}{dt} \underset{\sim}{\gamma}_2 = \mathcal{H}_{21} \underset{\sim}{\gamma}_1$$

$$\Rightarrow \quad i\hbar \frac{d}{dt} \gamma_{2n} = V_{12} \sum_m \Omega_{mn} \exp\left\{ \frac{i}{\hbar} \int (W_{2n} - W_{1m})\, dt \right\} \gamma_{1m}$$

$$\Rightarrow \quad \hbar \frac{d}{dt} R_{2n} = V_{12} \sum_m \Omega_{mn} (I_{1m} \cos p_{mn} - R_{1m} \sin p_{mn})$$

and $$\hbar \frac{d}{dt} I_{2n} = V_{12} \sum_m \Omega_{mn} (-R_{1m} \cos p_{mn} - I_{1m} \sin p_{mn})$$

where $$p_{mn} = \frac{1}{\hbar}\int_0^t (W_{1m} - W_{2n})\,dt$$

$$= (E_{1m} - E_{2n})\frac{t}{\hbar} + \frac{1}{\hbar}\int_0^t (V_{11} - V_{22})\,dt$$

Note that the complete integrals $\int_0^t (V_{11} - V_{22})dt$ were not worked out at each step; $\int_0^{t_o} (V_{11} - V_{22})\,dt$ was calculated for a grid of values t_0, and for any t the nearest t_0 was found, and the integral from t_0 to t evaluated; this was then added to the integral from 0 to t_0, already known.

At $E = 10^5$ cpe, with $f = 3.5$, using the original equations (2-54) & (2-58) took 13 sec, whereas using the transformed equations took 17 sec. At $E = 100$ cpe, with $f = 0.2$, using the original equations took 336 sec and gave a total transition probability of 0.9973; using the transformed equations took 237 sec and gave a total probability of 1.0000. This improvement in time and unitarity was found for several other low energies, and the transformed equations were used throughout in the low energy regime.

Plots of transition probability as a function of collision energy appear in figs 14-19; results from the present calculations are labelled "Exact". It can be seen from fig. 13 that strong interaction takes place during about half of the collision computed; the approximate number of X_2 vibrations (at $\nu = 4.5$ /dps) occurring during this part of the collision was calculated for various collision energies, and these numbers are shown in brackets on the energy scales of figs 14, 15 & 19.

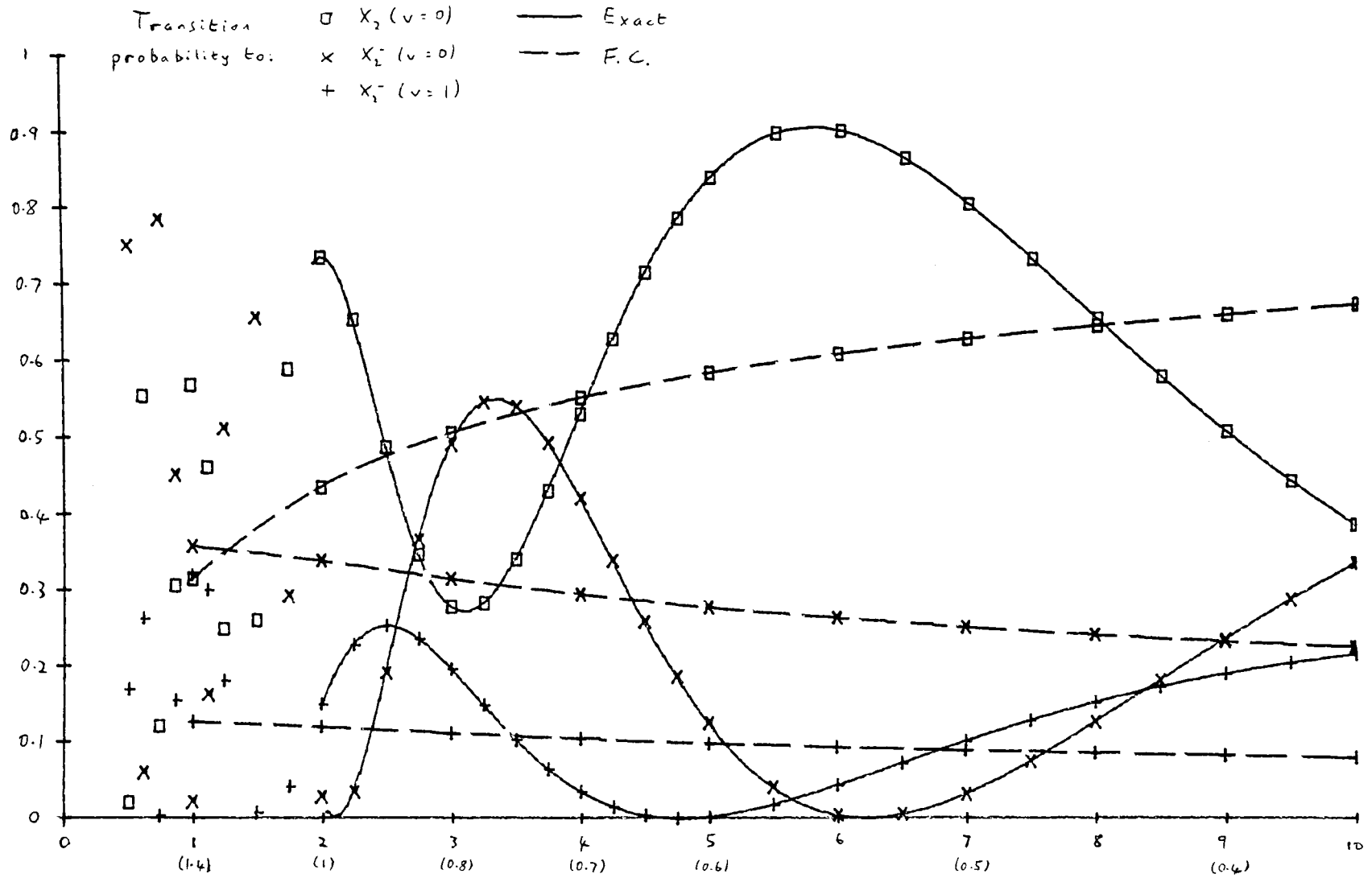

Fig. 14. Variation of transition probabilities with collision energy, by Krogh's method (numbers in brackets show approx. number of X_2 vibrations during the interactive part of the collision)

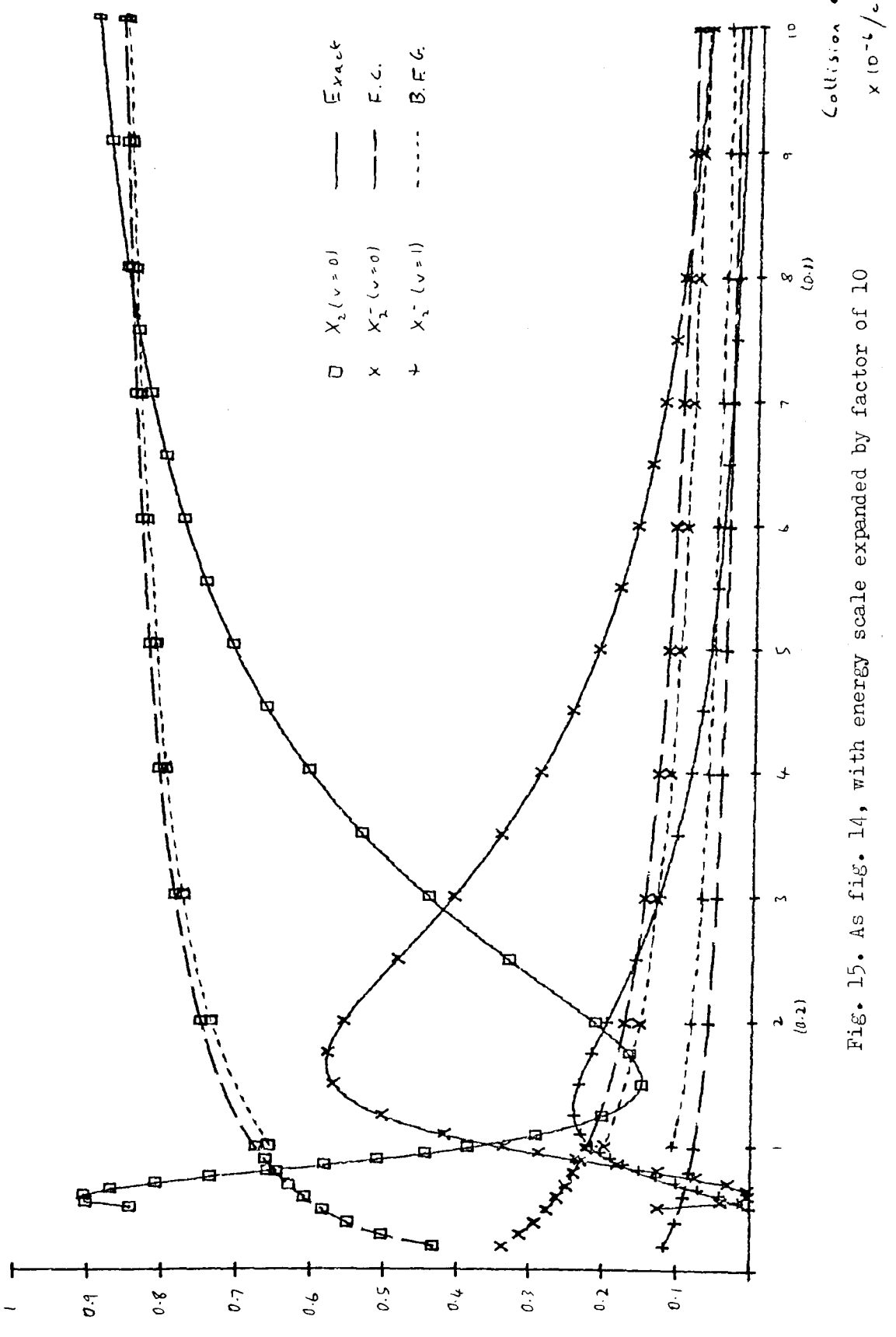

Fig. 15. As fig. 14, with energy scale expanded by factor of 10

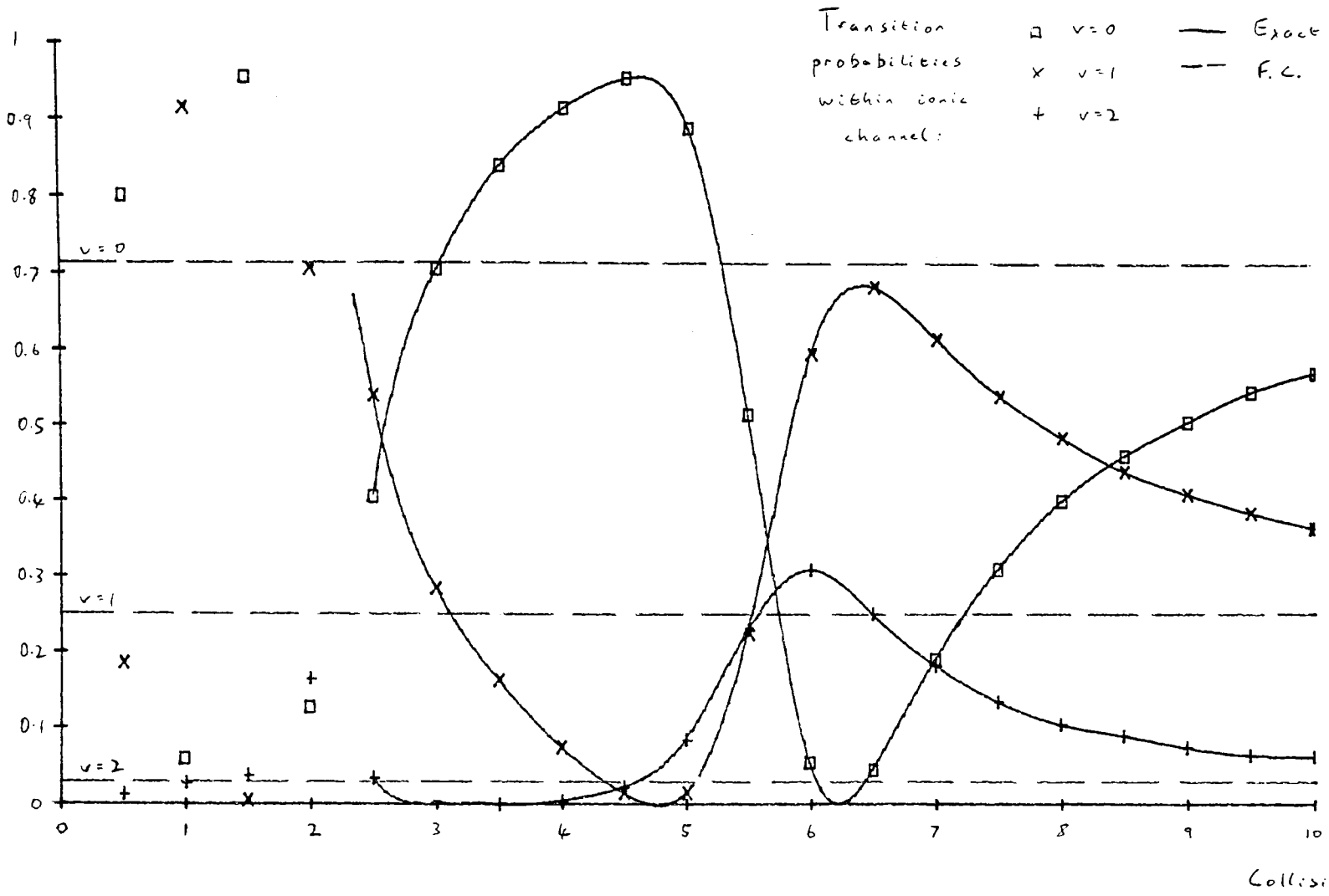

Fig. 16. Vibrational energy distribution in ionic level, as a function of collision energy

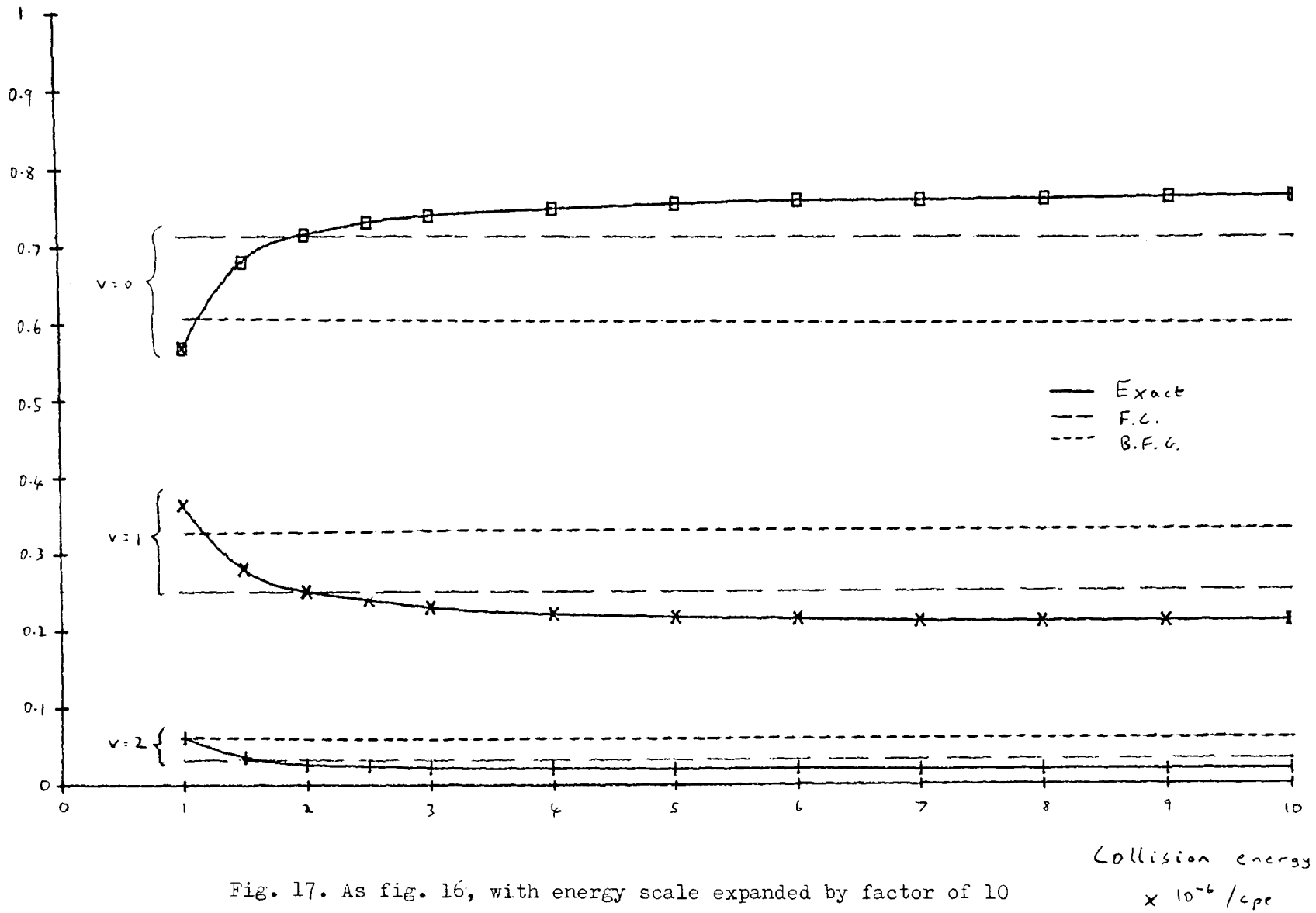

Fig. 17. As fig. 16, with energy scale expanded by factor of 10

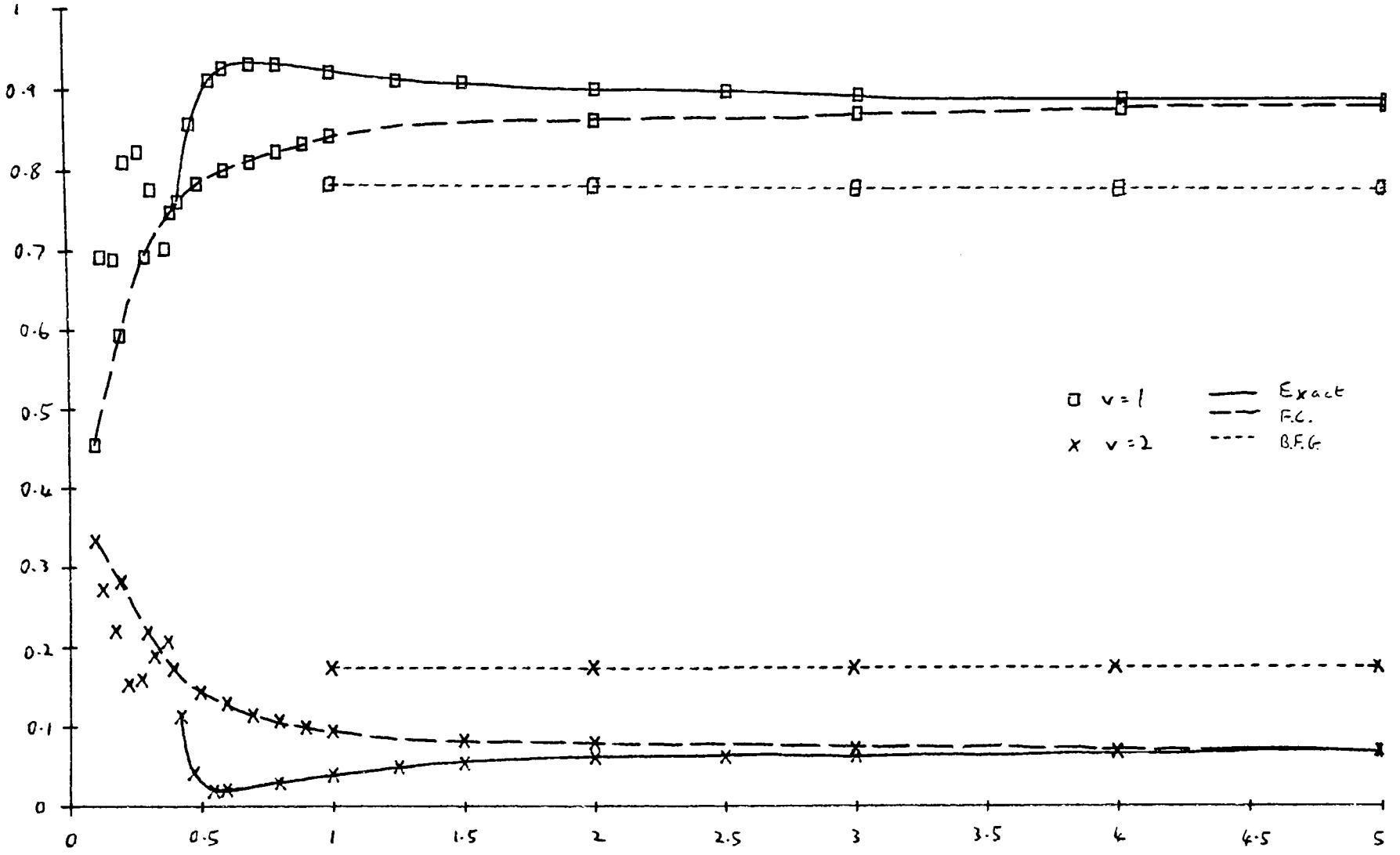

Fig. 18. Vibrational energy distribution in covalent channel

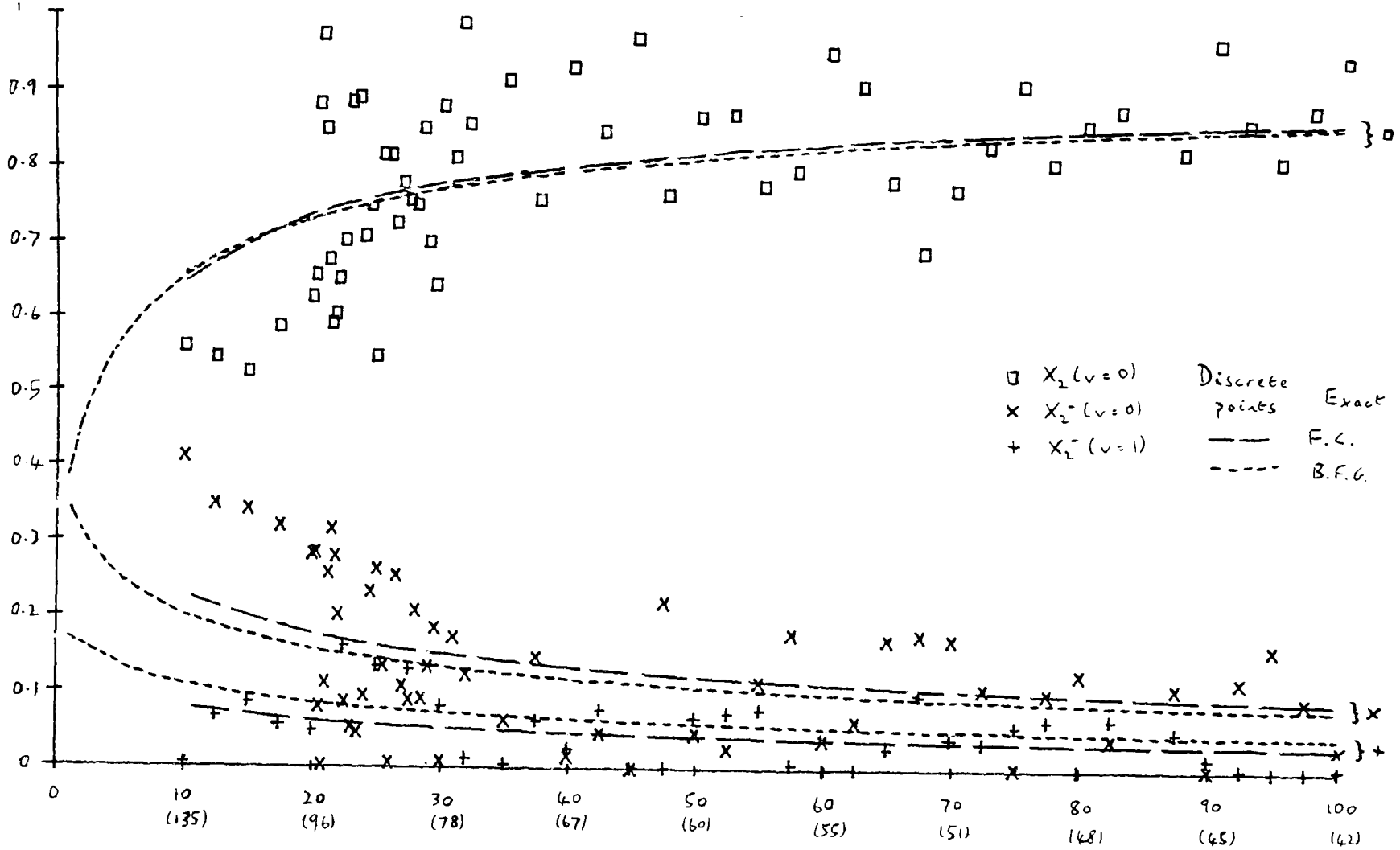

Fig. 19. Variation of transition probabilities with collision energy in low energy region

F Discussion of results.

Some of the calculations described above were repeated using the high energy Franck-Condon method (described in chapter II section F; results shown as points labelled "F.C." in figs 14-19), and the low energy Bauer, Fisher & Gilmore method (described in chapter II section G; results shown as points labelled "B.F.G." in figs 14-19).

Consider the Franck-Condon method. Calculations were performed using equations (2-83), (2-84) & (2-85). Probabilities for population of the initial ground covalent vibrational level from the two possible routes involving no transitions and two transitions were added together. The transition probability P in these equations was calculated using the LZS formula (2-42); in this, the crossing distance $r_c = 9.21$ Å, obtained from (3-6), was used, and the slopes $F_i(r) = \frac{\partial}{\partial r} V_{ii}(r)$ were obtained from (3-3) & (3-4):

$$V_{11}(r) = \varepsilon \left\{ \left(\frac{\sigma}{r}\right)^{12} - 2\left(\frac{\sigma}{r}\right)^{6} \right\} \qquad (3\text{-}3)$$

$$\Rightarrow \quad F_1(r) = \frac{12\varepsilon}{r} \left\{ \left(\frac{\sigma}{r}\right)^{6} - \left(\frac{\sigma}{r}\right)^{12} \right\} \qquad (3\text{-}55)$$

$$V_{22}(r) = -\frac{e^2}{4\pi\varepsilon_0 r} - \frac{e^2(\alpha_1 + \alpha_2)}{8\pi\varepsilon_0 r^4} + Ae^{-r/k} + \text{const.} \qquad (3\text{-}4)$$

$$\Rightarrow F_2(r) = \frac{e^2}{4\pi\varepsilon_0 r^2} \quad \frac{2e^2(\alpha_1 + \alpha_2)}{4\pi\varepsilon_0 r^5} - \frac{A}{k} e^{-r/k} \qquad (3\text{-}56)$$

The validity criterion (2-80) suggests that we can expect the approximation to become valid above the velocity given by $A = 1$; this corresponds to a collision energy E_{FC} given by:

$$E_{FC} = \frac{1}{2}\mu\left(\frac{2\pi X_{nn'}^{2}}{\hbar|F_1 - F_2|}\right)^2 \qquad (3\text{-}57)$$

Putting $X_{nn'}$ equal to its maximum value for the levels of interest, of ~ 25 cpe, this gives $E_{FC} \sim 3 \times 10^6$ cpe (~ 18 keV).

Now consider the Bauer, Fisher & Gilmore method. Calculations were performed using equations (2-91), (2-92) & (2-93). The slopes $F_i(r)$ in the LZS formula were calculated using (3-55) & (3-56), and the various crossing points r_{pq} were calculated from:

$$V_{11}(r_{pq}) + E_{1n} = V_{22}(r_{pq}) + E_{2m}$$

The values found were as follows:

r_{pq}/Å: Covalent p:	1	2	3	4	5
Ionic q:					
6	9.418	10.672	12.257	14.321	17.112
7	8.730	9.794	11.111	12.778	14.952
8	8.148	9.066	10.181	11.561	13.309
9	7.650	8.452	9.411	10.577	12 019
10	7.220	7.929	8.765	9.765	10.980

From the validity criterion (2-87), we can estimate a collision energy E_{BFG} below which the method will be hoped to be valid:

$$E_{BFG} = \frac{1}{2}\mu\left(\frac{(\Delta E)^2}{8\hbar|F_1 - F_2|}\right)^2$$

Putting $\Delta E \sim 25$ cpe, then $E_{BFG} \sim 40$ cpe ($\sim .25$ eV), which is somewhat higher than thermal (~ 5 cpe). With $f = 0.2$, and the nominal crossing radius $r_c = 9.21$ Å, $V_{12}(r_c) = 1.1$ cpe, so condition (2-90) is reasonably

well satisfied. Note that at the low energy of 40 cpe, the impact parameter approximation is not good; however it provides a framework within which the performance of the BFG method can be tested.

Note also that the energies E_{FC} and E_{BFG} both depend to the fourth power on a quantity which varies according to the actual pair of levels involved in a crossing of the network, i.e. X_{nn}, and ΔE respectively.

In fig. 14, the transition probabilities to $X_2(v = 0)$ and $X_2^-(v = 0,1)$ are plotted as a function of collision energy in the range 0 to 10^6 cpe. The exact results are seen to oscillate, the oscillations becoming more rapid as the energy is decreased. The FC results seem to agree reasonably with the exact results as they would be with the oscillations averaged out, and it is possible that if interference between ingoing and outgoing trajectories were included in the FC treatment, then similar oscillations would be produced. In fig. 15, the scale is increased by a factor of ten, and the oscillations in the exact results seem to die out (as was confirmed by calculations up to 10^{10} cpe). At energies considerably above E_{FC}, the FC results approach agreement; however, this is partly because both models predict completely diabatic behaviour (i.e. no transition out of the initial ground state covalent level) in the high energy limit. Perhaps more useful is the comparison in figs 16 & 17, in which the final distribution over the vibrational levels of the ionic channel, which in the FC model is completely independent of any assumptions about interference between ingoing and outgoing trajectories, is shown as a function of collision energy over the same energy ranges $0\text{-}10^6$ cpe and $0\text{-}10^7$ cpe. The final probabilities for the bottom three levels $v = 0, 1, 2$ of X_2^- were divided by the total probability for all five levels considered in X_2^- to give these distributions. In the

FC model, the distribution is given by (2-85): $|c_{2m}|^2 \propto (\Omega_{0m})^2$, which is independent of the collision energy. As can be seen, the exact results again have oscillations. Such oscillations of transition probabilities within a single electronic channel can be distinguished from covalent versus ionic oscillations in that they could not be produced in the FC model by including interference between ingoing and outgoing trajectories. The oscillations again die out in the region of the energy E_{FC}. However, the exact results appear to approach asymptotes which are not coincident with the FC results. It was thought that the FC results may be in error because of the slight departure from orthogonality of the overlap matrix used, since the result (2-85) comes from $|c_{2m}|^2 \propto (\Omega_{m0}^{-1})^2$ via this orthogonality. However, reference to (3-27) & (3-28) shows that replacing Ω_{0m} by Ω_{m0}^{-1} has no appreciable effect on the results. Also, since the sum of the five probabilities $(\Omega_{0m})^2$ is 0.9993 (or $\sum_{m=0}^{4} (\Omega_{m0}^{-1})^2 = 0.9995$), re-normalising the results will have no significant effect. Hence the difference between the asymptotes for the exact and FC methods seems to be a real effect; calculations at energies up to 10^{10} cpe show no indication of the exact results turning back towards the FC ones.

Also expected to be independent of any assumptions about interference between ingoing and outgoing trajectories is the distribution over the covalent vibrational levels other than the initial ground one; these are reached by two transitions, and the distribution in the FC approximation is given by (2-83). This distribution is plotted as a function of energy over the range $0\text{-}5 \times 10^5$ cpe in fig. 18, and here it can be seen that the two methods do approach agreement in the region of E_{FC}.

Turning now to the low energy regime, fig. 19 contains a plot of the transition probabilities to $X_2(v = 0)$ and $X_2^-(v = 0,1)$ as a function of collision energy over the range 0-100 cpe. It can be seen that the exact results now oscillate much more rapidly, and the points plotted are not sufficiently close together to resolve these oscillations. Also plotted are results using both the low energy BFG and the high energy FC methods; these show surprisingly similar behaviour with energy, and also, for the three most highly populated states shown, are in reasonable agreement on the transition probabilities. Both methods seem to give good estimates of the exact results as they would be with the oscillations averaged out. Results obtained from the BFG method at high energies are also shown in figs 15 & 17. In fig. 15, it can be seen that there is a remarkable similarity in the transition probabilities predicted by the two approximations at high energies also. However, it can be seen in fig. 17 that in predicting distributions in the ionic level, the BFG method is not as good as the FC method.

G Summary and conclusions.

Distributions among the vibrational levels of X_2 and X_2^- after alkali / halogen electron transfer collisions $M + X_2 \rightarrow M^+ + X_2^-$ were investigated, and the performance of the high energy Franck-Condon (FC) and low energy Bauer, Fisher & Gilmore (BFG) sequential Landau-Zener approximations in calculating such distributions was evaluated by comparison of the results obtained from them with those from exact calculations within the framework of the multi-curve crossing formulation of the classical trajectory approximation.

(i) Calculation of the overlap integrals between the wavefunctions of two different Morse oscillators was investigated, using solutions

of the oscillators obtained by the finite element method with cubic splines. Consideration of the corresponding harmonic oscillator problem showed that the results were good to an absolute accuracy of about $\pm$ 0.001; calculation of 256 elements, including calculation of the relevant eigenvectors, took about 900 sec of computer time. Our method would be much improved if the method of solution of the generalised matrix eigenvalue problem made use of the fact that the matrices are banded.

(ii) Solution of the coupled differential equations arising from the multi-curve crossing problem was attempted by the Magnus method, with the overall scattering matrix accumulated from the product of approximate time evolution matrices (corresponding to truncating the Born series to first order) over small time increments. It was found that considerable improvement in computation time and unitarity of the S matrix could be achieved by transformation of the basis to remove terms from the diagonal of the H matrix. However, it was found that the particular method used was still inferior to solution of the coupled equations as an initial value problem by Krogh's method, although this is partly because the latter gives effectively only one column of the S matrix rather than all of it.

(iii) The FC and BFG approximations were compared with the exact solution of the multi-curve crossing problem using Krogh's method, at various collision energies and a particular impact parameter and diatom orientation.

Considering the probabilities for transition into $X_2(v = 0)$ and $X_2^-(v = 0,1)$, it was found that the FC and BFG results had similar behaviour and agreed surprisingly well with each other at both high and low energies. No oscillations in the probabilities as a function

of collision energy were produced, since in the implementation of both methods interference between ingoing and outgoing trajectories was not taken into account. The exact results were found to oscillate, but the FC and BFG results seemed to agree with what these results would be if the oscillations were averaged out. At high energies, the oscillations die out, and the three methods approach agreement, but this is to be expected as they all have the same, diabatic, behaviour in the limit of high energy.

Considering the distributions over the vibrational levels of X_2^- and over the excited levels of X_2, the FC method predicts no oscillations in these, regardless of interference between ingoing and outgoing trajectories. The exact results still have oscillations, but these die out in the region in which the FC method is expected to become valid. The results for $X_2(v = 1,2)$ then approach agreement, but in the ionic levels ($v = 0,1,2$) there is a slight residual disagreement between the exact and FC results which has not been explained; there is, as expected, however, a much greater disagreement between these and the BFG predictions at these high energies.

Several further calculations suggest themselves, e.g. at intermediate energies, but in particular the variation of the results with impact parameter would be interesting; it is thought that the oscillations of the exact results with collision energy may be averaged out by rapid oscillations with impact parameter, when predicting the results of real experiments, in which all impact parameters have to be taken into account; in this case the FC and BFG methods, which use very small amounts of computer time at all energies, might well be more useful. As a preliminary investigation, the calculation for $E = 10^5$ cpe (with $f = 3.5$) was repeated for several values of b, and the results are given below:

	Final probability in:		
b/Å	X_2 (v = 0)	X_2^-(v = 0)	X_2^-(v = 1)
1.5	.3904	.4363	.0715
2.0	.1485	.7885	.0002
2.5	.4661	.3112	.1314
3.0	.1414	.7433	.0566
3.5	.5932	.0195	.3017
4.0	.4495	.2556	.2133
4.5	.4828	.1705	.2687
5.0	.5700	.0211	.3221
5.5	.2608	.6271	.0269
6.0	.3482	.3045	.2743
6.5	.3996	.4650	.0375
7.0	.4167	.0960	.3562
7.5	.0959	.6618	.1682
8.0	.5951	.3679	.0056
8.5	.9384	.0320	.0157
9.0	.9519	.0135	.0287

It can be seen that there is indeed a rapid variation with impact parameter.

CHAPTER IV

TRAJECTORY STUDIES OF REACTIVE SCATTERING OF ALKALI METAL ATOMS WITH HALOGEN MOLECULES

A Introduction.

Since the early days of molecular beams, reactive scattering has been particularly well studied in collisions involving an alkali metal atom and some molecule containing one or more halogen atoms (see e.g. Birely et al, 1967; Gillen, Rulis & Bernstein, 1971; Lin, Mascord & Grice, 1974; Van der Meulen, Rulis & DeVries, 1975; Grice, 1975; Sholeen et al, 1976). Two extreme types of behaviour were soon recognised, the "rebound" reactions, e.g. those involving alkyl halides:

$$M + RX \rightarrow MX + R \qquad (4\text{-}1)$$

characterised by relatively small total reactive cross sections, backward product scattering in the C.M. (centre of mass) frame, and appearance of the exothermicity of the reaction mainly in product translation; and "stripping" reactions, e.g. those involving diatomic halogen and interhalogen molecules:

$$M + XY \rightarrow MX + Y \qquad (4\text{-}2)$$

characterised by very large total cross sections, forward product scattering in the C.M. frame, and appearance of the exothermicity mainly in MX vibration. Stripping reactions have been understood as occurring in two stages, viz. an electron jump:

$$M + XY \rightarrow M^+ + XY^- \qquad (4\text{-}3)$$

i.e. the type of process considered in chapter III, followed by reaction initiated by the Coulomb attraction between the oppositely charged ions:

$$M^+ + XY^- \rightarrow MX + Y \qquad (4\text{-}4)$$

The motion subsequent to the electron jump has been studied by considering classical trajectories over a potential energy surface for MXY with Monte Carlo averaging of the initial conditions (see e.g. Godfrey & Karplus, 1968; Blais, 1968 & 1969; Kuntz, Nemeth & Polanyi, 1969; Evers & DeVries, 1976).

In a previous work (Gover, 1975), such trajectory calculations were performed in two dimensions over a simple ionic surface designed to investigate the effect on the calculated scattering of varying the amount of weakening of the bond in XY^- by the field of the approaching M^+ ion, this weakening being considered the central cause of the reaction. The PES used was:

$$V(r,\rho) = D\, e^{\beta(\rho_e-\rho)}\left(e^{\beta(\rho_e-\rho)} - 2\left\{1 - e^{\alpha(r_e-r)}\right\}\right) - \frac{e^2}{4\pi\varepsilon_0 r} - \frac{e^2(\alpha_1+\alpha_2)}{8\pi\varepsilon_0 r^4} + Ae^{-r/k} \qquad (4\text{-}5)$$

where r & ρ are the magnitudes of the vectors

$\vec{r}$ = displacement of X from M;

$\vec{\rho}$ = " " Y " X

and the products are MX + Y.

The first term is a Morse potential for XY^-, with the attractive part reduced by the presence of the M^+, and decreasing as r decreases; α was chosen as a variable parameter determining the rate at which this occurs; the parameter r_0, which determines the distance at which

this attraction becomes repulsion, was in practice determined by the requirement that the total reactive cross section be a constant. The remaining terms are a simplefied Rittner (1951) potential for M^+X^-. Calculations were performed for the systems $K + I_2$ and $K + Br_2$; the parameters used are collected together below:

	$\rho_e/\AA$	D/cpe	ν/cm^{-1}	$\beta/\AA^{-1}$	μ/ppg
I_2 (a)	2.67	247	215	1.87	105.37
I_2^- (a)	3.1 ± 0.1	112±50	115±50	1.5	
Br_2 (b)	2.28	315	323	1.97	66.41
Br_2^- (b)	2.8 ± 0.1	184±100	150±50	1.2	

	$\alpha_1/\AA^3$	$\alpha_2/\AA^3$	A/cpe	k/Å
$K + I_2$ (c)	0.84	7.16	3.32×10^6	0.311
$K + Br_2$ (c)		4.83	1.60×10^6	0.328

References: (a) Person, 1963

(b) Kendall & Grice, 1972

(c) Rittner, 1951

The surface (4-5) is of the attractive or early downhill type, as can be seen from the example plotted in fig. 20.

It was assumed that all reactive encounters start with an electron jump, the probability of which is independent of any of the initial conditions, and hence can be considered as unity. Each trajectory is started on the ionic surface, reaction taking place with the halogen atom nearer to the alkali atom, and stays on it for the remainder of the encounter, the starting conditions being determined by its intersection with the covalent surface; since initial reactant vibration was ignored, as also was the slight r-dependence of the covalent surface due to weak Van der Waals

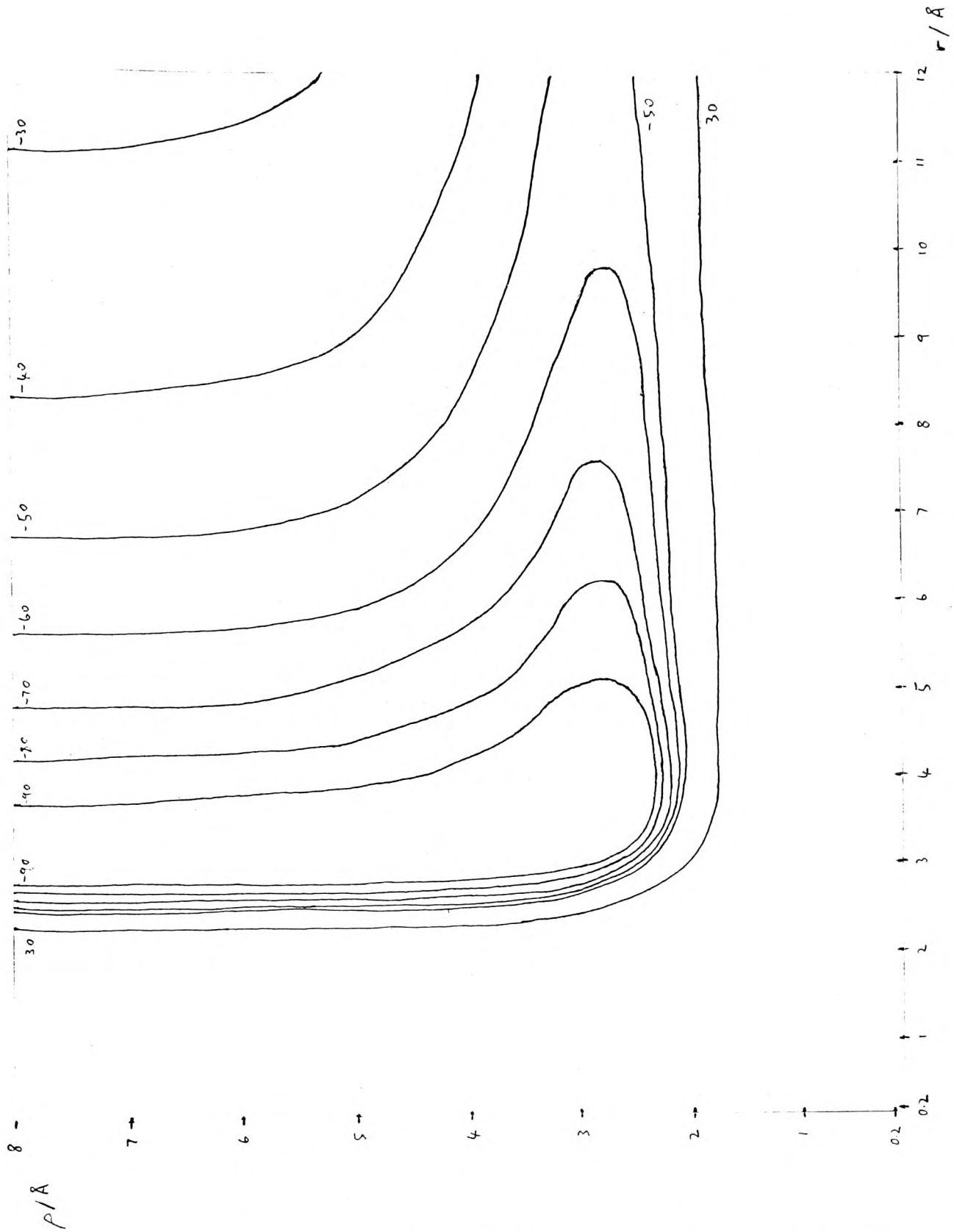

Fig. 20. Potential energy surface for $K + Br_2$ ($\alpha = 2$ Å^{-1}; $r_0 = 2.91$ Å)
The energy contours are in kcal/mol

attraction, this was effectively replaced by a flat surface at the level of the bottom of the XY well. Hence the method is a simple SHT method, and uses a diabatic formulation, although at thermal energies the motion is essentially adiabatic, and Evers & DeVries (1976) have shown that use of the lower adiabatic surface is preferable.

It was found in this earlier work that variation of the single parameter α produced a considerable change in the scattering results, it being possible to change from stripping to rebound behaviour by a fairly small increase in α (e.g. from 1 to 3 Å^{-1} for $K + Br_2$). By comparison with the experimental results of Gillen, Kulis & Bernstein (1971), it was decided that the "best" value of α for $K + I_2$ was ~ 1.4 Å^{-1}. The effect of increasing α is: to increase the product repulsion, making the surface less attractive, with the result that the scattering becomes more backward, and the ratio of product translational to vibrational energy increases. Also it was found that the final conditions become less sensitive to the initial ones, and the trajectories require fewer steps for their integration.

B Inclusion of initial vibrational energy.

The previous study (Gover, 1975) ignored the presence of reactant zero point energy, which was a serious limitation. In particular, when considering the distribution of product translational energy, the theoretical results tended to give very sharp cut-offs at high energy instead of the smooth tail observed experimentally (see e.g. Gillen et al, 1971). Initial X_2 vibration was included by the following crude method: five initial values of ρ, spaced about the equilibrium separation ρ_e, were selected, and a set of trajectory calculations was performed for each of these, with the number of trajectories weighted by a Gaussian distribution (with the width determined by the

square of the ground state vibrational wavefunction $\psi_0^2(\rho)$) about ρ_e. This corresponds to the electron jump probability being governed by the high energy Franck-Condon model described in chapter II section F; the Franck-Condon factor is equal to the square of the overlap of the ground vibrational wavefunction of X_2 with a high vibrational level of X_2^- represented by a delta function centred on the initial value of ρ, corresponding to a "vertical" transition, as shown in fig. 21.

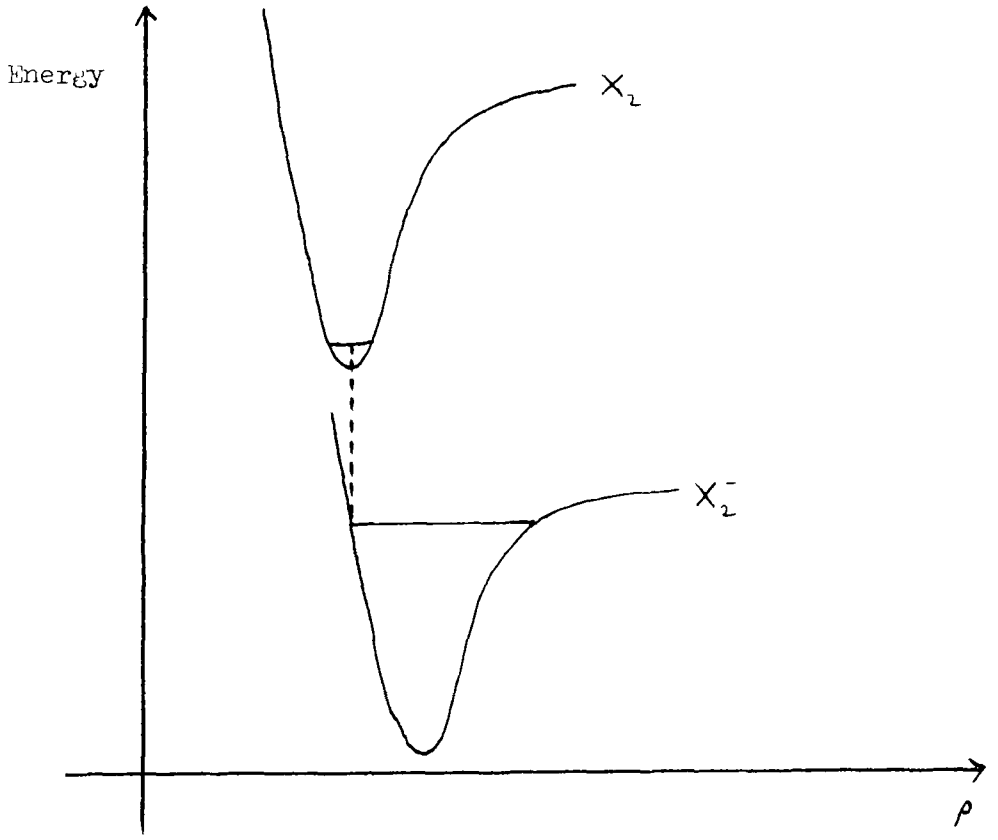

Fig. 21. A vertical transition from the ground vibrational state of X_2 to a high vibrational state of X_2^-.

If the initial value of ρ is ρ_i,

and X_2 ground state wavefunction $= \psi(\rho)$ say,

X_2^- " $\propto \delta(\rho - \rho_i)$

then overlap $\propto \int_{-\infty}^{\infty} \psi(\rho)\, \delta(\rho - \rho_i)\, d\rho$

$= \psi(\rho_i)$

$\propto \exp\{-q^2 (\rho_i - \rho_e)^2/2\}$

where $q = \sqrt{\frac{\mu\omega}{\hbar}}$

$\Rightarrow$ probability $\propto \exp\{-q^2 (\rho_i - \rho_e)^2\}$

giving rise to a Gaussian distribution in $\sqrt{\frac{2\mu\omega}{\hbar}}(\rho - \rho_e)$ of the electron jump probability, and hence trajectory weighting, about ρ_e.

C Calculations for $K + I_2$.

Trajectory calculations with the addition of initial diatom vibration were performed for the system $K + I_2$, and compared with the detailed cross section measurements of Gillen, Kulis & Bernstein (1971). The measurements were made at three values of the initial reactant relative translational energy, and the middle one of these, $E = 2.67$ kcal mol^{-1} ($= 11.2$ kJ mol^{-1}, equivalent to relative velocity 815 ms^{-1}), was chosen for the comparisons. The values for ρ_i used were (/Å): 2.62, 2.65, 2.67, 2.69, 2.72, the outer values being roughly at the classical turning points of the ground state vibrational motion. For I_2, $\sqrt{\frac{2\mu\omega}{\hbar}} = 28.41$ Å^{-1}, and a Gaussian

distribution gives the following weightings:

ρ_i/Å	Weighting w	1/(1-w)
2.62, 2.72	0.365	1.6
2.65, 2.69	0.851	6.7
2.67	1	∞

The starting value for r in each case was r_i, determined by the intersection of the ionic and covalent surfaces:

$$V(r_i, \rho_i) + I_K - E_{aI} + D_{I_2} = 0$$

The results of the new calculations with the previously determined "best" value of $\alpha = 1.4$ Å^{-1} are plotted in fig. 22, which is a polar plot of C.M. product scattering angle against final product relative velocity $\dot{D}$. Also shown on the velocity scale is the final velocity of the KI with respect to the C.M., w'_{KI}, and the translational energy corresponding to this, E'_{trans}. Each dot represents the outcome of a counted trajectory; since it is not possible to indicate fractions of trajectories in such a plot, the weighting described in part B was crudely applied by not counting 2 in 3 trajectories for $\rho_i = 2.62$, 2.72, and 2 in 13 trajectories for $\rho_i = 2.65$, 2.69 Å. The contours are obtained from the velocity-angle polar plot of Gillen et al by deweighting the experimental distribution by the final product velocity w'_{KI} to convert experimentally measured fluxes to number densities, which correspond to the analysis of the calculations (this was not done in the earlier work, and the comparison there is not valid). The experimental contours are not continued into the backward hemisphere, since sufficient measurements were not made in this region.

Figs 23 & 24 are corresponding plots for $\alpha = 1.0$ Å^{-1} and $\alpha = 2.0$ Å^{-1}.

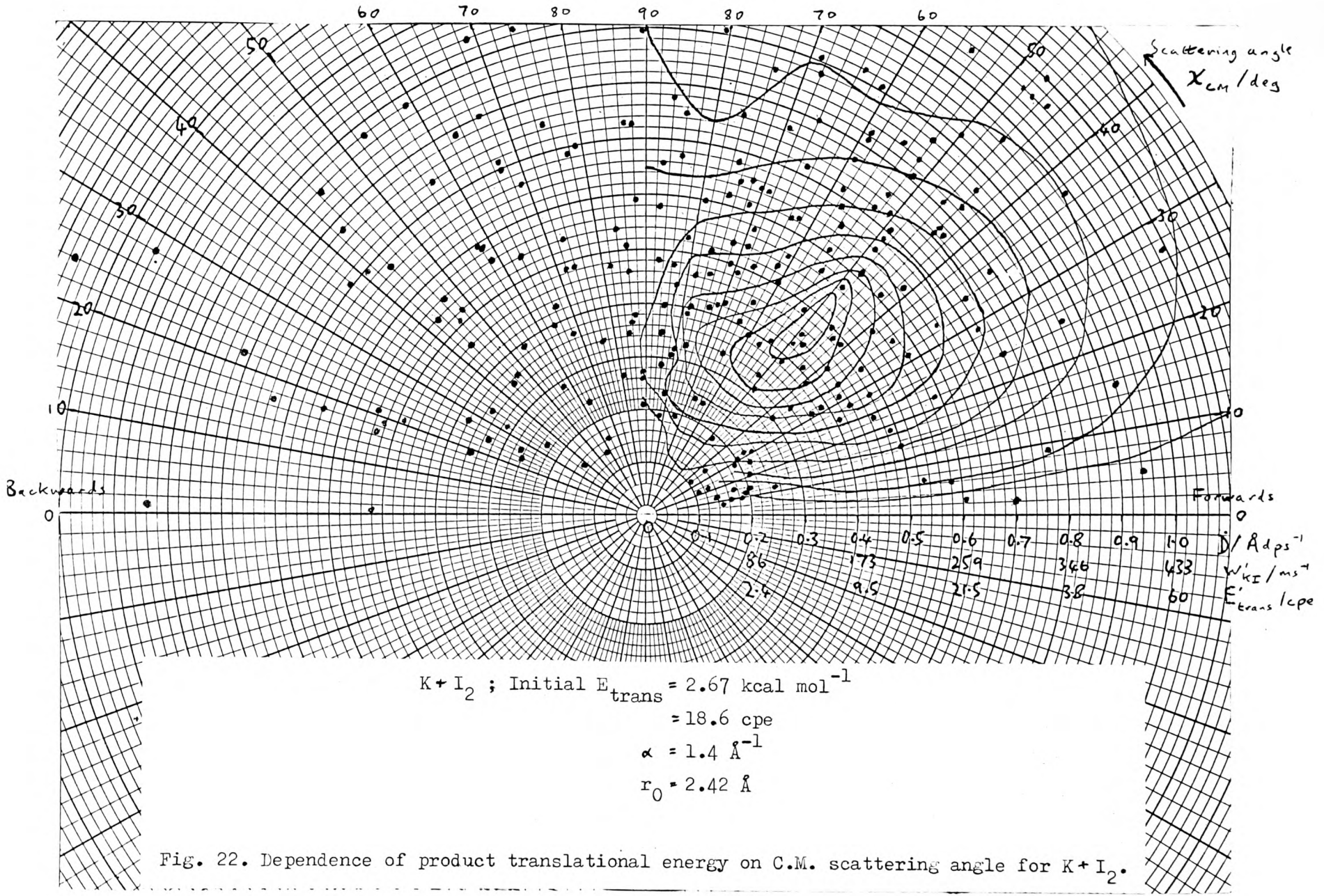

$K + I_2$; Initial E_{trans} = 2.67 kcal mol^{-1}

= 18.6 cpe

α = 1.4 $Å^{-1}$

r_0 = 2.42 Å

Fig. 22. Dependence of product translational energy on C.M. scattering angle for $K + I_2$.

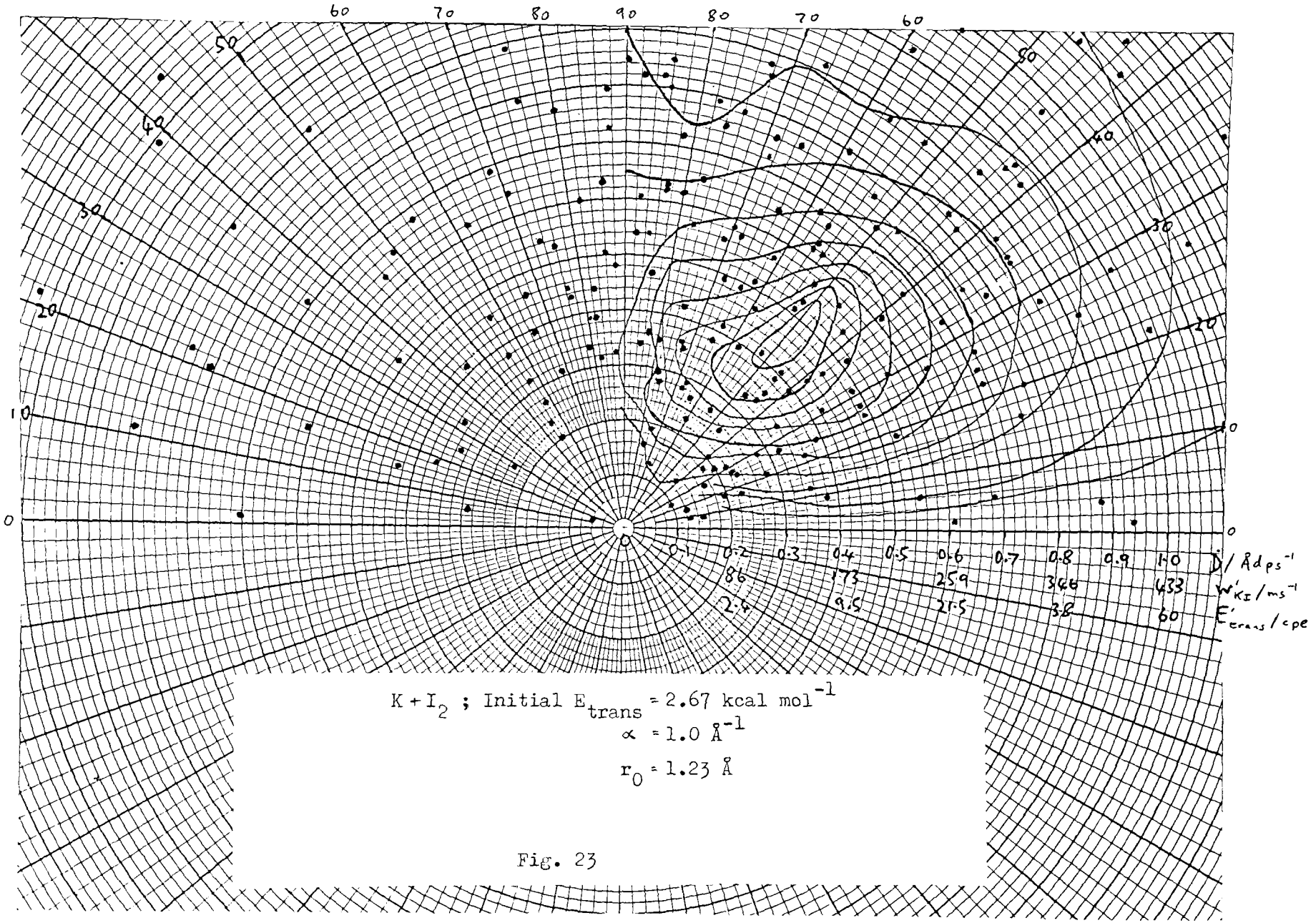

$K + I_2$; Initial $E_{trans} = 2.67$ kcal mol^{-1}

$\alpha = 1.0$ Å^{-1}

$r_0 = 1.23$ Å

Fig. 23

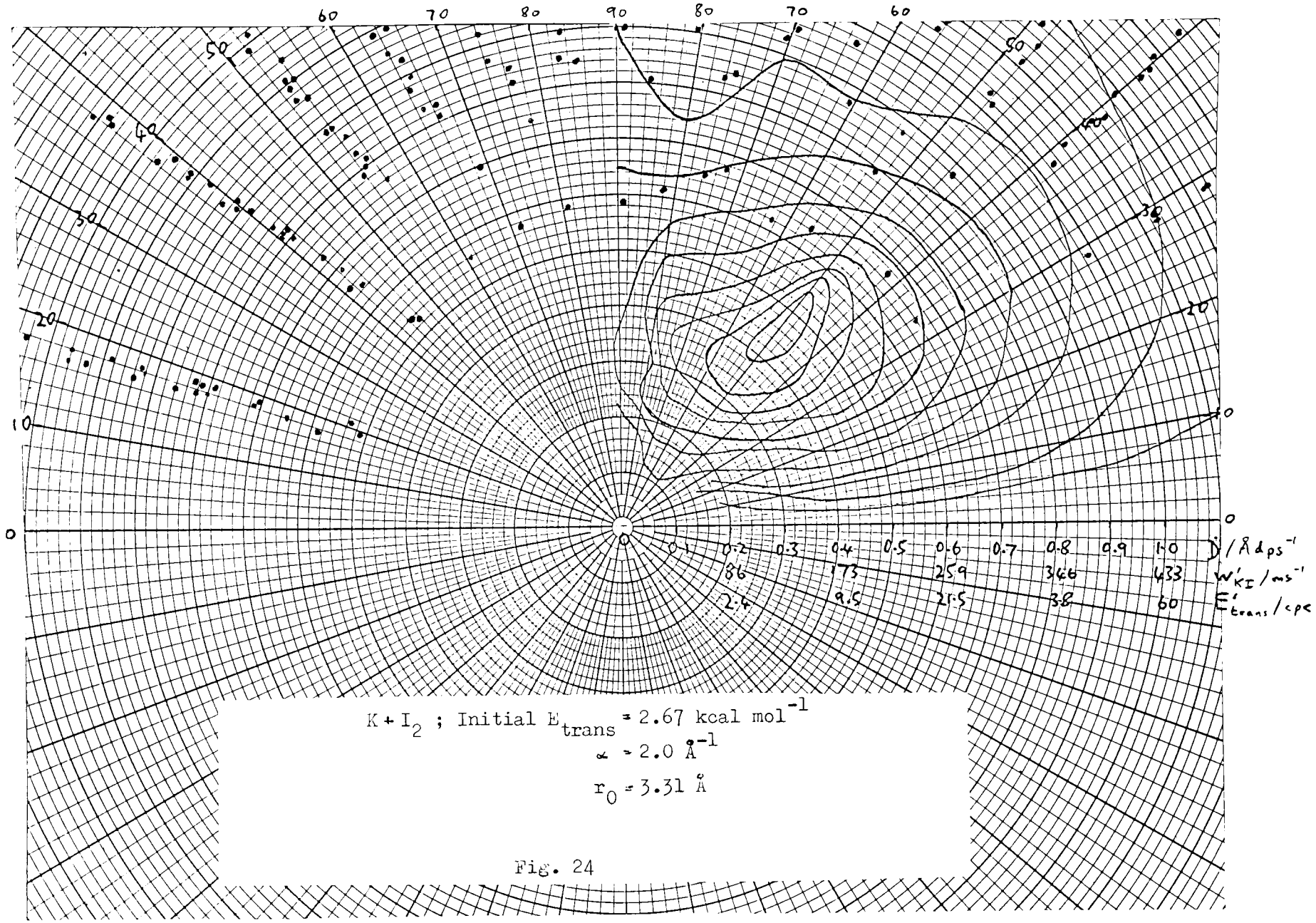

$K + I_2$; Initial $E_{trans} = 2.67$ kcal mol^{-1}

$\alpha = 2.0$ Å^{-1}

$r_0 = 3.31$ Å

Fig. 24

The somewhat regular distribution of points in fig. 24 is caused by the choice of starting values in the Monte Carlo method; rather than using random values of the impact parameter and initial diatom orientation, the values were obtained from regularly spaced grids of values of b^2 and $\sin\gamma$, which functions have flat probability distributions (see Gover, 1975); it was found that as α is increased, the final conditions vary more smoothly with the initial conditions, and approach a systematically spaced grid. However, for all three values of α, the effect of including initial diatom vibration is a considerable smearing out of the results. Although the results for $\alpha = 2$ Å^{-1} clearly agree poorly with experiment and $\alpha = 1.4$ Å^{-1} appears to give better agreement than $\alpha = 1.0$ Å^{-1}, it is not easy to decide from such diagrams on the optimum value of α, and whether this gives good agreement with experiment.

More detailed plots for our "best" value of $\alpha = 1.4$ Å^{-1} appear in figs 25 & 26. In fig. 25, experimental and theoretical angular distributions, averaged over all final velocities, are compared. These are $\sin\chi$-weighted distributions, which take out of plane scattering into account. The theoretical results were weighted by w'_{KI} to give fluxes, which are suitable for comparison with the experimental results. It can be seen that there is qualitative agreement although a quantitative comparison leaves a little to be desired. In fig. 26, sections through the polar plot of fig. 22, but again velocity-weighted to give fluxes, are shown at six different C.M. scattering angles, with the experimental results normalised to give the same total area under the six curves taken together. For each angle χ, trajectories falling in the range $\chi - 10^o$ to $\chi + 10^o$ were counted. Although the distributions generally agree in peaking at fairly low product translational energy (corresponding to high internal energy),

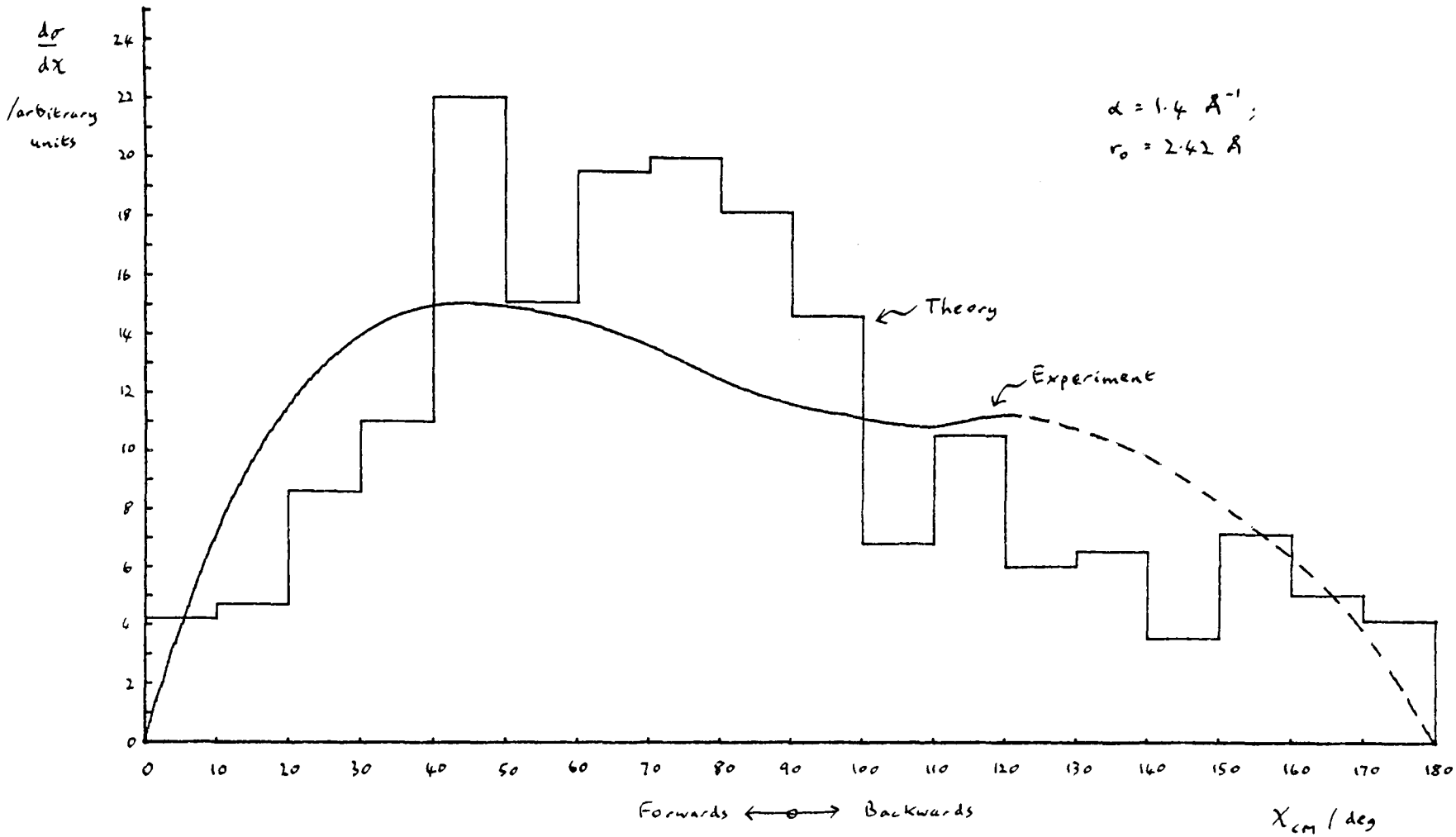

Fig. 25. Computed C.M. KI angular distribution, compared with experiment.

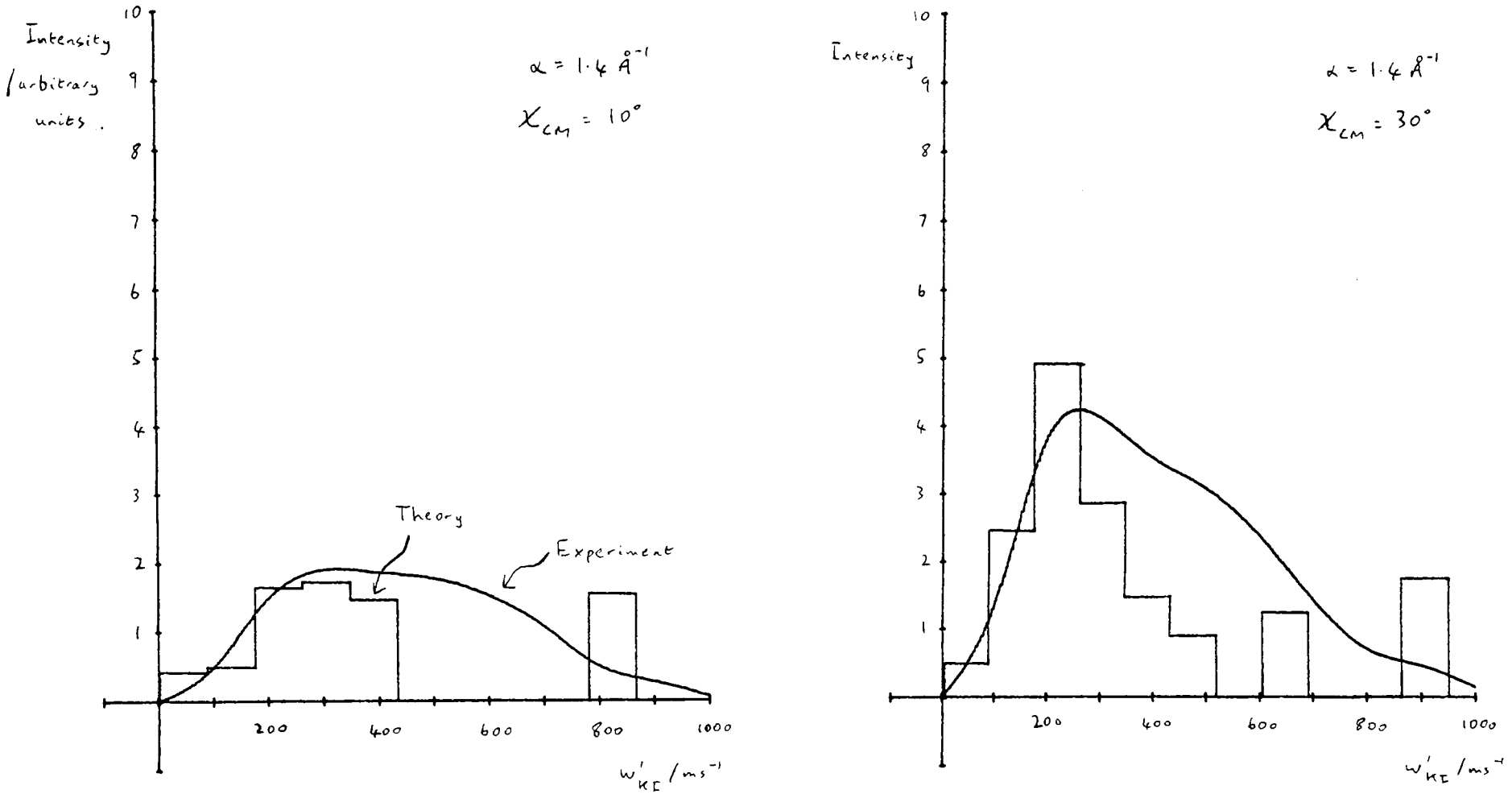

Fig. 26. Computed and experimental KI velocity distributions at various C.M. scattering angles.

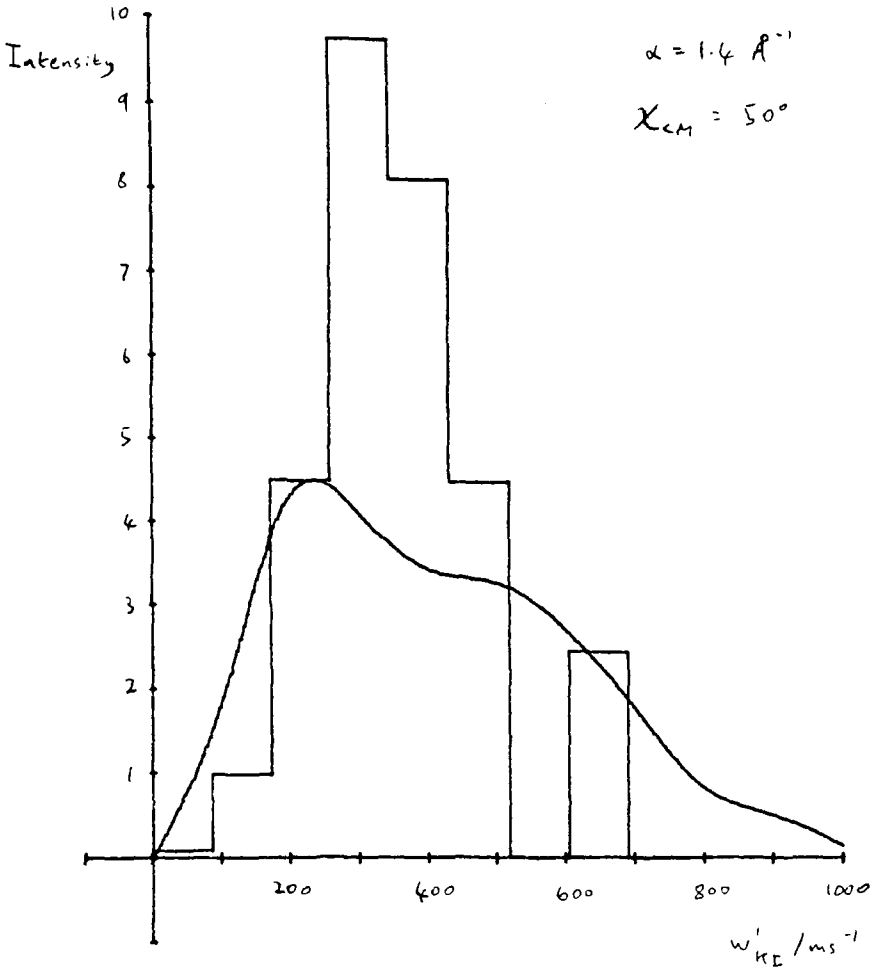

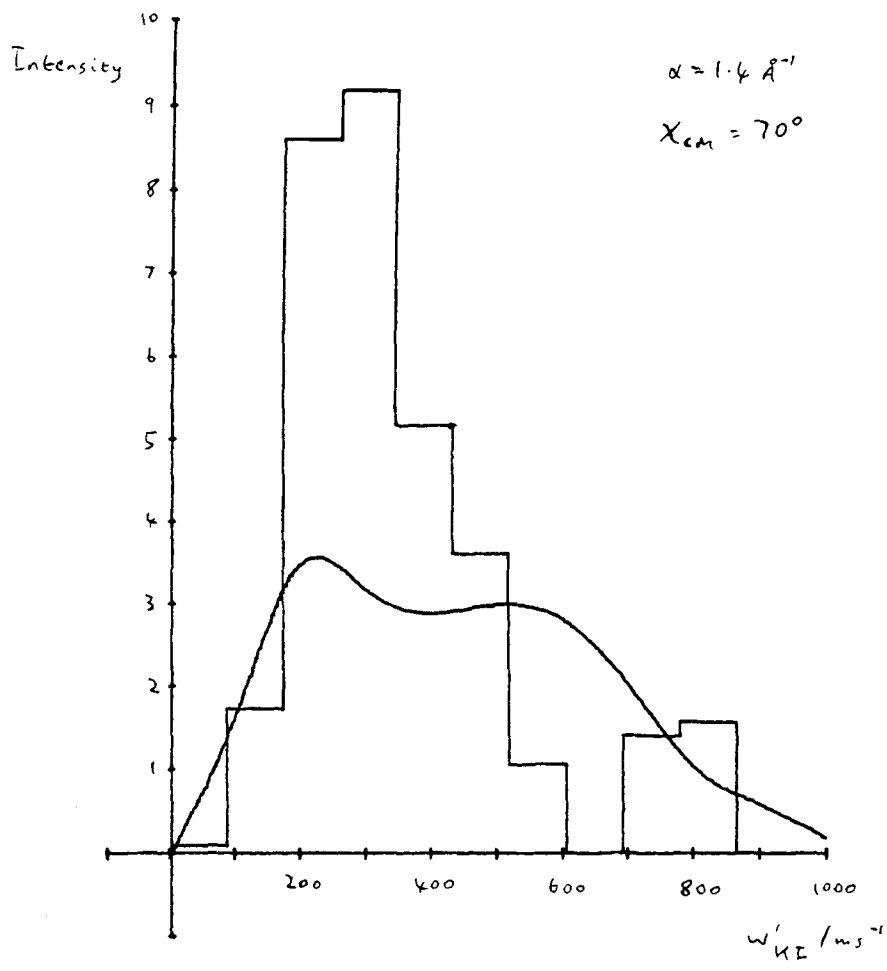

Fig. 26 continued

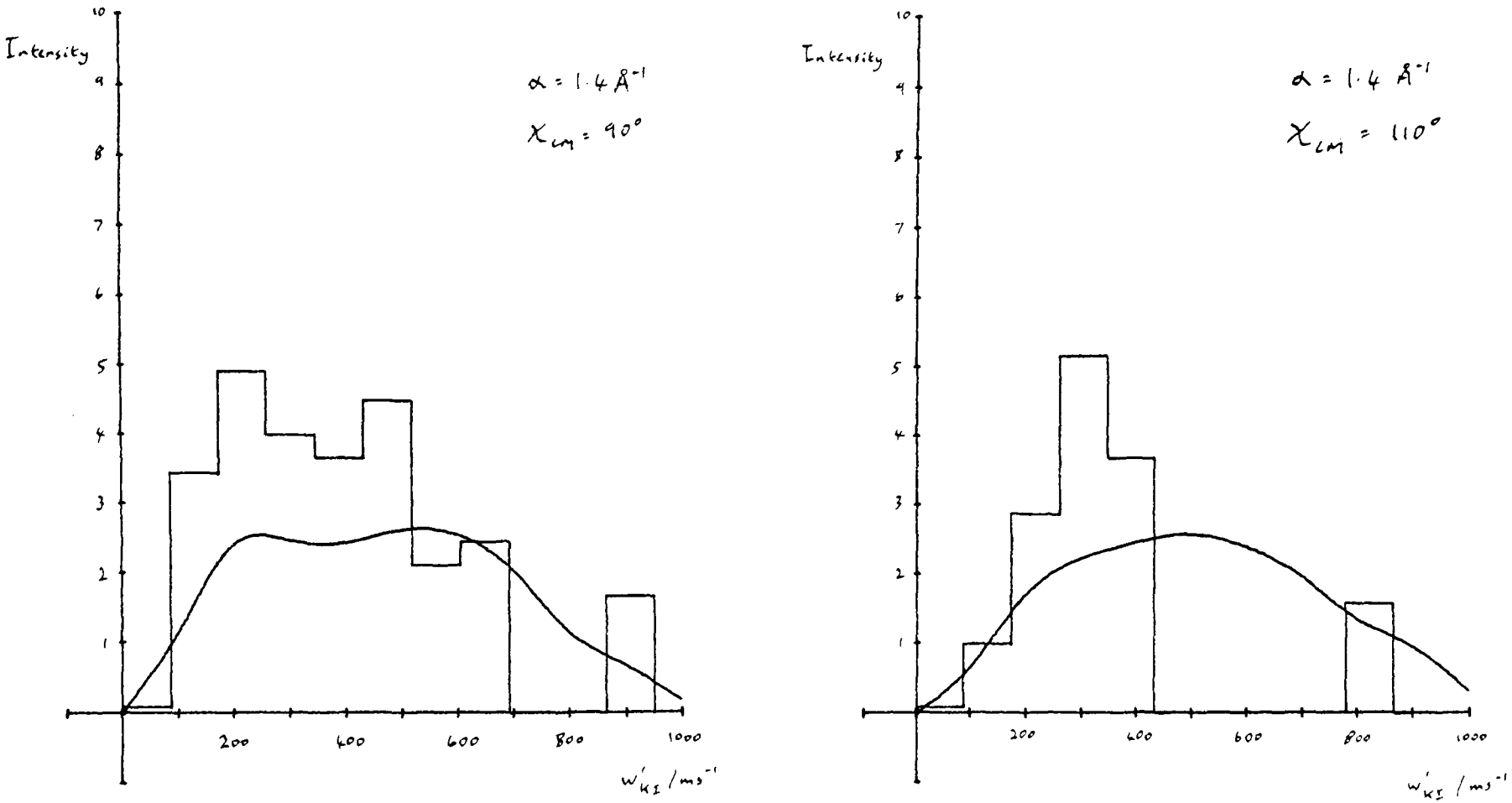

Fig. 26 continued

the overall agreement is fairly poor.

While polar velocity-angle plots contain the maximum information about the scattering, it is not easy to compare results with experiment using them. Hence it is desirable to find a few quantities which characterise the distributions and compare these. For various ranges of χ_{CM}, it was decided to calculate three numbers, which were: the percentage of the total flux falling within that range, the mean velocity, and the flux-weighted mean velocity (i.e. the next higher moment of the velocity distribution). These quantities were calculated from the experimental results (using velocity distributions at the middle of each angular range), and for the three sets of trajectory calculations. Three further sets of trajectory calculations, at intermediate values of α, were also performed, and the results are collected together in table 4.

Examining this table, it can be seen that it is still not easy to decide on an optimum value of α from the numbers presented. One factor contributing to this is the coarseness of the grid of starting values of the trajectories. As described above, use of systematically chosen pseudo-random instead of random starting conditions tends to produce a bunching effect in the final conditions, which is accentuated by the fairly small number of trajectories calculated (~ 300 for each calculation), and would be gradually smoothed out with an increasing number of trajectories. This is thought to be responsible for the oscillations observed in the plots of figs 25 & 26, also 28 & 29, and will make the numbers in table 4 fairly unreliable as each one is calculated from only a few trajectories.

Thus it is instructive to calculate properties of the distribution which involve a large number of trajectories. The quantities chosen,

	χ_{CM}/deg	Expt.	Theory ; α /Å^{-1}					
			1.0	1.2	1.4	1.6	1.8	2.0
% total flux	0-20	7.1	6.4	7.1	4.7	3.4	2.3	1.1
	20-40	14.4	14.9	14.7	10.4	10.8	6.6	4.9
	40-60	15.8	17.1	16.8	19.7	16.2	13.0	13.1
	60-80	14.4	16.8	18.0	21.0	21.4	19.7	15.8
	80-100	12.5	16.8	15.0	17.5	18.7	22.4	25.5
	100-120	11.8	10.8	10.4	9.3	11.9	14.4	15.7
Mean vel/ms^{-1}	0-20	341	303	214	227	198	292	506
	20-40	303	292	324	224	284	366	497
	40-60	293	336	300	315	299	403	512
	60-80	305	289	307	290	306	378	479
	80-100	332	370	299	291	282	385	484
	100-120	374	365	345	281	276	342	465
Flux-wtd mean vel/ms^{-1}	0-20	451	457	325	386	280	379	519
	20-40	410	413	454	352	358	425	511
	40-60	410	424	391	361	341	425	530
	60-80	435	408	373	356	375	402	494
	80-100	467	457	407	396	332	413	501
	100-120	502	460	398	351	307	371	488

Table 4.

which were calculated for scattering into the C.M. region $[0^{\circ}, 180^{\circ}]$, were the overall mean velocity, the velocity weighted mean velocity, and the mean C.M. scattering angle. These are shown below:

	Expt.	Theory ; α /Å^{-1}					
		1.0	1.2	1.4	1.6	1.8	2.0
Mean vel/ms^{-1}	321	327	304	283	288	374	485
Vel-wtd mean vel/ms^{-1}	442	433	396	366	343	405	503
Mean χ_{CM}/deg	62.2	63.3	62.3	65.5	68.7	74.6	78.1

These quantities vary quite smoothly with α, indicating that they contain information from enough trajectories to smooth out any bunching, as can be seen from fig. 27, in which they are plotted as a function of α, with the experimental results shown as straight lines. From this graph and the table, it is clear that, of the six values of α considered, α = 1.0 Å^{-1} is the optimum. In figs 28 & 29, angular and velocity distributions corresponding to those of figs 25 & 26 are plotted for this value of α.

D Calculations for Cs + I_2.

Having decided that for K + I_2 the optimum α is 1.0 Å^{-1}, it is interesting to test whether the optimum value of α is independent of the alkali metal, which it might reasonably be expected to be, if the I_2 bond weakening effect modelled is purely dependent on the electrical charge of the approaching ion, by repeating the calculation with the same α and r_0 for Cs + I_2. For this, the following parameters had to be changed:

Mass of Cs = 220.694 ppg

$\Rightarrow \mu_{Cs,I_2}$ = 144.846 ppg; μ_{CsI} = 107.798 ppg;

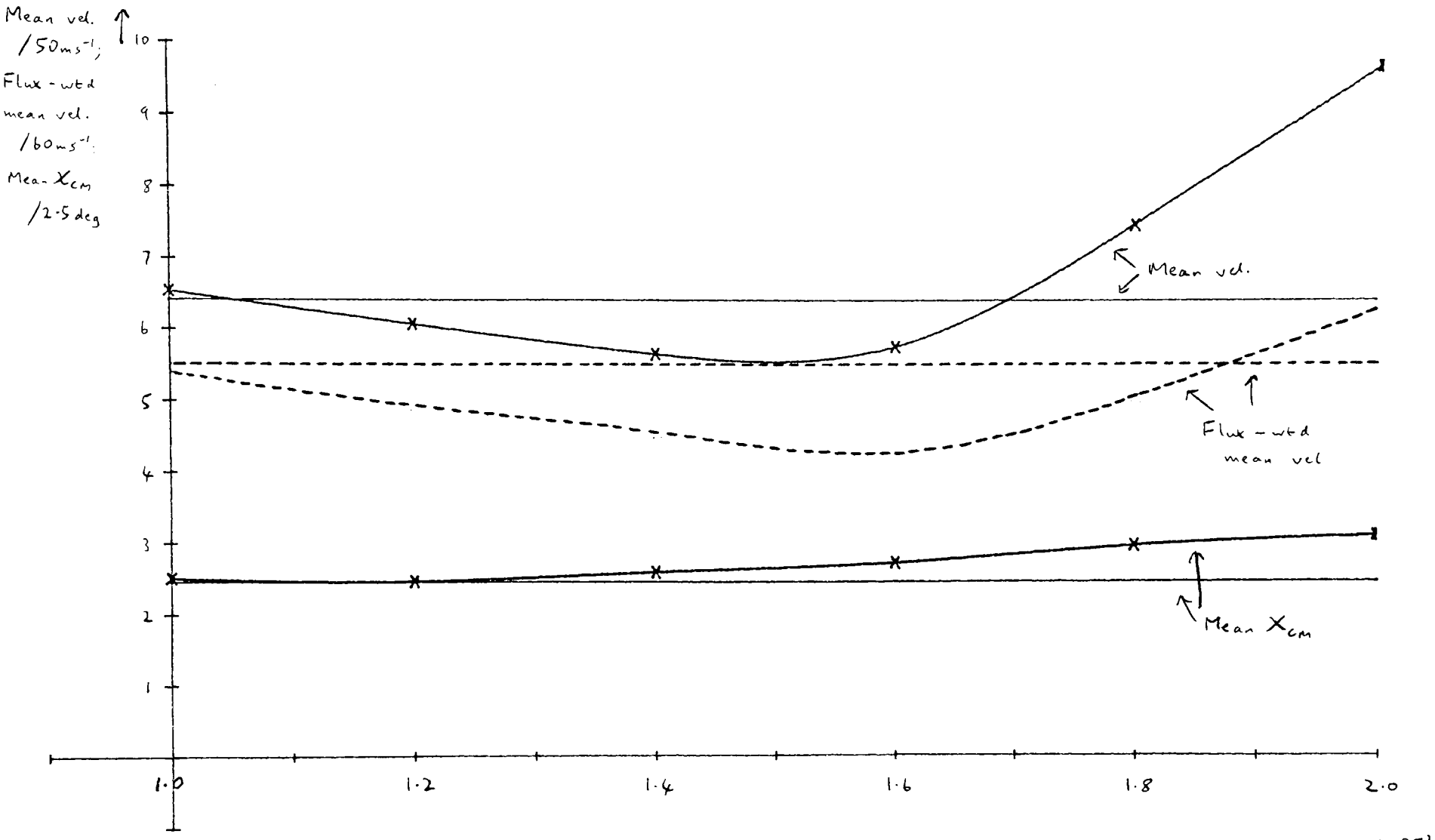

Fig. 27. Variation of various properties of the scattering with α for $K+I_2$.

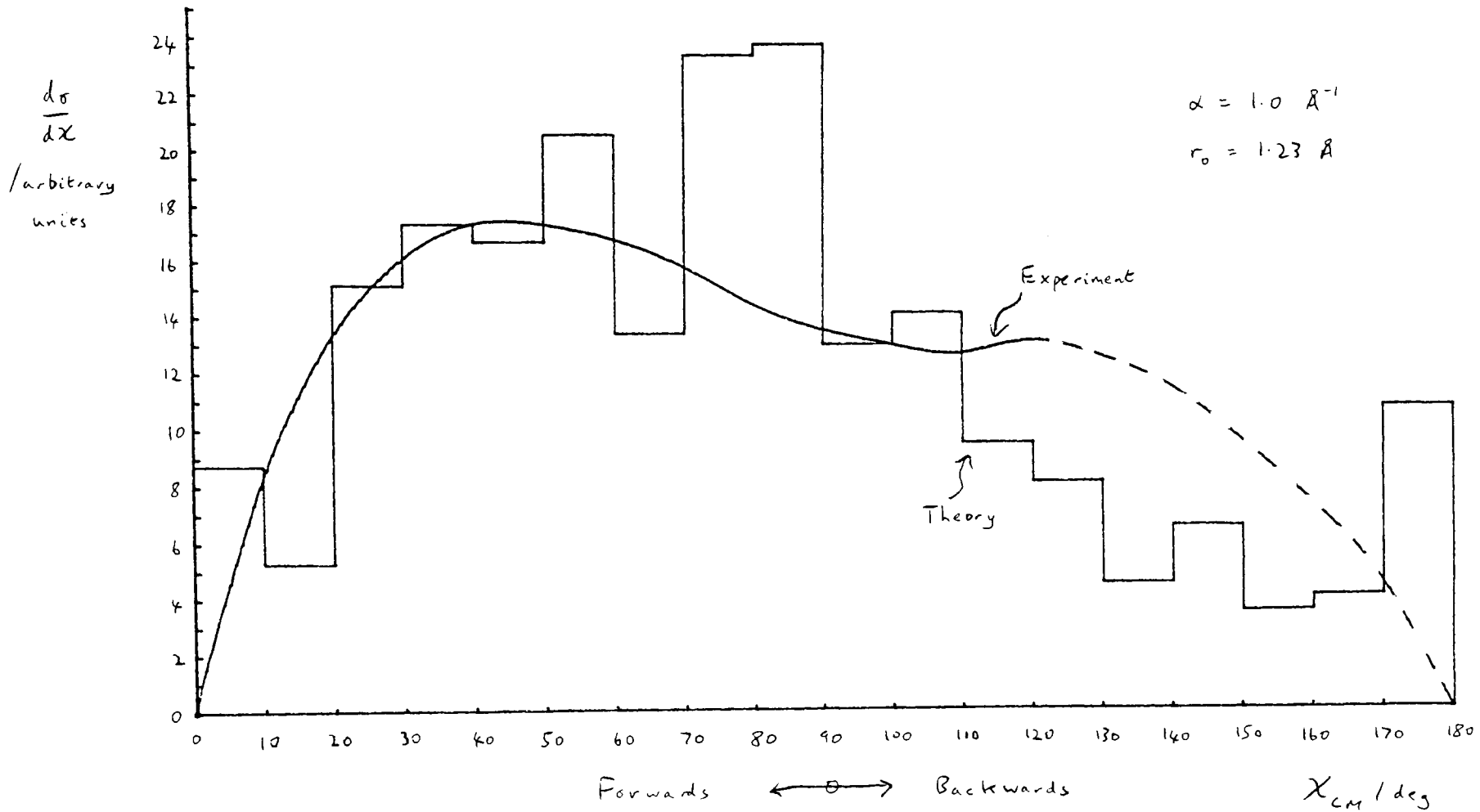

Fig. 28. C.M. KI angular distribution for $\alpha = 1.0$ Å^{-1}.

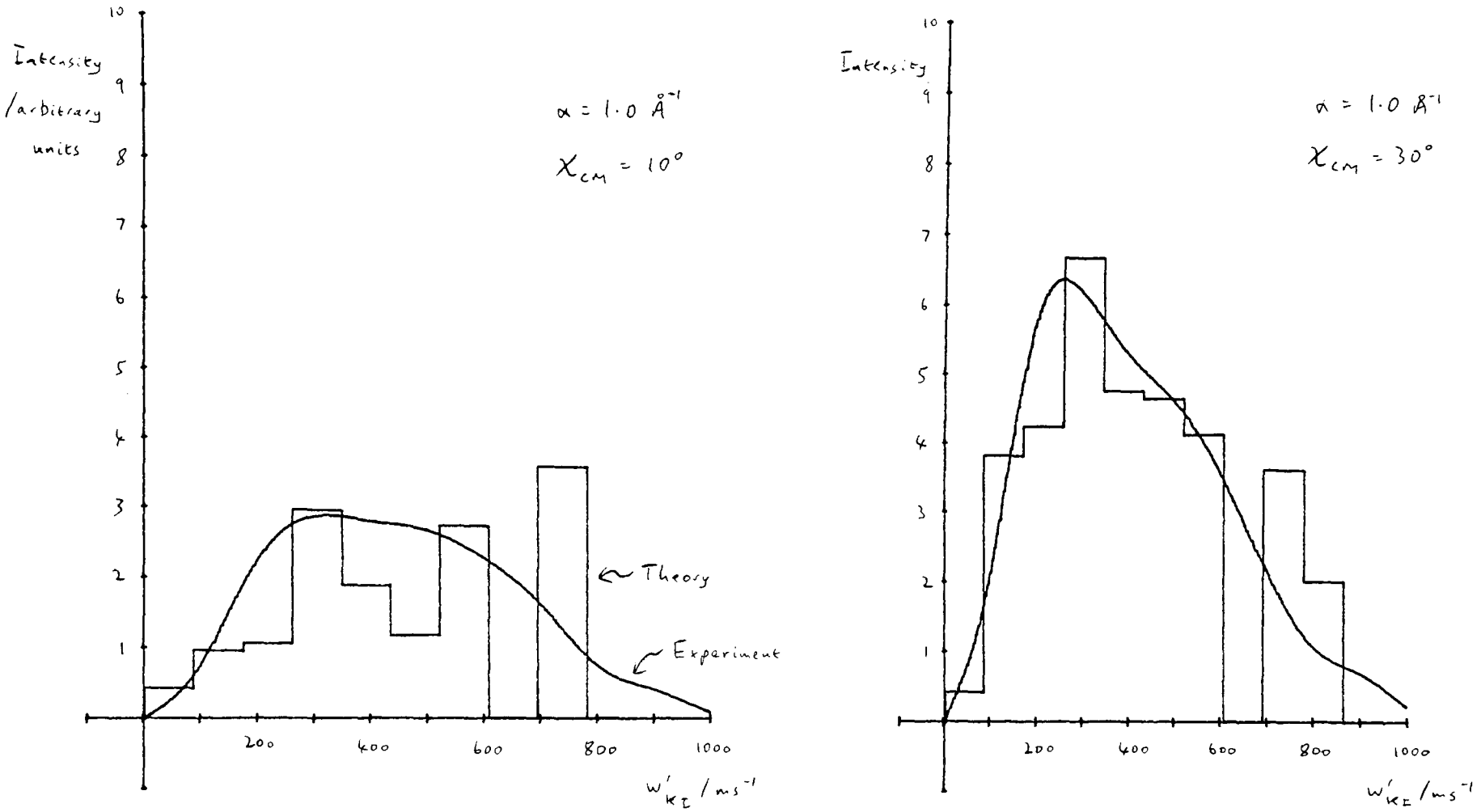

Fig. 29. Computed ($\alpha = 1.0$ Å^{-1}) and experimental KI velocity distributions at various C.M. scattering angles.

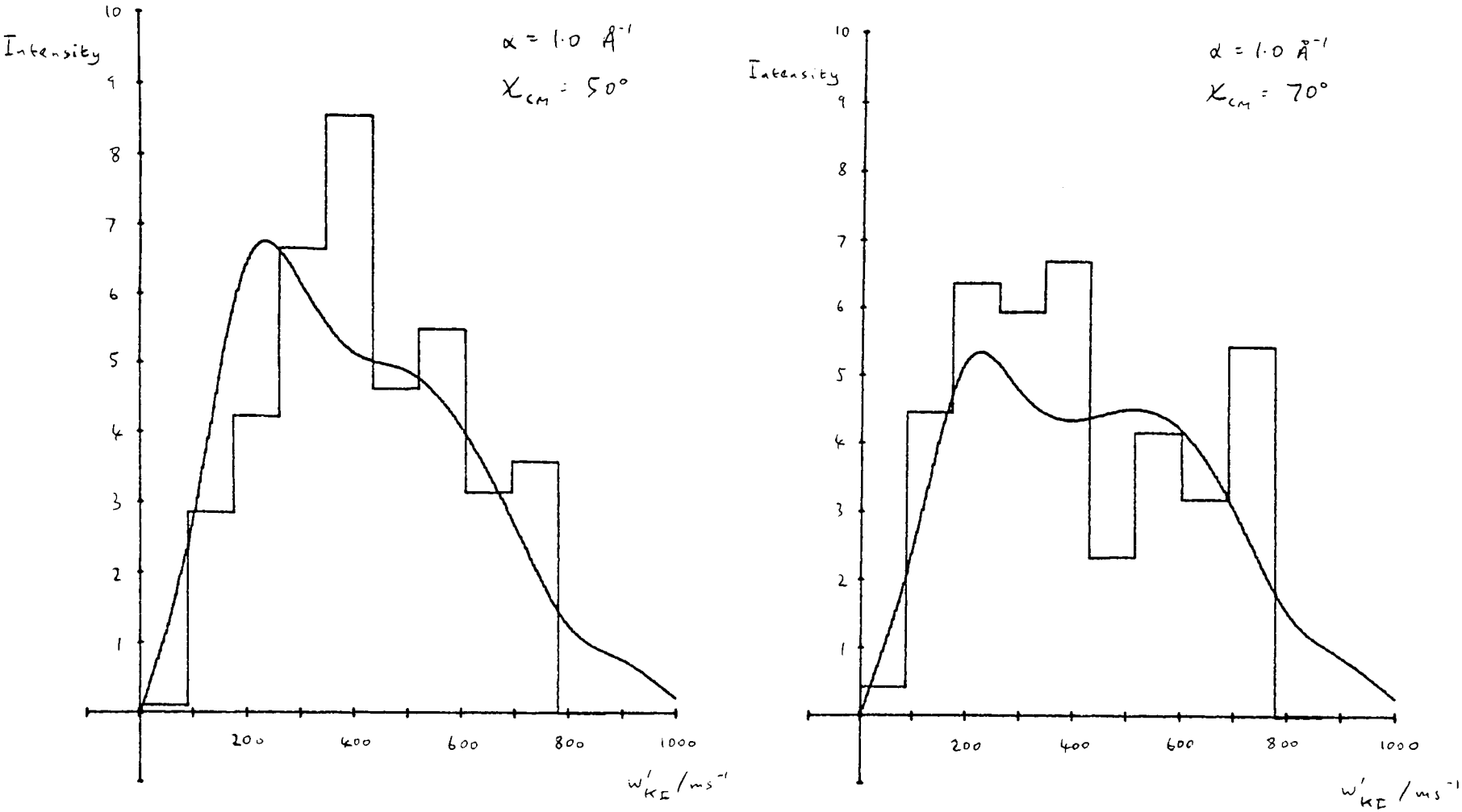

Fig. 29 continued

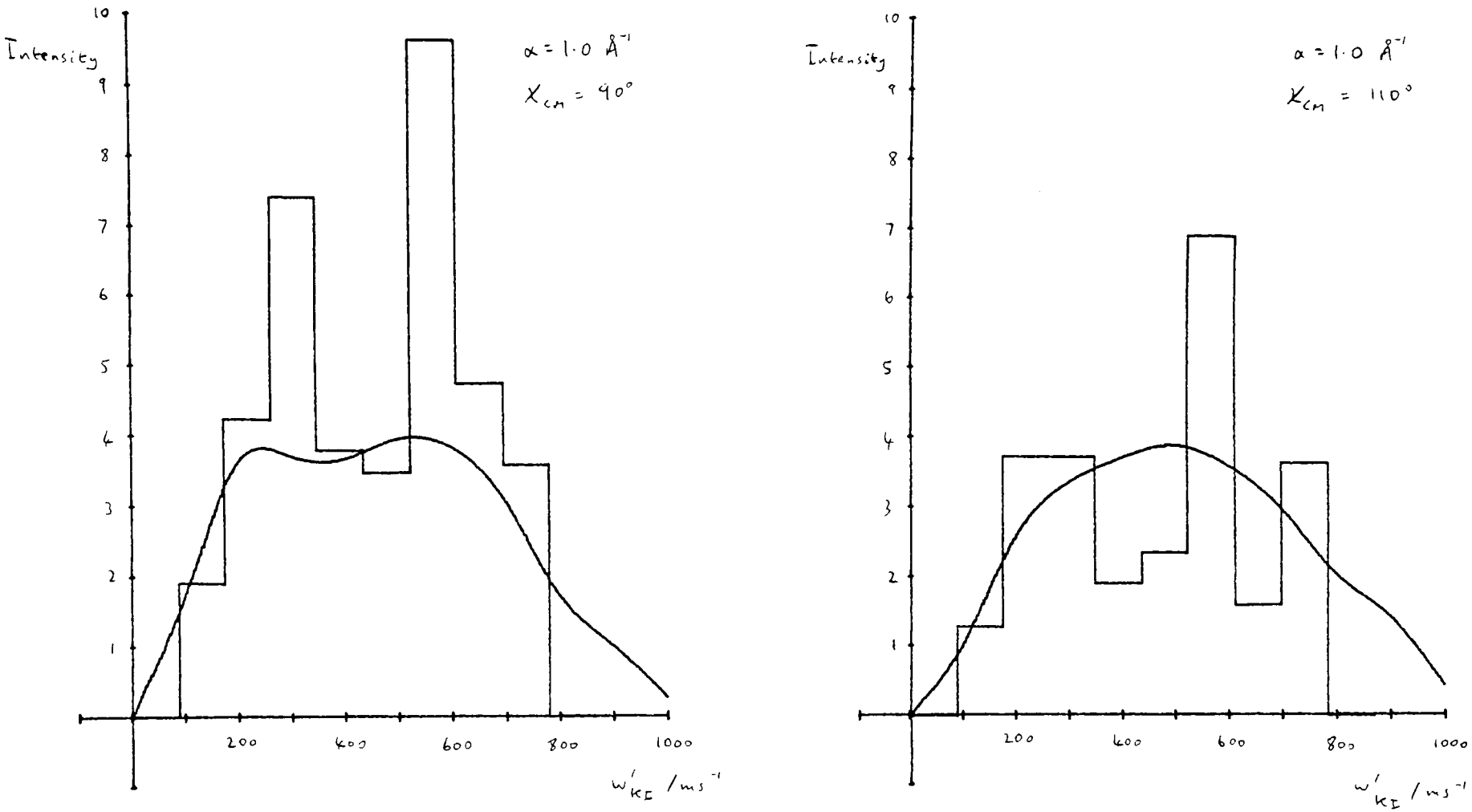

Fig. 29 continued

$$\mu_{I,CsI} = 141.576 \text{ ppg};$$

$$a = \frac{m_I}{2\mu_{I,CsI}} = 0.74423 \text{ ; (see Gover, 1975)}$$

$$b = \frac{\mu_{Cs,I_2}}{2\mu_{I,CsI}} = 0.51155.$$

$$\alpha_{Cs^+} = 2.44 \text{ Å}^3; \quad A = 35200 \text{ eV} = 5.64 \times 10^6 \text{ cpe};$$

$$k = 0.308 \text{ Å} \quad \text{(Rittner, 1951)}$$

The initial relative translational energy used was

$$E_{trans} = 1.14 \text{ kcal mol}^{-1}$$

corresponding to a relative velocity of 0.331 Å dps^{-1}. This then allows comparison with the experimental results of Birely et al (1967).

In fig. 30, the $\sin\chi$-weighted angular distributions from the theoretical and experimental results are plotted, normalised to the same total area. From this it can be seen that the agreement is not as good as for $K + I_2$, indicating that for $Cs + I_2$ different optimum values for α and r_0 are required, and hence that the bond weakening effect as modelled cannot be taken to be independent of the nature of the alkali metal atom.

E Summary and conclusions.

Following the work of (Gover, 1975), further classical trajectory calculations have been carried out for the reactive system $K + I_2 \rightarrow KI + I$, and more detailed comparison made with experiment.

(i) Allowance for the spread of initial diatom separations as a result of ground state vibration, in the crude manner described,

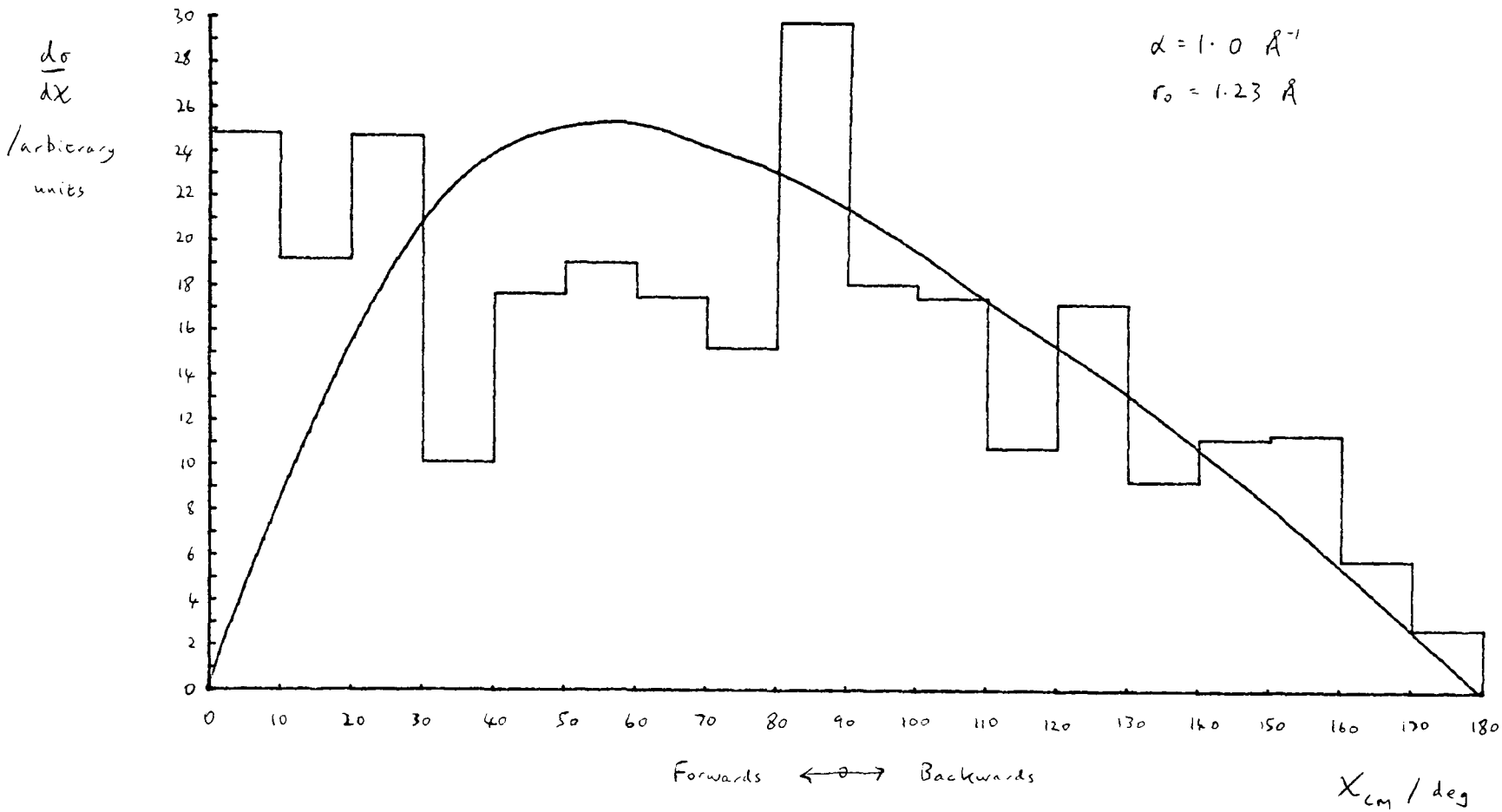

Fig. 30. Comparison of theoretical and experimental product angular distributions, for $Cs + I_2$.

was responsible for a general smearing out of the results. However, owing to the relatively small number of trajectories calculated, and the systematic method of choosing starting conditions, it was found that there was still a tendency for the results to bunch together. Thus comparison of theory with experiment using polar velocity-angle plots and sections through them has proved a little difficult.

(ii) The following quantities were calculated from theory and experiment for trajectories falling in 20 degree regions of the C.M. scattering angle: percentage of the total flux falling in the region, mean velocity, and flux-weighted mean velocity. Comparisons with these numbers are still difficult, as each number is calculated from only a small fraction of the trajectories. Thus, numbers dependent on nearly all trajectories were calculated, viz. the mean C.M. scattering angle, overall mean velocity, and flux-weighted mean velocity, for the trajectories falling in the χ_{CM} range 0^{o} - 120^{o}. Since these numbers vary smoothly with the one parameter α, it is thought that they contain information from sufficient trajectories. On the basis of this comparison, $\alpha = 1.0$ Å^{-1} was chosen as the "best" value for $K + I_2$.

(iii) The calculation was repeated for $Cs + I_2$ with the same best values for α and r_0. Agreement with experiment was not as good as for $K + I_2$, indicating that the I_2 bond weakening effect as modelled cannot in fact be described as independent of the nature of the alkali ion and merely dependent on its charge.

CHAPTER V

CHARGE NEUTRALISATION IN $Na^+ + I^-$ COLLISIONS AS A POSSIBLE LASER PUMPING MECHANISM

A Introduction.

The type of collision considered in this chapter is the reverse of that considered in the previous two, i.e. mutual charge neutralisation of oppositely charged ions. A few beam experiments, using the technique of merging beams, have been performed on such collisions, e.g. with $N^+ + O^-$ (Aberth et al, 1968), $H^+ + H^-$ (Moseley et al, 1970), $Na^+ + O^-$ (Weiner et al, 1970; 1971). In the latter case, it was observed that excited sodium atoms Na(3d) were formed with high probability. By analogy with this, and because of the observation of intense sodium D line emission in shock generated sodium iodide plasmas, Gait & Berry (1977) have suggested that Na(3p) could be formed with high efficiency in the process $Na^+ + I^- \rightarrow Na + I$, and that it may be possible in this way to produce a population inversion of Na(3p) with respect to the ground state Na(3s). In this chapter, calculations on this system, using the multi-curve crossing formalism developed above, are reported.

Considering the electronic states of the Na atom, and ignoring the internal states of the I atom, two covalent channels are energetically accessible:

$$Na^+ + I^- \longrightarrow \begin{cases} Na(3s) + I \\ \\ Na(3p) + I \end{cases} \qquad (5\text{-}1)$$

The diabatic curves for these three channels are sketched in fig. 31, and the labelling of the channels which will be used throughout is indicated. Since only two atoms are involved, there is only one degree of freedom, the internuclear distance r, and these are true potential energy "surfaces".

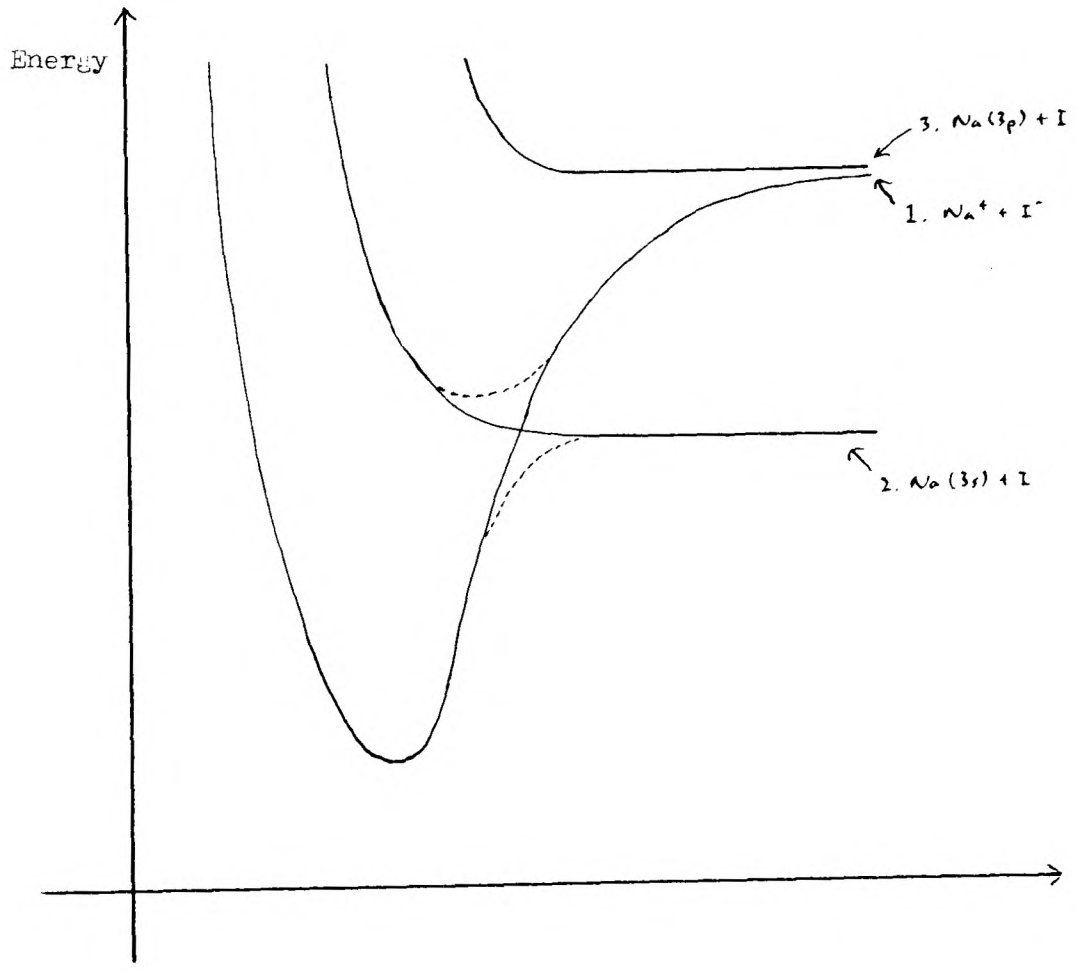

Fig. 31.

Note that, although curves 1 and 3 do not cross, they almost coincide asymptotically, because of the accidental near equality of the first ionisation potentials of Na(3p) and I^-. It has been

suggested (Gait & Berry, 1977) that this proximity of the curves over a large range of r could be responsible for a considerable probability of transition between the diabatic curves 1 and 3.

Using published expressions for the diagonal matrix elements H_{11} and H_{22}, and calculated values for H_{12} and H_{13}, the probability of such a transition was investigated in the framework of the classical trajectory approximation.

B The coupled equations.

Consider the time-dependent coupled equations of the classical trajectory approximation:

$$\sum_j H_{ij}\, c_j(t) = i\hbar \frac{d}{dt}\, c_i(t) \qquad (2\text{-}23)$$

With i,j = 1, 2, 3, these were applied to the three diabatic states shown in fig. 31. This in itself is an approximation, since the three states do not form a complete basis set, and in particular the overlap $\langle i|j \rangle$ between ionic and covalent states may be considerably different from zero.

Splitting the coefficients into real and imaginary parts, this produces 6 simultaneous first order differential equations:

Putting $c_i(t) = R_i(t) + i\, I_i(t)$,

$$i\hbar \frac{d}{dt}(R_i + i\, I_i) = \sum_j H_{ij}(R_j + i I_j)$$

$$\Rightarrow \hbar \frac{d}{dt} R_i = \sum_j H_{ij}\, I_j$$

and

$$\hbar \frac{d}{dt} I_i = -\sum_j H_{ij}\, R_j$$

These equations were solved using Krogh's method. The evaluation of

the ⋕ matrix elements H_{ij} and the classical trajectory are considered in sections C & D.

C Calculation of the ⋕ matrix elements.

(i) Diagonal elements.

The diagonal elements were obtained from those given by Delvigne & Los (1973). For the ionic diabatic potential, a Kittner (1951) potential was used:

$$H_{11}(r) = U_{ion}(r) = -\frac{e^2}{4\pi\varepsilon_0 r} - \frac{e^2(\alpha_{Na^+} + \alpha_{I^-})}{8\pi\varepsilon_0 r^4} - \frac{e^2\alpha_{Na^+}\alpha_{I^-}}{2\pi\varepsilon_0 r^7}$$

$$- \frac{C_{ion}}{r^6} + A_{ion}\, e^{-r/k_{ion}} \qquad (5\text{-}2)$$

This establishes the zero of energy as infinitely separated $Na^+ + I^-$. The values of the parameters used were:

$$\alpha_{Na^+} = 0.408\ \text{Å}^3;$$

$$\alpha_{I^-} = 6.431\ \text{Å}^3;$$

$$C_{ion} = 1810\ \text{cpe Å}^6; \quad (\sim 11\ \text{eV Å}^6)$$

$$A_{ion} = 3.066 \times 10^5\ \text{cpe}; \quad (\sim 1.8\ \text{keV})$$

$$k_{ion} = 0.3489\ \text{Å}.$$

The ground state covalent diabatic potential contains a C_6 long range attraction and an exponential short range repulsion:

$$H_{22}(r) = U_{cov}(r) = -\frac{C_{cov}}{r^6} + A_{cov}\, e^{-r/k_{cov}} - \Delta E_1 \qquad (5\text{-}3)$$

where $\Delta E_1 = I_{Na} - E_{aI}$,

with the parameters

$$C_{cov} = 1.602 \times 10^5 \text{ cpe } \text{Å}^6 \; ; \quad (\sim 0.9 \text{ keV } \text{Å}^6)$$

$$A_{cov} = 5.047 \times 10^5 \text{ cpe} \; ; \quad (\sim 3.1 \text{ keV})$$

$$k_{cov} = 0.435 \text{ Å}$$

and I_{Na} = 1st ionisation potential of Na = 823.3 cpe;

E_{aI} = electron affinity of I = 490.8 cpe (Berry & Reimann, 1963)

$$\Rightarrow \quad \Delta E_1 = 332.5 \text{ cpe.}$$

The curves $H_{11}(r)$ & $H_{22}(r)$ cross at a point $r = r_c$ given by

$$H_{11}(r_c) = H_{22}(r_c)$$

$$\Rightarrow \quad r_c = 6.97 \text{ Å}$$

The excited state covalent diabatic curve $H_{33}(r)$ was assumed to be parallel to $H_{22}(r)$ and separated from it by the asymptotic energy difference, which is the energy of the sodium "D" line:

$$H_{33}(r) = U_{cov}(r) + \Delta E_2 \qquad (5\text{-}4)$$

where $\Delta E_2 = E(\text{Na } 3p\ ^2P_{\frac{1}{2}}) - E(\text{Na } 3s\ ^2S_{\frac{1}{2}})$

$= 337.2$ cpe (Moore, 1949)

Notice that this is very nearly equal to ΔE_1, hence, as described in section A above, H_{11} and H_{33} come very close together asymptotically:

$$H_{33}(\infty) - H_{11}(\infty) = U_{cov}(\infty) + \Delta E_2 - 0$$

$$= - \Delta E_1 + \Delta E_2$$

$$= 4.7 \text{ cpe} \quad (\sim 0.025 \text{ eV})$$

(c.f. well depth of Na^+I^- ~910 cpe).

H_{11}, H_{22} and H_{33} are plotted as functions of r in fig. 33, where it can be seen that, although H_{11} and H_{33} become very close asymptotically (the asymptote of H_{11} being at zero), owing to the extreme long range nature of the Coulomb attraction, this condition is only approached at very large separations.

(ii) Introduction to calculation of off-diagonal elements.

Since H_{22} and H_{33} never come close together, $H_{23}(r)$ was assumed to be zero.

Very little work has been done on the variation of the off-diagonal integrals with r. Hence it was decided to calculate H_{12} and H_{13} at various values of r, and fit these to a simple functional form. They were estimated by the method described by Magee (1940; 1952), Berry (1957), Grice & Herschbach (1974), and Adelman & Herschbach (1977).

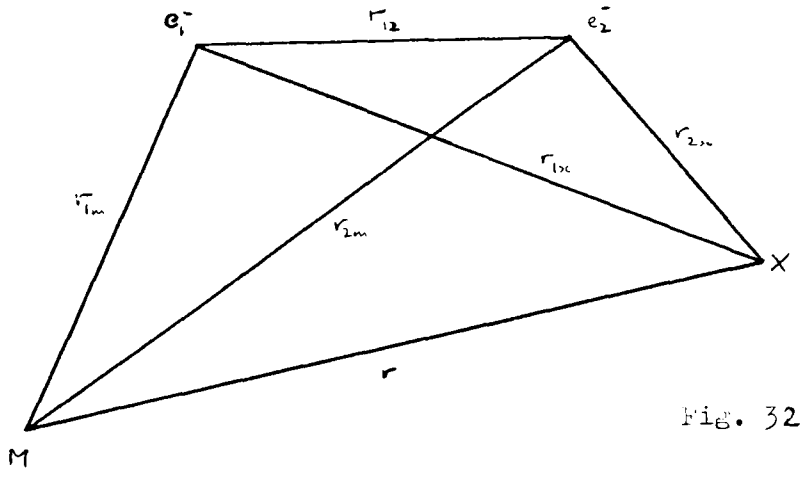

Fig. 32

Following Magee (1952), we use a two-electron approximation, with the various distances involved being labelled as shown in fig. 32 for a general M / X system. For ease of writing and later

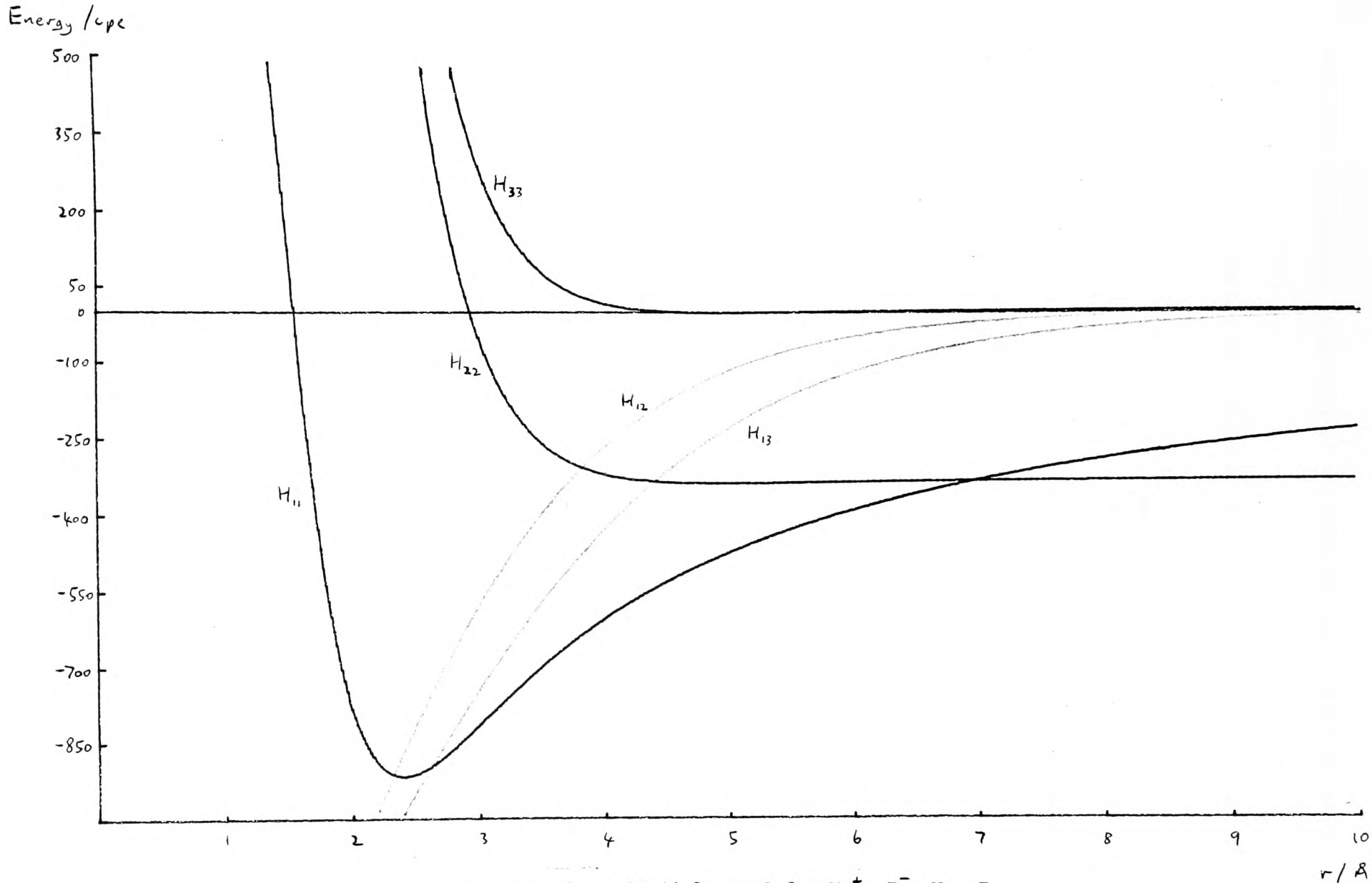

Fig. 33. The potentials used for $Na^+ + I^- \rightarrow Na + I$

numerical calculation, this part of the work was done in atomic units, in which $\hbar = m_e = e = 1$.

The Hamiltonian for the system is then

$$H = -\nabla_1^2 - \nabla_2^2 - \frac{1}{r_{1m}} - \frac{1}{r_{2x}} - \frac{1}{r_{1x}} - \frac{1}{r_{2m}} + \frac{1}{r_{12}} + \frac{1}{r} \qquad (5\text{-}5)$$

In the ionic configuration $M^+ + X^-$, both electrons are on the halogen atom, and the wavefunction can be written as a simple product

$$|i\rangle = x'(1)\, x'(2) \qquad (5\text{-}6)$$

where x' is the appropriate atomic orbital of X^-.

In the covalent configuration $M + X$, one electron is on each atom, and the wavefunction is assumed to be a symmetrised product:

$$|c\rangle = \frac{1}{\sqrt{2}} \{ m(1)\, x(2) + m(2)\, x(1) \}$$

where m and x are the appropriate orbitals of M & X respectively.

Combining this with (5-5) & (5-6),

$$H_{ic} = \langle i|H|c\rangle$$

$$= \frac{1}{\sqrt{2}} \iint (m(1)\, x(2) + m(2)\, x(1))\, H(1,2)\, x'(1)\, x'(2)\, d\tau_1\, d\tau_2$$

$$= \sqrt{2} \iint m(1)\, x(2)\, H\, x'(1)\, x'(2)\, d\tau_1\, d\tau_2$$

$$\Rightarrow \frac{1}{\sqrt{2}} H_{ic} = \iint m(1)\, x(2) \left[-\nabla_1^2 - \nabla_2^2 - \frac{1}{r_{1m}} - \frac{1}{r_{2x}} - \frac{1}{r_{1x}} - \frac{1}{r_{2m}} + \frac{1}{r_{12}} + \frac{1}{r} \right] x'(1)\, x'(2)\, d\tau_1\, d\tau_2$$

Now, put $\int m(1)\, x'(1)\, d\tau_1 = S_{mx'}$; $\int x(2)\, x'(2)\, d\tau_2 = S_{xx'}$

and assume $S_{xx'} = 1$

Also, note that

$$\left[-\nabla_1^2 - \nabla_2^2 - \frac{1}{r_{1x}} - \frac{1}{r_{2x}} + \frac{1}{r_{12}} \right] x'(1)\, x'(2) = E(M^+ + X^-)\, x'(1)\, x'(2)$$

where $E(A + B)$ means the energy of infinitely separated A & B.

$$\therefore \frac{H_{ic}}{\sqrt{2}} = E(M^+ + X^-) S_{mx'} S_{xx'} + \iint m(1)x(2) \left[-\frac{1}{r_{1m}} - \frac{1}{r_{2m}} + \frac{1}{r} \right] x'(1)x'(2)\, d\tau_1 d\tau_2$$

But the energy scale is defined such that $E(M^+ + X^-) = 0$

$$\Rightarrow \frac{H_{ic}}{\sqrt{2}} = - S_{xx'} \int m(1) \frac{1}{r_{1m}} x'(1)\, d\tau_1 - S_{mx'} \int x(2) \frac{1}{r_{2m}} x'(2)\, d\tau_2$$

$$+ \iint m(1)\, x(2) \frac{1}{r} x'(1)\, x'(2)\, d\tau_1\, d\tau_2$$

Now, if electron 1 is the one which is transferred, and r is large, which it generally is in alkali / halogen systems, with their large crossing distances, then $r_{2m} \simeq r$, and, as an approximation, we cancel the last two terms, to give

$$H_{ic} = -\sqrt{2} \int m(1) \frac{1}{r_{1m}} x'(1)\, d\tau_1 \qquad (5\text{-}7)$$

Using this approximation, $H_{ii} = \langle i|H|i\rangle$ is also readily calculated:

$$H_{ii} = - \int x'(1) \frac{1}{r_{1m}} x'(1)\, d\tau_1 - \int x'(2) \frac{1}{r_{2m}} x'(2)\, d\tau_2$$

$$+ \iint x'(1)\, x'(2)\, \frac{1}{r}\, x'(1)\, x'(2)\, d\tau_1\, d\tau_2$$

$$= -2 \int x'(2)\, \frac{1}{r_{2m}}\, x'(2)\, d\tau_2 + \iint x'(1)\, x'(2)\, \frac{1}{r}\, x'(1)\, x'(2)\, d\tau_1\, d\tau_2$$

$$= -\frac{1}{r} S_{xx'}$$

Hence, again putting $S_{xx'} = 1$,

$$H_{ii} = -\frac{1}{r} \tag{5-8}$$

and it can be seen that the approximation is equivalent to taking only the first term in the Kittner expression, which is acceptable for large r.

The overlap $S_{ic} = \langle i|c \rangle$ is also readily calculated, to give

$$S_{ic} = \sqrt{2}\, S_{mx'}\, S_{xx'}$$

or, with $S_{xx'} = 1$ again,

$$S_{ic} = \sqrt{2}\, S_{mx'} \tag{5-9}$$

Using the notation $m(1) = |m\rangle$; $x(1) = |x\rangle$;

$x'(1) = |x'\rangle$; $r_{1m} = \rho_m$

and substituting (5-7), (5-8), and (5-9) in (2-28), we get

$$\Delta V(r_c) = 2 \left| \frac{H_{ii}\, S_{ic} - H_{ic}}{1 - S_{ic}^2} \right|$$

$$= 2\sqrt{2} \left| \frac{\langle x|x' \rangle \langle m| \frac{1}{\rho_m} - \frac{1}{r}|x' \rangle}{1 - S^2} \right| \tag{5-10}$$

with $S = \sqrt{2} \langle x|x' \rangle \langle m|x' \rangle$

where all quantities are evaluated at $r = r_c$, and $\langle x|x' \rangle = 1$ has been restored. (5-10) is the expression used by Grice & Herschbach (1974) to calculate $\Delta V(r_c)$ (see also Bates & Moiseiwitsch, 1954; Bates & Boyd, 1956; Adelman & Herschbach, 1977). The values calculated in this way are often converted back to H_{ic} values using the simpler formula (2-30) (see e.g. Baede, 1975), which is a little suspect here, since even if S is quite small, as it is shown below to be in this system, $H_{ii}(r_c)$ may be significantly large, e.g. ~ -330 cpe in this case.

(iii) Calculation of wavefunctions.

Consider the evaluation of the wavefunctions in (5-7). The operator $\left(\frac{1}{\rho_m} - \frac{1}{r}\right)$ is the so-called post-interaction operator; it vanishes at the X nucleus, so an asymptotic expression can be used for $|x'\rangle$, whereas it is large near the M nucleus, so we need a better approximation for $|m\rangle$.

Hence, following Grice & Herschbach (1974), for $|x'\rangle$ ($^1S_0$) we use the pseudopotential form:

$$\left.\begin{aligned} |x'\rangle &= N_x \rho_x^{-1} \exp(-\gamma \rho_x) \qquad \text{for } \rho_x \geq \rho_{x0} \\ &\text{or} \quad 0 \qquad\qquad\qquad\quad \text{for } \rho_x < \rho_{x0} \end{aligned}\right\} \quad (5\text{-}11)$$

where ρ_x is the distance of the electron from the X nucleus;

and $\gamma = \sqrt{2 E_a}$

where E_a = electron affinity of X;

and N_x is a normalising constant:

$$N_x = \sqrt{\frac{\gamma}{2\pi}} \exp(\gamma \rho_{x0})$$

This then ensures that

$$\iiint \psi_{x'}^{2}\, \rho_x^{2} \sin\theta \, d\rho_x \, d\theta \, d\phi = 1$$

For X = I, the parameters take the values

$$E_a = 3.063 \text{ eV}$$
$$= 1.125 \times 10^{-1} \text{ Hartree}$$

$$\rho_{x0} = 2.01\, a_0 \qquad \text{(Grice \& Herschbach, 1974)}$$

For $|m\rangle$, Grice & Herschbach (1974) suggest using a Whittaker function solution. This is derived as follows: assume the outer electron on the alkali metal atom is in a Coulomb field of effective nuclear charge 1. Then find a "Coulomb" wavefunction which vanishes at $\rho_m = \infty$, and truncate it at an inner boundary by applying an infinite repulsive wall at its outermost zero. The radial Coulomb wavefunction multiplied by ρ_m satisfies the equation (in a.u.):

$$\left(-\frac{1}{2}\frac{d^2}{d\rho_m^2} - \frac{1}{\rho_m} + \frac{L(L+1)}{2\rho_m^2} + I \right) \psi = 0 \qquad (5\text{-}12)$$

where $I = -E$ (i.e. is an ionisation potential);

and L = angular momentum quantum number.

Now, this is an example of a general form called Whittaker's equation:

$$\left(\frac{d^2}{dz^2} - \frac{1}{4} + \frac{\kappa}{z} + \frac{\frac{1}{4} - \mu^2}{z^2} \right) F_{\kappa,\mu}(z) = 0 \qquad (5\text{-}13)$$

Equations (5-12) & (5-13) can be compared by an appropriate scaling:

Let $\rho_m = \alpha z$

$$\Rightarrow \quad \frac{d^2}{d\rho_m^2} = \frac{1}{\alpha^2}\frac{d^2}{dz^2}$$

Substituting in (5-12)

$$\Rightarrow \left(-\frac{1}{2\alpha^2}\frac{d^2}{dz^2} - \frac{1}{\alpha z} + \frac{L(L+1)}{2\alpha^2 z^2} + I \right)\psi = 0$$

$$\Rightarrow \left(\frac{d^2}{dz^2} + \frac{2\alpha}{z} - \frac{L(L+1)}{z^2} - 2\alpha^2 I \right)\psi = 0$$

Comparing coefficients with (5-13),

$$\alpha = \sqrt{\frac{1}{8I}} = \frac{1}{2\nu} \qquad \text{where} \qquad \nu = \sqrt{2I} \ ;$$

$$\kappa = 2\alpha = \frac{1}{\nu} \ ;$$

$$\mu^2 = \tfrac{1}{4} + L(L+1)$$

$$= (L+\tfrac{1}{2})^2$$

$$\Rightarrow \mu = L + \tfrac{1}{2}$$

Hence, applying the repulsive wall at the outermost zero $\rho_m = \rho_{m0}$, the radial part of the wavefunction is given by:

$$\left.\begin{aligned} R_L(\rho_m) &= \frac{1}{\rho_m} F_{1/\nu,\, L+\frac{1}{2}}(2\nu\rho_m) && \rho_m \geqslant \rho_{m0} \\ &\text{or} \quad 0 && \rho_m < \rho_{m0} \end{aligned}\right\} \quad (5\text{-}14)$$

The function $F_{\kappa,\mu}(z)$ is called Whittaker's function. There are two possible solutions for it (see Abramowitz & Stegun, 1964):

$$M_{\kappa,\mu}(z) = e^{-\frac{1}{2}z}\, z^{\mu+\frac{1}{2}}\, M(\tfrac{1}{2}+\mu-\kappa, 1+2\mu, z);$$

$$W_{\kappa,\mu}(z) = e^{-\frac{1}{2}z}\, z^{\mu+\frac{1}{2}} U(\tfrac{1}{2}+\mu-\kappa, 1+2\mu, z) \qquad (5\text{-}15)$$

The function $W_{\kappa,\mu}(z)$ has already been met in the solution of the Morse oscillator (eqn. (3-9)).

In the H-atom problem, the Whittaker function approach can be used, and applying boundary conditions at $\rho = 0$ and $\rho = \infty$ gives conditions on the possible values for E, and the familiar radial wavefunctions; here, however, the technique is to apply the right hand boundary condition and use the experimentally determined E; in general this will mean that the solution diverges at the origin, but this is avoided by truncating it at its outermost finite zero.

Since, in the limit of large z, M(a,b,z) contains a term in e^z, the $M_{\kappa,\mu}(z)$ solution is unacceptable. U(a,b,z) has the asymptotic form:

$$\lim_{|z|\to\infty} U(a,b,z) = z^{-a}\,(1+O(|z|^{-1})) \qquad (5\text{-}16)$$

Since this becomes multiplied by $e^{-\frac{1}{2}z}$, this is acceptable, and the final form for (5-14) is

$$\left.\begin{aligned} R_L(\rho_m) &= (2\nu)^{L+1}\,\rho_m^{L}\, e^{-\nu\rho_m} U(L+1-1/\nu, 2(L+1), 2\nu\rho_m) \\ &\qquad\qquad\qquad\qquad\qquad\qquad \rho_m \geqslant \rho_{m0} \\ \text{or} \quad &0 \qquad\qquad\qquad\qquad\qquad\qquad \rho_m < \rho_{m0} \end{aligned}\right\} \qquad (5\text{-}17)$$

Evaluation of U raises two types of problem. First the power series expansion about the origin for U (Abramowitz & Stegun, 1964) is invalid for integral values of b (= 2(L+1)). Secondly the alternative logarithmic form was found to converge very slowly.

Equation (5-12) was therefore instead solved numerically using a Runge-Kutta method available from the NAG library. It was split into

two simultaneous first order differential equations by using ψ and $\frac{d\psi}{d\rho_m}$ as independent variables; integration was performed inwards from a large starting value of ρ_m, with initial conditions $\psi = 0$ and $\frac{d\psi}{d\rho_m}$ = asymptotic value at initial ρ_m, which was calculated as follows:

From (5-16) & (5-17),

$$\lim_{\rho_m \to \infty} \psi(\rho_m) = e^{-\frac{1}{2}z} z^{\mu+\frac{1}{2}} z^{-a}$$

$$= e^{-\nu\rho_m} (2\nu)^{\kappa} \rho_m^{\kappa}$$

$$\Rightarrow \lim_{\rho_m \to \infty} \frac{d\psi}{d\rho_m} = (2\nu)^{\kappa} \rho_m^{\kappa-1} e^{-\nu\rho_m} (\kappa - \nu\rho_m)$$

Note that since the wavefunction is later normalised, the starting value for the slope is in fact arbitrary.

This calculation was performed for Na(3s) and Na(3p), and the wavefunctions stored as values at a grid of ρ_m values. If the solution is $\psi_L(\rho_m)$, then the final wavefunction required is the product of radial and angular parts:

$$|m_L\rangle = N \psi_L(\rho_m) \frac{1}{\rho_m} G_L(\theta, \phi) \qquad (5\text{-}19)$$

where G is the angular part, and N is a normalising constant.

The parameters used were as follows:

For Na(3s),

$L = 0$;

$I = 823.3$ cpe $= 0.1889$ Hartree

$\Rightarrow \nu = 0.6147$ a.u.;

$G(\theta, \phi) = 1.$

On performing the integration, the outermost zero was found to occur at

$$\rho_{m0}(3s) = 0.9080\ a_0$$

which is in agreement with the value found by Grice & Herschbach (1974).

The normalisation condition is

$$\frac{1}{N_s^2} = \int_0^{2\pi}\int_0^{\pi}\int_{\rho_{m0}}^{\infty} \psi_s^2(\rho_m)\,\frac{1}{\rho_m^2}\,\rho_m^2 \sin\theta\, d\rho_m d\theta d\phi$$

$$= 4\pi J$$

where $$J = \int_{0.908}^{\infty} \psi_s^2(\rho_m)\, d\rho_m$$

and this was estimated from the numerical results by cubic spline fitting.

For Na(3p),

$$L = 1;$$

$$I = 486.1 \text{ cpe} = 0.1115 \text{ Hartree}$$

$$\Rightarrow \nu = 0.4723 \text{ a.u.};$$

$$G(\theta, \phi) = \cos\theta.$$

The outermost zero was found to be at

$$\rho_{m0}(3p) = 1.0333\ a_0$$

and the normalisation condition used was

$$\frac{1}{N_p^2} = \int_0^{2\pi}\int_0^{\pi}\int_{\rho_{m0}}^{\infty} \frac{\psi_p^2(\rho_m)}{\rho_m^2} \cos^2\theta\, \rho_m^2 \sin^2\theta\, d\rho_m d\theta d\phi$$

$$= \frac{4\pi}{3} I$$

where $$I = \int_{1.0333}^{\infty} \psi_p^2 (\rho_m)\, d\rho_m$$

The radial parts of the wavefunctions, including the normalising constants, for Na(3s) and Na(3p) are plotted in figs 34 & 35.

(iv) Calculation of off-diagonal elements.

The integrals H_{12} and H_{13} were calculated numerically using (5-7), (5-11), and the stored values for the sodium wavefunctions, which were interpolated by cubic spline fitting.

Since the wavefunctions $|m\rangle$ and $|x'\rangle$ are truncated at $\rho_m = \rho_{m0}$ and $\rho_x = \rho_{x0}$, the integration was performed outwards from these boundaries, using ρ_m, ρ_x, and ϕ as integration variables (using ρ_m, θ and ϕ for instance would involve integrating across a discontinuity at $\rho_x = \rho_{x0}$). It is therefore necessary to obtain the volume element. Referring to the diagram:

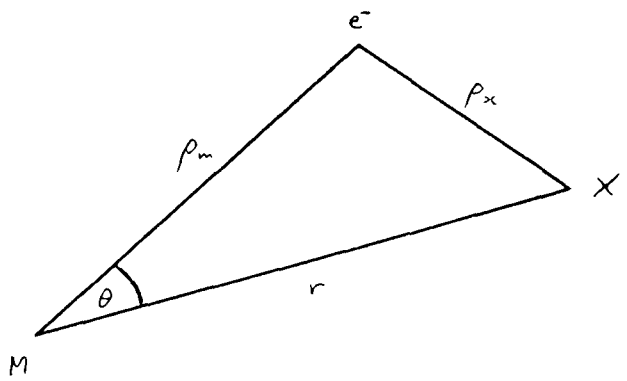

we know that the volume element may be expressed in the spherical polar form

$$dS = \rho_m^2 \sin\theta\, d\rho_m\, d\theta\, d\phi$$

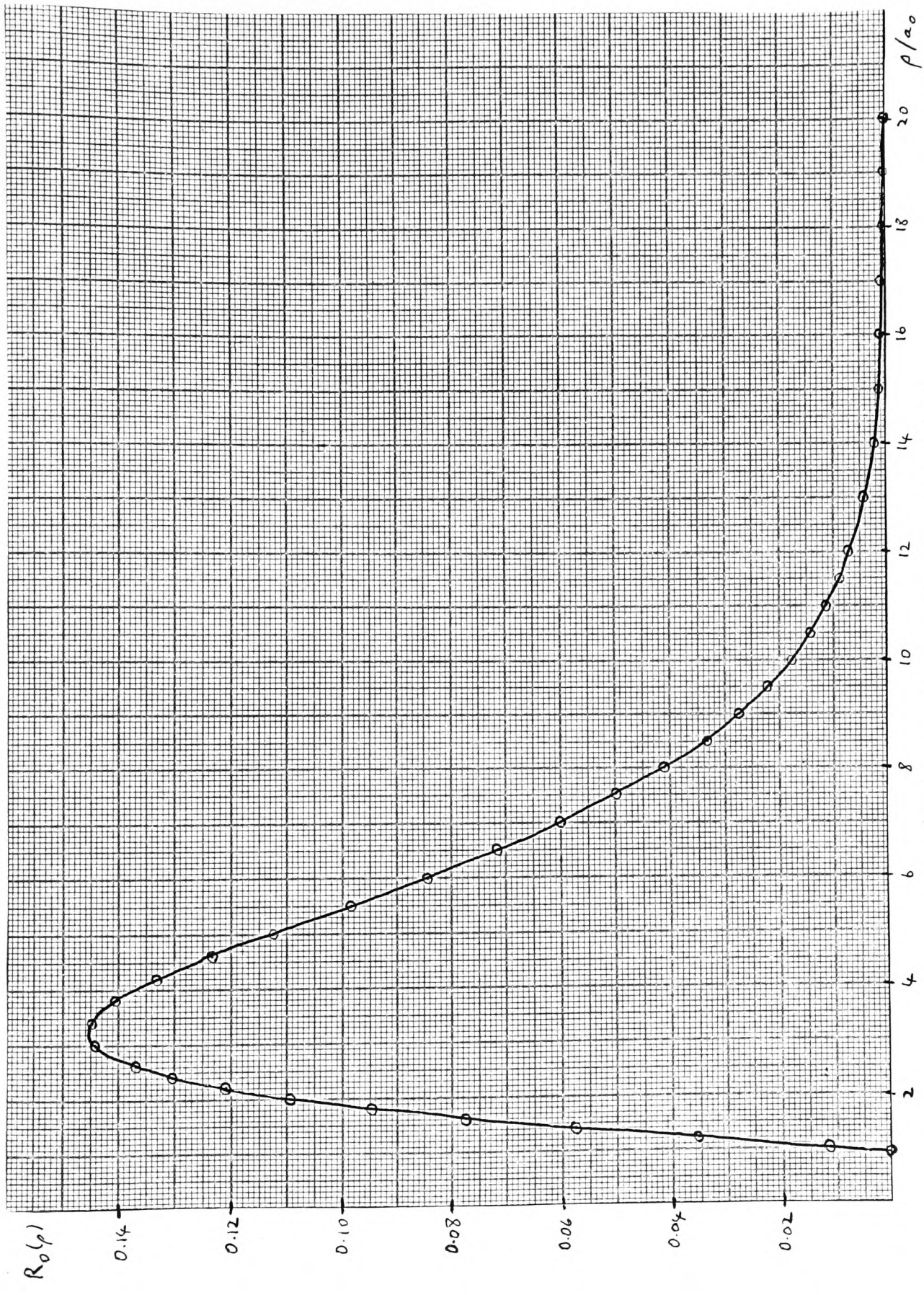

Fig. 34. Radial wavefunction for Na(3s)

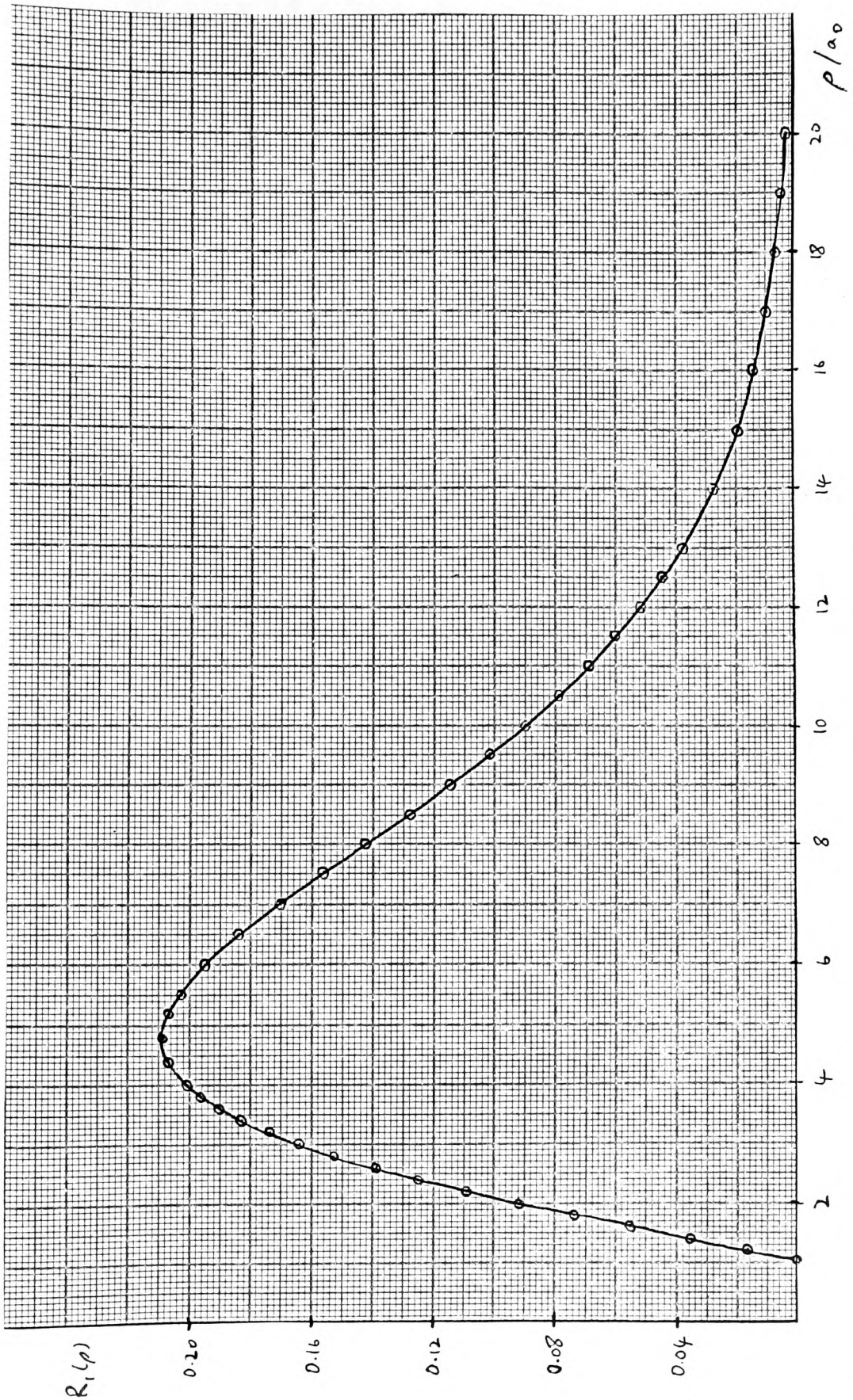

Fig. 35. Radial wavefunction for Na(3p).

But $$d\rho_m d\theta = \frac{\partial(\rho_m, \theta)}{\partial(\rho_m, \rho_x)} d\rho_m d\rho_x$$

$$= \left(\frac{\partial\theta}{\partial\rho_x}\right)_{\rho_m} d\rho_m d\rho_x$$

$$\therefore dS = \rho_m^2 \sin\theta \left(\frac{\partial\theta}{\partial\rho_x}\right)_{\rho_m} d\rho_m d\rho_x d\phi$$

Now, $$\rho_x^2 = \rho_m^2 + r^2 - 2\rho_m r\cos\theta$$

$$\Rightarrow 2\rho_x = 2\rho_m r \sin\theta \left(\frac{\partial\theta}{\partial\rho_x}\right)_{\rho_m}$$

$$\left(\frac{\partial\theta}{\partial\rho_x}\right)_{\rho_m} = \frac{\rho_x}{\rho_m r \sin\theta}$$

$$\Rightarrow dS = \frac{\rho_m \rho_x}{r} d\rho_m d\rho_x d\phi \qquad (5\text{-}20)$$

As a check, it can be shown that

$$J\left(\frac{x_m, y_m, z_m}{\rho_m, \rho_x, \phi}\right) = J\left(\frac{x_x, y_x, z_x}{\rho_m, \rho_x, \phi}\right) = \frac{\rho_m \rho_x}{r}$$

and this element is also obtained geometrically.

The limits are clearly:

$$\left.\begin{array}{ll} \phi: & [0, 2\pi] \ ; \\ \rho_x: & [\rho_{x0}, \infty] \ ; \\ \rho_m: & [\mathrm{Max}(\rho_{m0}, |\rho_x - r|), \ r + \rho_x] \end{array}\right\} \qquad (5\text{-}21)$$

where $\mathrm{Max}(x,y)$ = larger of x & y

provided $\rho_{m0} < r$, which is satisfied, since all r values chosen were greater than ρ_{m0}.

The use of these novel integration variables was first checked by using them to calculate an integral given by Eyring, Walter & Kimble (1944):

$$I = \int_{\text{all space}} \frac{\psi_m \psi_x}{\rho_m} \, d\tau = e^{-r}(1+r)$$

where $\psi_m = \frac{1}{\sqrt{\pi}} e^{-\rho_m}$; $\psi_x = \frac{1}{\sqrt{\pi}} e^{-\rho_x}$

Using our integration coordinates, this can be shown as follows:

$$I = \int_0^{2\pi} d\phi \, \frac{1}{(\sqrt{\pi})^2} \int_0^{\infty} \int_{|r-\rho_x|}^{r+\rho_x} \frac{e^{-\rho_m} e^{-\rho_x}}{\rho_m} \, \frac{\rho_m \rho_x}{r} \, d\rho_m d\rho_x$$

$$= \frac{2}{r} \int_0^{\infty} \int_{|r-\rho_x|}^{r+\rho_x} e^{-\rho_m} e^{-\rho_x} \rho_x \, d\rho_m d\rho_x$$

$$= \frac{2}{r} \int_0^{\infty} \left[e^{-y} \right]_{r+x}^{|r-x|} e^{-x} x \, dx$$

$$= \frac{2}{r} \int_0^{\infty} e^{-|r-x|} e^{-x} x \, dx - \frac{2}{r} \int_0^{\infty} e^{-(r+x)} e^{-x} x \, dx$$

$$= \frac{2}{r} \int_0^{r} e^{-(r-x)} e^{-x} x \, dx + \frac{2}{r} \int_r^{\infty} e^{-(x-r)} e^{-x} x \, dx$$

$$- \frac{2 e^{-r}}{r} \int_0^{\infty} e^{-2x} x \, dx$$

$$= r e^{-r} + e^{-r}\left(1 + \frac{1}{2r}\right) - \frac{e^{-r}}{2r}$$

$$= e^{-r}(1+r)$$

which is the correct result.

The off-diagonal elements H_{12} & H_{13} were now calculated, for various values of r, using the following formulae:

$$H_{12} = \int_0^{2\pi} \int_{\rho_{x0}}^{\infty} \int_{(\rho_{m0}, |r-\rho_x|)}^{r+\rho_x} \frac{1}{\rho_m} \psi_s(\rho_m) \frac{1}{\rho_m} N_s \frac{N_x}{\rho_x} \exp(-\gamma\rho_x) \frac{\rho_m \rho_x}{r} d\rho_m d\rho_x d\phi$$

$$= 2\pi N_s N_x \iint \frac{\psi_s(\rho_m)}{r\rho_m} \exp(-\gamma\rho_x)\, d\rho_m d\rho_x \qquad (5\text{-}22)$$

Similarly,

$$H_{13} = 2\pi N_p N_x \iint \frac{\psi_p(\rho_m)}{r\rho_m} \cos\theta \exp(-\gamma\rho_x)\, d\rho_m d\rho_x \qquad (5\text{-}23)$$

where $$\cos\theta = \frac{r^2 + \rho_m^2 - \rho_x^2}{2r\rho_m}$$

The integration was done by Patterson's method, available from the NAG library, and, to ensure reliability of the results, the integration range for ρ_x was split into small segments. The contributions from the segments were summed, until each contribution was too small to affect the fourth figure of the total, and was less than half the previous contribution. The results of the calculations are shown in table 6.

Consider H_{12}. Because of its occurrence in the LZS formula, the value at the crossing point, $H_{12}(r_c)$, has attracted most attention. For the system $M^+ + X^- \rightarrow M(ns\ ^2S) + X$, Grice & Herschbach (1974) arrived at the following empirical formula:

$$\Delta V(r_c) = \exp\left[(r_c^0 - r_c)/\Delta r\right] \qquad (5\text{-}24)$$

r/a_0	H_{12}/Hartree	ln(H_{12}/r)	H_{13}/Hartree	ln(H_{13}/r)
4	-2.188(-1)	-2.906	-1.597(-1)	-3.220
6	-1.149(-1)	-3.956	-1.313(-1)	-3.822
8	-5.083(-2)	-5.059	-8.102(-2)	-4.593
10	-2.077(-2)	-6.177	-4.379(-2)	-5.431
12	-8.132(-3)	-7.297	-2.197(-2)	-6.303
14	-3.105(-3)	-8.414	-1.052(-2)	-7.194
16	-1.167(-3)	-9.526	-4.870(-3)	-8.097
18	-4.344(-4)	-10.632	-2.202(-3)	-9.009

Table 6.

where the parameters r_c^0 and Δr depend on the halogen but not on the metal. For M + I, they determined

$$r_c^0 \approx 0.58\ a_0;$$
$$\Delta r \approx 2.27\ a_0.$$

Using our value for M = Na of $r_c = 6.97$ Å $= 13.2\ a_0$, (5-24) gives

$$\Delta V(r_c) \approx 3.85 \times 10^{-3} \text{ Hartree}$$

Grice & Herschbach also fitted their results to the formula of Olson et al (1971) (see eqn. (1-7)), and obtained

$$\Delta V(r_c) = \nu\gamma \times 2.44\ r_c^* \exp(-0.996\ r_c^*) \qquad (5\text{-}25)$$

where $$r_c^* = \frac{(\nu + \gamma)}{2} r_c$$

and $$\nu = \sqrt{2\ I_M}$$

$$\gamma = \sqrt{2 E_{aI}}$$

For Na + I, $\nu = 0.6147$ a.u.; $\gamma = 0.4746$ a.u. and (5-25) with these values gives

$$\Delta V(r_c) = 3.98 \times 10^{-3} \text{ Hartree}$$

Inspired by the form of (5-25), and assuming that the behaviour of H_{13} is similar to that of H_{12}, it was decided to find out whether the data in table 6 for both integrals fit a simple functional form

$$H_{ic} = - Ar \exp(-Br) \qquad (5\text{-}26)$$

$$\Rightarrow \quad \ln\left(\left|\frac{H_{ic}}{r}\right|\right) = \ln A - Br$$

If (5-26) is a good description of the behaviour, then a plot of $\ln\left(\left|\frac{H_{ic}}{r}\right|\right)$ against r will be a straight line. Such plots appear in figs 36 & 37, and it can be seen that, apart from the short range region for H_{13}, this behaviour is well followed. Hence the data were fitted to the form (5-26), and, reverting to LaBudde's system of units, the values of the slopes and intercepts gave the following:

$$H_{12}(r) = - A_s r \exp(- B_s r) ; \qquad (5\text{-}27)$$

$$H_{13}(r) = - A_p r \exp(- B_p r) \qquad (5\text{-}28)$$

where $A_s = 4.61 \times 10^3$ cpe; $B_s = 1.06$ Å^{-1};

$A_p = 3.15 \times 10^3$ cpe; $B_p = 0.85$ Å^{-1}

As a check, (5-27) was used to calculate $H_{12}(r_c)$; with $r_c = 6.97$ Å, this gives $H_{12}(r_c) = -19.87$ cpe. The overlap S_{12} between $Na^+ + I^-$ and Na(3s) + I at the crossing point was also calculated, using the same

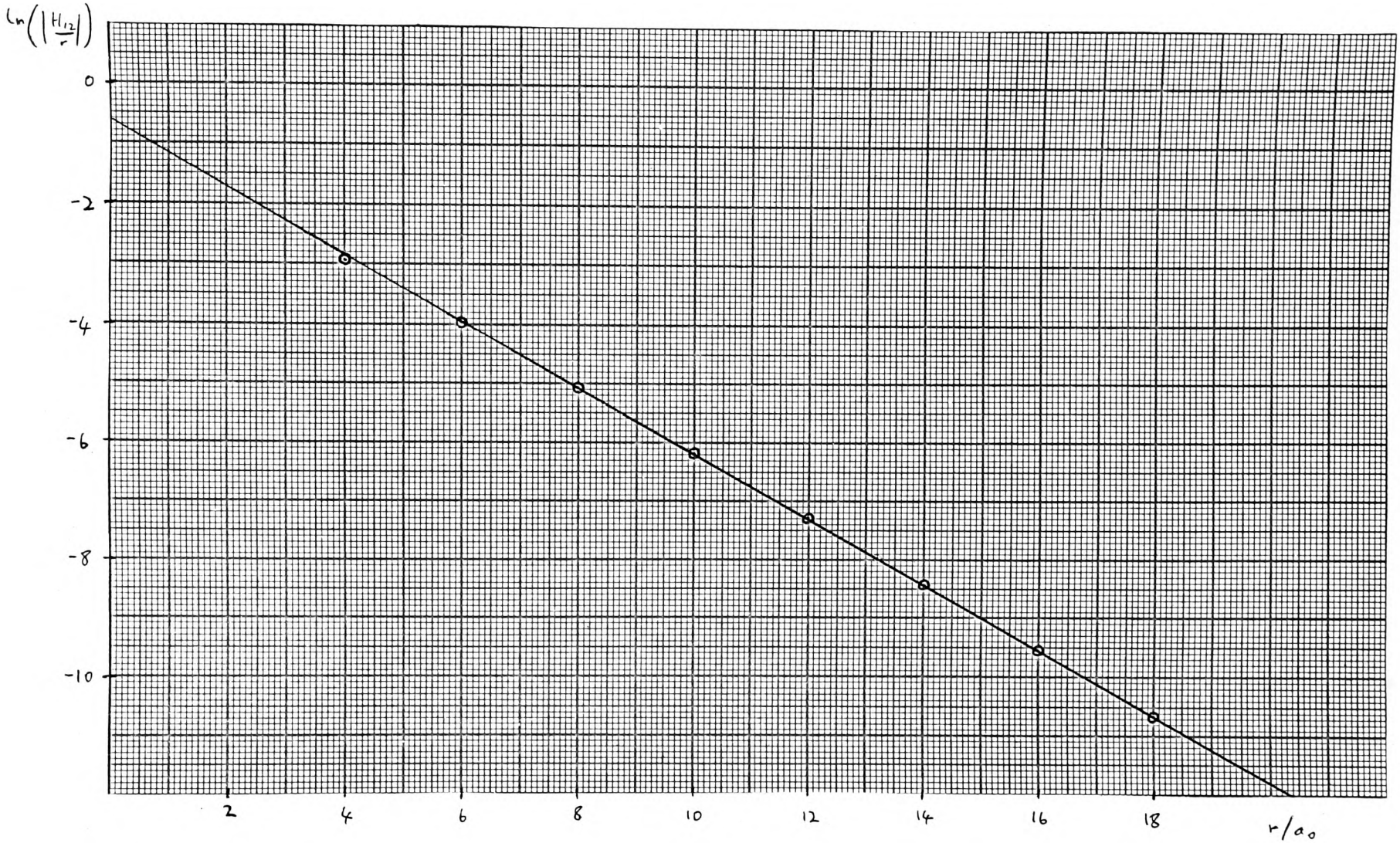

Fig. 36.

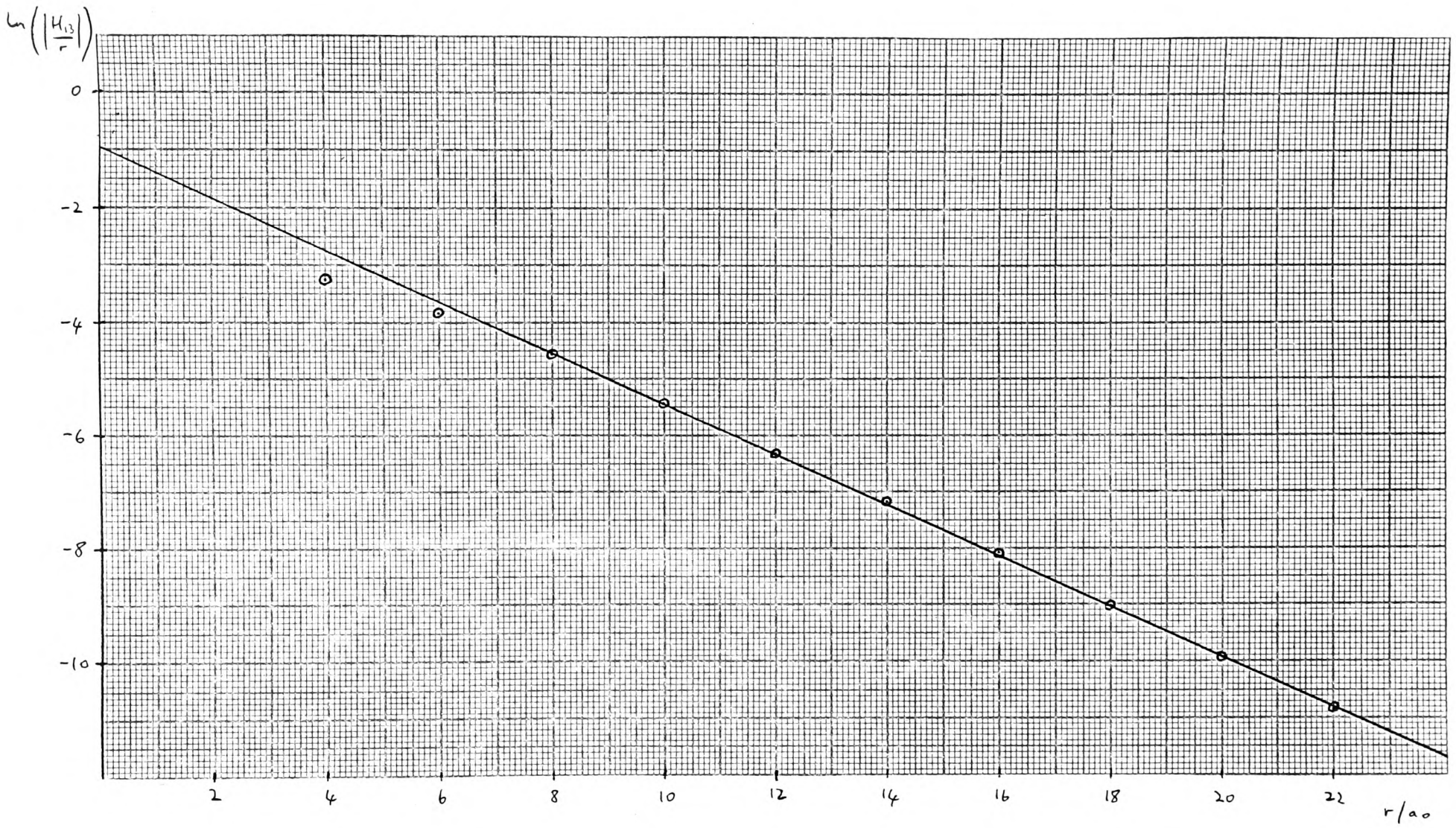
$\ln\left(\left|\frac{H_{13}}{r}\right|\right)$
0
-2
-4
-6
-8
-10
2
4
6
8
10
12
14
16
18
20
22
r/a₀

Fig. 37

method as that described for H_{12} and H_{13} above, and found to be 3.35×10^{-2}, which is fairly small; substituting these values in (5-10) then gives

$$\Delta V(r_c) = 17.60 \text{ cpe} \qquad (\text{c.f. } 2|H_{12}(r_c)| = 39.74 \text{ cpe})$$

$$= 4.04 \text{ Hartree}$$

and this agrees well with the results from the empirical formulae (5-24) & (5-25).

In summary, the expressions used for the five non-zero matrix elements were those given in eqns (5-2), (5-3), (5-4), (5-27) & (5-28).

D The classical trajectory.

Since the impact parameter approximation becomes invalid at low collision energies, the classical trajectory was calculated in two dimensions under the influence of an effective potential V(r). Referring to the diagram:

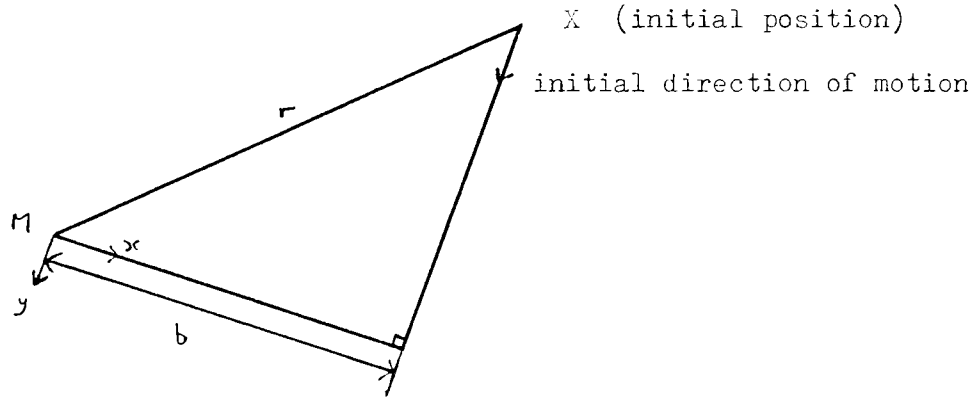

the Newton's second law form of the classical equations of motion (LaBudde, 1973) is

$$\mu \ddot{\vec{r}} = -\frac{\partial V}{\partial \vec{r}}$$

$$\Rightarrow \quad \mu \ddot{x}\,\hat{i} + \mu \ddot{y}\,\hat{j} = - \frac{\partial V}{\partial x}\,\hat{i} - \frac{\partial V}{\partial y}\,\hat{j}$$

where x and y are the x- and y-components of $\vec{r}$

and $\hat{i}$ and $\hat{j}$ are unit vectors along the x- and y-axes

$$\Rightarrow \quad \mu \ddot{x} = - \frac{\partial V}{\partial x} \quad ; \qquad \mu \ddot{y} = - \frac{\partial V}{\partial y}$$

hence, putting $\dot{x} = v_x$; $\dot{y} = v_y$, we have four first order differential equations

$$\dot{v}_x = - \frac{1}{\mu} \frac{\partial V}{\partial x} \; ; \qquad \dot{v}_y = - \frac{1}{\mu} \frac{\partial V}{\partial y} \; ; \qquad \dot{x} = v_x \; ; \qquad \dot{y} = v_y$$

where $$\frac{\partial V}{\partial q} = \frac{\partial V}{\partial r} \frac{\partial r}{\partial q} = \frac{q}{r} \frac{\partial V}{\partial r} \qquad (q = x,y)$$

These four equations were combined with the six coupled equations from (2-23) to give an overall system of ten simultaneous first order differential equations, which were solved using Krogh's method (see chapters III & IV).

Since non-adiabatic transitions are expected, the choice of V for the classical trajectory is not clear cut. The ionic diabatic potential was used, since we are considering transitions out of the ionic state; we are interested in what happens from the time when the effect of the Coulomb attraction is first felt, which will be very early, because of the long-range nature of the Coulomb potential, until the relatively small interaction region has been passed; the initial approach, which is definitely under the influence of the ionic potential, occupies most of this time, so use of the ionic potential is preferred. In the LCS formalism, this would then ensure the correct velocity at the crossing point. The choice of potential

is more critical for the trajectory after the interaction region has been passed, but since we are only interested in transition probabilities, which are not changed by this trajectory, this is not relevant.

Thus a simplefied Rittner potential was used:

$$V = -\frac{e^2}{4\pi\varepsilon_0 r} - \frac{e^2(\alpha_1+\alpha_2)}{8\pi\varepsilon_0 r^4} + A e^{-r/k}$$

$$\Rightarrow \frac{\partial V}{\partial r} = \frac{e^2}{4\pi\varepsilon_0 r^2} - \frac{e^2(\alpha_1+\alpha_2)}{2\pi\varepsilon_0 r^5} - \frac{A}{k} e^{-r/k}$$

Since the interactions H_{12} & H_{13} fall off exponentially, it is acceptable to integrate the probabilities only over the region in which they change appreciably (this might not be the case for a long range interaction, e.g. $\sim r^{-1}$; see Lebeda & Thorson, 1970). However, the trajectory must be started much further out, so that it follows the correct route in the region in which interaction is occurring. Thus the method used was to integrate the four classical trajectory equations in from some large initial $r = r_i$ with initial velocity $v = \sqrt{\frac{2E}{\mu}}$, where E is the collision energy, until $r = r_0$ say, then integrate all ten equations until $r = r_0$ again, then stop.

E Discussion of results.

The results of the various calculations performed are given in table 7. By varying r_0 and r_i, it was found that the results could be relied on to an absolute accuracy of $\pm$ 0.001 with $r_0 = 20$ Å; $r_i = 500$ Å (integration between r_i and r_0 was very fast, so that increasing r_i made no significant increase in the computation time). Thus the small transition probabilities are unreliable but definitely small.

Collision energy/cpe	b/Å	Final probabilities in:		
		$Na^+ + I^-$	Na(3s) + I	Na(3p) + I
1	5	9.981(-1)	1.733(-3)	1.766(-10)
10	2	9.771(-1)	2.360(-2)	1.500(-10)
	5	9.928(-1)	7.399(-3)	1.094(-4)
	8	9.884(-1)	1.082(-2)	7.661(-11)
100	2	9.588(-1)	4.084(-2)	8.024(-10)
	5	9.970(-1)	1.118(-3)	2.812(-10)
	8	9.786(-1)	2.056(-2)	3.698(-6)
6×10^4	5	6.182(-1)	3.820(-1)	2.579(-7)
8×10^4	2	4.195(-1)	5.806(-1)	6.615(-7)
	5	8.189(-1)	1.812(-1)	2.568(-7)
10^5	2	9.795(-1)	2.047(-2)	6.295(-7)
	5	4.514(-1)	5.487(-1)	2.410(-7)
	8	9.615(-1)	3.861(-2)	4.340(-8)
10^6	2	8.986(-1)	1.012(-1)	1.499(-4)
	5	7.835(-1)	2.165(-1)	6.040(-5)
	8	9.694(-1)	3.058(-2)	2.661(-6)
10^7	5	6.392(-1)	3.490(-1)	1.169(-2)
10^8	2	1.387(-1)	1.336(-1)	7.277(-1)
	5	6.566(-1)	6.761(-2)	2.758(-1)
	8	9.915(-1)	4.921(-4)	7.969(-3)

Table 7.

The immediate conclusion from these results is that, at energies from somewhat above thermal (which is ~ 5 cpe) up to the region where the LZS probability for staying on diabatic curve 1 during a passage through the crossing point r_c is ~ 0.5 (at $\sim 8 \times 10^4$ cpe), the probability of transition to excited sodium Na(3p) + I is very small. Referring back to fig. 32, this seems quite reasonable, for, as stated earlier, although asymptotically H_{11} and H_{33} become very close, this is only approached at very large separations, and in particular, in the outer region, this energy difference never becomes comparatively small to H_{13}. However, as the collision energy is increased still further, considerable population of Na(3p) does appear to become possible, in the region of 10^8 cpe (~ 625 keV), which is an extremely high energy. At such an energy, the trajectory is essentially a straight line, so the distance of closest approach will be equal to the impact parameter. Thus when b = 2 Å, the high probability of transition to channel 3 may be explained by the fact that H_{13} becomes comparable with $(H_{33} - H_{11})$ in the region of the H_{11} potential well.

At more reasonable collision energies, however, formation of a population inversion of Na(3p) with respsct to Na(3s) does not seem to be possible. The possibility is, though, presumably more favourable the smaller the asymptotic separation $H_{33}(\infty) - H_{11}(\infty)$, and it is worth examining other alkali / halogen combinations in this respect. The separation is given by:

$$H_{33}(\infty) - H_{11}(\infty) = E\left\{M(^2P_{\frac{1}{2}}\ np) + X\right\} - E(M^+ + X^-)$$

$$= E\left\{M(^2P_{\frac{1}{2}}\ np)\right\} - E(M^+) + E(X) - E(X^-)$$

$$= E_{aX} - I(M\ ^2P_{\frac{1}{2}}\ np)$$

Using published values for the electron affinities E_{aX} (CRC Handbook of Chemistry and Physics, 1972) and excited state ionisation potentials I (Moore, 1949), the separations are as follows (/cpe):

	F	Cl	Br	I
Li	-15	11	-29	-77
Na	66	92	52	5
K	115	141	101	53
Rb	133	159	119	71
Cs	151	177	137	89

It can be seen that the smallest positive value indeed occurs for Na/I. However, for three combinations involving Li, the separation is negative, i.e. there is an actual crossing; this would indicate that formation of a population inversion by collisional charge neutralisation would be much more favourable in these cases.

F Summary and conclusions.

Calculations within the classical trajectory approximation were performed on the process $Na^+ + I^- \rightarrow Na + I$, to investigate the possibility of forming a population inversion of excited Na(3p) with respect to Na(3s) via such a collision.

(i) The integrals H_{12} & H_{13}, between $Na^+ + I^-$ and Na(3s) + I and Na(3p) + I respectively, were calculated for various values of the internuclear separation r. It was found that the results fit quite well the simple form

$$H_{ic}(r) = - A\, r \exp(-Br)$$

with $A = 4.61 \times 10^3$ cpe; $B = 1.06$ Å^{-1} for Na(3s) and $A = 3.15 \times 10^3$ cpe; $B = 0.85$ Å^{-1} for Na(3p); and it was confirmed that the value for

$H_{12}(r_c)$ calculated from this is in agreement with published values.

(ii) It was found that, within the approximations of the classical trajectory formulation on the three state basis $Na^+ + I^-$, $Na(3s) + I$, and $Na(3p) + I$, transitions into $Na(3p) + I$ only become significant ($P > 0.1$) at extremely high collision energies ($E \sim 500$ keV). The mechanism postulated for the enhanced population of Na(3p) observed, i.e. transition as a result of the asymptotic near coincidence of the diabatic curves for $Na(3p) + I$ and $Na^+ + I^-$, does not appear to be important, since the energy separation in fact falls much more slowly than the interaction integral H_{13} with increasing r.

(iii) Consideration of other alkali / halogen pairs shows that with Li + F, Br, I an actual crossing occurs between the ionic state and the excited covalent state, so it is thought that conditions may be more favourable for forming a population inversion in these systems. It should be noted that possible uncertainty ($\sim \pm 0.03$ eV; see Berry & Reimann, 1963) in the electron affinity of iodine allows the formal possibility of a distant crossing ($r \geq 2.3 \times 10^4$ Å) between H_{11} and H_{33} even for NaI, but the magnitude of the interaction H_{13} at this distance ($< 10^{-99}$ cpe) rules out any possibility of significant population inversion due to a curve crossing mechanism.

References

W. Aberth, J. R. Peterson, D. C. Lorentz, C. J. Cook, $N^+ + O^-$ neutralisation cross-section measurements using a superimposed-beam technique, Phys. Rev. Lett., 20, 979 (1968).

M. Abramowitz & I. A. Stegun, Handbook of mathematical functions (NBS, 1964).

S. A. Adelman & D. R. Herschbach, Asymptotic approximation for ionic-covalent configuration mixing in hydrogen and alkali hydrides, Mol. Phys., 33, 793 (1977).

R. W. Anderson & D. R. Herschbach, Inversion of orbiting scattering from elastic collisions of reactive molecules, J. C. P., 62, 2666 (1975).

J. A. Aten, C. W. A. Evers, A. E. DeVries, J. Los, Energy transfer and differential scattering for ion-pair formation in Na, K, Cs + I_2 collisions, Chem. Phys, 23, 125 (1977).

J. A. Aten, M. M. Hubers, A. W. Kleyn, J. Los, Simple trajectory calculations on ion-pair formation in alkali atom - halogen molecule collisions, Chem. Phys., 18, 311 (1976).

J. A. Aten, G. E. H. Lanting, J. Los, The energy dependence of differential cross-sections for ion-pair formation in Na, K, Cs + I_2 collisions, Chem. Phys., 19, 241 (1977).

D. J. Auerbach, M. M. Hubers, A. P. M. Laede, J. Los, Chemi-ionisation in alkali - heteronuclear halogen collisions: role of excited molecular ion states, Chem. Phys., 2, 107 (1973).

A. P. M. Laede, Charge transfer between neutrals at hyperthermal energies, Adv. Chem. Phys., XXX, 463 (1975).

A. P. M. Baede, J. Los, Total cross-sections for charge transfer and production of free electrons by collisions between alkali atoms and some molecules, Physica, 52, 422 (1971).

A. P. M. Baede, A. M. C. Moutinho, A. E. DeVries, J. Los, Total cross-sections for charge transfer between alkali atoms and halogen molecules, Chem. Phys. Lett., 3, 530 (1969).

G. G. Balint-Kurti & M. Karplus, Potential energy surfaces for simple chemical reactions: $Li + F_2 \rightarrow LiF + F$, Chem. Phys Lett., 11, 203 (1971).

G. G. Balint-Kurti & M. Karplus, Potential energy surfaces for simple chemical reactions: $Li + F_2 \rightarrow LiF + F$, Mol. Phys., 25, 393 (1973).

D. R. Bates, Collisions involving the crossing of potential energy curves, Proc. Roy. Soc., A 257, 22 (1960).

D. R. Bates & T. J. M. Boyd, Inelastic heavy particle collisions involving the crossing of potential energy curves IV: Ionic recombination, Proc. Phys. Soc., A 69, 910 (1956).

D. R. Bates & D. S. F. Crothers, Semiclassical treatment of atomic collisions, Proc. Roy. Soc., A 315, 465 (1970).

D. R. Bates & B. L. Moiseiwitsch, Inelastic heavy particle collisions involving the crossing of potential energy curves I: Charge transfer from H atoms to Be^{2+}, Si^{2+}, & Mg^{2+} ions, Proc. Phys. Soc., A 67, 805 (1954).

E. Bauer, E. R. Fisher, F. R. Gilmore, De-excitation of electronically excited sodium by nitrogen, J. C. P., 51, 4173 (1969).

R. S. Berry, Interaction of vibrational and electronic motion in alkali halide molecules, J. C. P., 27, 1288 (1957).

R. S. Berry & C. W. Reimann, Absorption spectrum of gaseous F^- and electron affinities of the halogen atoms, J. C. P., 38, 1540 (1963).

J. H. Birely, R. R. Herm, A. R. Wilson, D. R. Herschbach, Molecular

beam kinetics: Reactions of K, Rb, and Cs with Br_2 and I_2, J. C. P., 47, 993 (1967).

J. H. Birely & D. R. Herschbach, Reactive scattering in molecular beams: velocity analysis of KBr formed in the K + Br_2 reaction, J. C. P., 44, 1690 (1966).

N. C. Blais, Monte Carlo trajectories: the dynamics of harpooning in alkali-halogen reactions, J. C. P., 49, 9 (1968).

N. C. Blais, Monte Carlo trajectories: further studies of alkali-halogen reactions, J. C. P., 51, 856 (1969).

M. S. Child, Curve-crossing and the WKB approximation, Mol. Phys., 20, 171 (1971).

M. S. Child, Non-adiabatic transitions, Farad. Disc., 53, 18 (1972).

M. S. Child, Franck-Condon transitions in multi-curve crossing processes, Farad. Disc., 55, 30 (1973).

M. S. Child, Molecular Collision Theory (Academic Press, London, 1974).

L. Collatz, The Numerical Treatment of Differential Equations (Springer, Berlin, 1966).

C. A. Coulson & K. Zalewski, Internal conversion and the crossing of molecular potential energy surfaces, Proc. Roy. Soc., A 268, 437 (1962).

D. S. F. Crothers, A critique of Zwaan-Stueckelberg phase integral techniques, Adv. Phys., 20, 405 (1971).

S. Datz & R. E. Minturn, Study of the reaction of Cs with Br_2 in crossed molecular beams, J. C. P., 41, 1153 (1964).

P. Davidovits & J. Maya, Cross-sections for the alkali atom - Cl_2 reactions, J. C. P., 61, 1082 (1974).

J. B. Delos & W. R. Thorson, Semiclassical theory of inelastic collisions II: Momentum space formulation, Phys. Rev., A 6, 720 (1972a).

J. B. Delos & W. R. Thorson, Studies of the potential curve crossing problem II, Phys. Rev., A 6, 728 (1972b). Erratum, Phys. Rev., A 9, 1026 (1974).

J. B. Delos, W. R. Thorson, S. Knudson, Semiclassical theory of inelastic collisions I: The classical picture and semiclassical formulation, Phys. Rev., A 6, 709 (1972).

G. A. L. Delvigne & J. Los, The differential cross-section for chemi-ionisation in alkali atom - halogen molecule collisions. Classical interpretation, Physica, 59, 61 (1972).

G. A. L. Delvigne & J. Los, Rainbow, Stuckelberg oscillations and rotational coupling on the differential cross-section of $Na + I \rightarrow Na^+ + I^-$, Physica, 67, 166 (1973).

Yu. N. Demkov, Charge transfer at small resonance defects, Sov. Phys. J. Exp. Th. Phys., 18, 138 (1964).

G. V. Dubrovskii, Non-adiabatic transitions in slow collisions between heavy particles, Sov. Phys. J. Exp. Th. Phys., 19, 591 (1964).

R. Düren, Differential cross-sections for alkali - halogen collisions from trajectory calculations on intersecting surfaces, J. Phys. B, 6, 1801 (1973).

C. W. A. Evers, Trajectory surface hopping study of ionizing collisions between Na, K and $Cs + I_2$ in the energy range 10 - 100 eV, Chem. Phys. 21, 355 (1977).

C. W. A. Evers & A. E. DeVries, Total reactive cross-section for $K + Br_2$ in the energy range 0 - 4 eV, Chem. Phys., 15, 201 (1976).

J. J. Ewing, R. Milstein, R. S. Berry, Curve crossing in collisional dissociation of alkali halide molecules, J. C. P., 54, 1752 (1971).

H. Eyring, J. Walter, G. E. Kimble, Quantum Chemistry (John Wiley, 1944).

E. R. Fisher & G. K. Smith, Vibration-electronic coupling in the

quenching of electronically excited alkali atoms by diatomics, Appl. Optics, 10, 1803 (1971).

M. A. D. Fluendy & K. P. Lawley, Chemical applications of molecular beams (Chapman & Hall, 1974).

P. D. Gait & R. S. Berry, Oscillations of the D line emission in shock generated sodium halide plasmas, J. C. P., 66, 2764 (1977).

K. T. Gillen, A. M. Kulis, R. B. Bernstein, Molecular beam study of the $K + I_2$ reaction: Differential cross section and energy dependence, J. C. P., 54, 2831 (1971).

E. A. Gislason & J. G. Sachs, Multiple crossing electron-jump model for reactions of metal atoms with diatomic halogen molecules, J. C. P., 62, 2678 (1975).

M. Godfrey & M. Karplus, Theoretical investigation of reactive collisions in molecular beams: $K + Br_2$, J. C. P., 49, 3602 (1968).

M. R. Gover, A model for the interpretation of alkali atom plus halogen molecule reactions, Part II thesis (Hertford College, Oxford, 1975).

R. Grice, Reactive scattering, in: Molecular Scattering: Physical and Chemical Applications, ed. K. P. Lawley, Adv. Chem. Phys. XXX, 247 (1975).

R. Grice & D. R. Herschbach, Long-range configuration interaction of ionic and covalent states, Mol. Phys., 27, 159 (1974).

A. E. Grosser & R. B. Bernstein, Internal energy of reaction products by velocity analysis II: Scattered KBr from the crossed molecular beam reaction $K + Br_2 \rightarrow KBr + Br$, J. C. P., 43, 1140 (1965).

J. Groszer & G. Meyer, Ionizing collisions of potassium atoms with molecules: excitation energy of the product molecular ion, Chem. Phys. Lett., 37, 82 (1976).

R. K. Helbing & E. W. Rothe, Crossed-beam study of ionisation of Cs by Br_2, J. C. P., 51, 1607 (1969).

D. R. Herschbach, Reactive scattering in molecular beams, Adv. Chem. Phys. X, 319 (1966).

G. Herzberg, Spectra of diatomic molecules (Van Nostrand, 1950).

M. M. Hubers, A. ... Kleyn, J. Los, Ion pair formation in alkali - halogen collisions at high velocities, Chem. Phys., 17, 303 (1976).

E. Hutchisson, Band spectra intensities for symmetrical diatomic molecules, Phys. Rev., 36, 410 (1930).

R. K. Janev, Nonadiabatic transitions between ionic and covalent states, in: Adv. At. Mol. Phys., 12, ed. D. R. Bates & B. Bederson, 1 (1976).

N. K. Kashihira, F. Schmidt-Bleek, S. Datz, Ionizing collisions of fast alkali atoms with Cl_2, Br_2, and O_2, J. C. P., 61, 160 (1974).

G. M. Kendall & R. Grice, Vibrational coordinates in the electron jump model, Mol. Phys., 24, 1373 (1972).

J. L. Kinsey, Molecular beam reactions, in: Chemical Kinetics, ed. J. C. Polanyi, MTP International Review of Science, Physical Chemistry, series 1, 9, 173 (1972).

A. Komornicki, T. F. George, K. Morokuma, Decoupling scheme for a semiclassical treatment of electronic transitions in atom - diatom collisions: Real-valued trajectories and local analytic continuation, J. C. P., 65, 48 (1976).

F. T. Krogh, Algorithms for changing the step size, SIAM J. Numer. Anal., 10, 949 (1973).

P. J. Kuntz, E. M. Nemeth, J. C. Polanyi, Distributions of reaction products IV: reactions forming an ionic bond, M+XC (2D), J. C. P., 50, 4607 (1969); Bit (3D), J. C. P., 50, 4623 (1969).

R. A. LaBudde, Classical mechanics of molecular collisions, PhD thesis, WIS-TCl-414 (1973).

K. Lacmann & D. R. Herschbach, Collisional excitation and ionisation

of K atoms by diatomic molecules; role of ion-pair states, Chem. Phys. Lett., 6, 106 (1970).

L. D. Landau, Zur Theorie der Energieübertragung II, Z. Phys. Sov. Un. 2, 46 (1932).

L. D. Landau & E. M. Lifshitz, Quantum Mechanics (Pergamon, 1958).

K. P. Lawley, Molecular Scattering: Physical and Chemical Applications, Adv. Chem. Phys. XXX (1975).

C. F. Lebeda & W. R. Thorson, Numerical integration of differential equations encountered in atomic collision theory, Can. J. Phys., 48, 2937 (1970).

R. D. Levine, Molecular collisions and reactive scattering, in: Theoretical Chemistry, ed. W. Byers Brown, MTP Int. Rev. Science, Physical Chemistry series 1, 1, 229 (1972).

W. Lichten, Resonant charge exchange in atomic collisions, Phys. Rev. 131, 229 (1963).

S. M. Lin, D. J. Mascord, R. Grice, Reactive scattering of a supersonic alkali atom beam K + I_2, IBr, CH_2I_2, CHI_3, CBr_4, Mol. Phys., 28, 975 (1974).

J. L. Magee, The gaseous reactions of the alkali metals and halogens, J. C. P., 8, 687 (1940).

J. L. Magee, Charge neutralisation by reaction between positive and negative ions, Disc. Farad. Soc., 12, 33 (1952).

W. Magnus, On the exponent solution of differential equations for a linear operator, Commun. Pure & Appl. Math., 7, 649 (1954).

W. H. Miller & T. F. George, Semiclassical theory of electronic transitions in low energy atomic and molecular collisions involving several nuclear degrees of freedom, J. C. P., 56, 5637 (1972).

R. E. Minturn, S. Datz, R. L. Becker, Alkali atom - halogen molecule reactions in molecular beams; The spectator stripping model,

J. C. P., 44, 1149 (1966).

L. Mirsky, An Introduction to Linear Algebra (Oxford University Press, 1971).

T. Mochizuki & K. Lacmann, Kinematic studies of electron transfer processes between alkali atoms and molecules. $K + O_2$, J. C. P., 65, 3257 (1976).

T. Mochizuki & K. Lacmann, Energy loss measurements in charge transfer reaction between $K + Cl_2$, Chem. Phys. Lett., 49, 604 (1977).

C. E. Moore, Atomic Energy Levels (NBS, 1949).

J. Moseley, W. Aberth, J. R. Peterson, $H^+ + H^-$ mutual neutralisation cross section obtained with superimposed beams, Phys. Rev. Lett., 24, 435 (1970).

N. F. Mott, On the theory of excitation by collisions with heavy particles, Proc. Camb. Philos. Soc., 27, 553 (1931).

A. M. C. Moutinho, J. A. Aten, J. Los, Temperature dependence of the total cross section for chemi-ionisation in alkali - halogen collisions, Physica, 53, 471 (1971).

A. M. C. Moutinho, J. A. Aten, J. Los, Chemi-ionisation in alkali - methylhalogen collisions, Chem. Phys., 5, 84 (1974).

A. M. C. Moutinho, A. P. M. Baede, J. Los, Charge transfer between alkali atoms and oxygen molecules, Physica, 51, 432 (1971).

E. E. Nikitin, Chemische Elementarprozesse, ed. H. Hartmann, p. 43 (Springer-Verlag, 1968).

C. Nyeland & J. Ross, Estimate of potential surface for KClCl, J. C. P.,54, 1665 (1971).

R. E. Olson, Charge transfer at large internuclear distances: Application to asymmetric alkali-ion - alkali-atom systems, Phys. Rev., A 6, 1822 (1972).

R. E. Olson, F. T. Smith, E. Bauer, Estimation of the coupling matrix

elements for one-electron transfer systems, Appl. Opt., 10, 1648 (1971).

P. Pechukas & J. C. Light, On the exponential form of time-displacement operators in quantum mechanics, J. C. P., 44, 3897 (1966).

W. B. Person, Electron affinities of some halogen molecules and the charge-transfer frequency, J. C. P., 38, 109 (1963).

E. S. Hittner, Binding energy and dipole moment of alkali halide molecules, J. C. P., 19, 1030 (1951).

J. Ross, Molecular Beams (ed), Adv. Chem. Phys., X (1966).

Ch. Schlier, Molecular beams and reaction kinetics (ed) (Academic Press, 1970).

I. J. Schoenberg, Contributions to the problem of approximation of equidistant data by analytic functions A, Q. Appl. Math., 4, 45 (1946).

E. Schrödinger, Quantisierung als Eigenwertproblem, Ann. d. Physik., 80, 486 (1926).

C. M. Sholeen, L. A. Gundel, R. R. Herm, Product magnetic deflection slotted disc velocity analysis molecular beam kinetics : $Li + Cl_2$, Br_2, ICl, J. C. P., 65, 3223 (1976).

B. W. Shore, Solving the radial Schrodinger equation by using cubic spline basis functions, J. C. P., 58, 3855 (1973a).

B. W. Shore, Comparison of matrix methods applied to the radial Schrödinger eigenvalue equation : The Morse potential, J. C. P., 59, 6450 (1973b).

B. W. Shore, Use of the Rayleigh-Ritz-Galerkin method with cubic splines for constructing single-particle bound-state radial wavefunctions : The Hydrogen atom and its spectrum, J. Phys., B 6, 1923 (1973c).

B. M. Smirnov, Formation and decay of negative ions, Soviet. Phys.

Dokl., 10, 218 (1965).

F. T. Smith, Diabatic and adiabatic representations for atomic collision problems, Phys. Rev., 179, 111 (1969).

E. C. G. Stückelberg, Theorie der unelastischen stösse zwischen atomen, Helv. Phys. Acta., 5, 369 (1932).

W. R. Thorson, Nonadiabatic effects in the high energy scattering of normal helium atoms, J. C. P., 39, 1431 (1963).

W. R. Thorson, Asymptotic Coriolis interaction in slow atom collisions, J. C. P., 50, 1702 (1969).

J. P. Toennies, Molecular beam scattering experiments on elastic, inelastic, and reactive collisions, in: Physical Chemistry VIA, ed W. Jost, chap. 5 (Academic Press, 1974).

J. C. Tully, Nonadiabatic processes in molecular collisions, in: Dynamics of Molecular Collisions B, ed. W. H. Miller, p. 217 (Plenum, 1976).

J. C. Tully & R. K. Preston, Trajectory Surface Hopping approach to non-adiabatic molecular collisions: the reaction of H^+ with D_2, J. C. P., 55, 562 (1971).

A. Van der Meulen, A. M. Kulis, A. E. DeVries, Molecular beam study of the K+ Br_2 reaction in the electronvolt energy region, Chem. Phys., 7, 1 (1975).

J. Weiner, W. B. Peatman, R. S. Berry, Electron transfer from O^- to the 3p level of Na^+ in 0 - 7 eV collisions, Phys. Rev. Lett., 25, 79 (1970).

J. Weiner, W. B. Peatman, R. S. Berry, Charge transfer in $Na^+ - O^-$ collisions at low relative energy, Phys. Rev., A4, 1824 (1971).

S. Wexler, Associative and non-associative ion pair formation by fast atoms, Ber. Bunsen-Gesselschaft, 77, 606 (1973).

R. R. Wilson, G. H. Kwei, J. A. Norris, R. K. Herm, J. H. Birely,

D. R. Herschbach, Reactive scattering in molecular beams: evidence for a stripping mechanism in reactions of alkali atoms with halogens, J. C. P., 41, 1154 (1964).

C. E. Young, R. J. Beuhler, S. Wexler, Dynamics of electron transfer collisions of fast Li atoms with neutral molecules, J. C. P., 61, 174 (1974).

J - M Yuan & D. A. Micha, Collision dynamics of three interacting atoms: electron transfer in the reactions of K + Br_2, BrI and I_2, J. C. P., 65, 4876 (1976).

C. Zener, Non-adiabatic crossing of energy levels, Proc. Roy. Soc., A 137, 696 (1932).